ACKNOWLEDGEMENTS

I would like to express my sincere thanks to my guides, Dr. Bhaskar Ramamurthi and Dr. K. Giridhar, for their valuable guidance. I would also like to thank Dr. Devendra Jalihal for giving me the opportunity to do System Administrative work for some of the Linux and Digital servers in our laboratory. This has greatly helped me to gain knowledge other than my regular research work. I thank Prof. Ashok Jhunjhunwalla for providing good computing facilities. I also thank Dr. R. Aravind for many useful interactions. Last but not the least, I thank my parents for their support and encouragement.

ABSTRACT

KEYWORDS: Wireless communications, maximum likelihood estimation, Viterbi algorithm, fading channels, noncoherent detection, differential detection.

Multilevel signalling has received much attention in high bit-rate wireless communications in recent years. While constant envelope signalling schemes such as Continuous Phase Modulation (CPM) allow power-efficient operation by using non-linear (Class-C) amplifiers, they are not as spectrally efficient as Quadrature Amplitude Modulation (QAM), especially for M-ary signalling. This thesis addresses the problem of recovering QAM-type multilevel signals transmitted through a variety of wireless communication channels, ranging from "very slow fading" channels, in which the channel gain and phase are constant over many symbol durations, to "slow fading" channels, where the channel gain and phase vary from symbol-to-symbol.

The first part of this thesis deals with noncoherent detection of multilevel signals in frequency-nonselective fading channels. First, an approximate noncoherent Maximum Likelihood (ML) detector is derived for detecting multilevel signals transmitted through frequency-nonselective, very slow fading channels. This detector is noncoherent in the sense that both the channel phase and gain are taken as unknown. This Maximum Likelihood detector for signals with Unknown Amplitude and Phase (ML-UAP) is then modified and implemented recursively using the Viterbi Algorithm (VA), to obtain a lower complexity Suboptimal Noncoherent VA for Multilevel signals (SNVA-M). Next, a forgetting-factor is introduced to deal with slow variations in gain and phase. The resulting Forgetting-factor based SNVA-M (FSNVA-M) does not require explicit carrier recovery or automatic gain control procedures. The FSNVA-M has a symbol-error-rate performance that is as good as the coherent detector for very slow Rayleigh fading channels, slow Rician fading channels with a large specular-to-diffuse power ratio, and AWGN channels.

It is however not suitable for slow Rayleigh fading channels, where the channel gain and phase change appreciably from one symbol to next.

For frequency-nonselective slow Rayleigh fading channels, three schemes based on detection of differentially encoded circular 8-QAM are presented. They are referred to as (i) the Symbol-by-Symbol Differential Detector for Multilevel signals (SSDD-M), (ii) Multiple Symbol Differential Detector using VA for Multilevel signals (MSDDVA-M) and (iii) the Quotient Space approach using the VA (QSVA). While SSDD-M and MSDDVA-M are extensions of the ML-UAP detector, the QSVA is an *ad hoc* approach that takes advantage of the inherent memory in the quotient operation. These schemes have been found to perform better than the conventional symbol-by-symbol detector for differentially encoded 8-PSK, in the absence of diversity. The MSDDVA-M is found to give the best performance out of all the differential detection schemes explored.

All the three proposed schemes for differentially encoded 8-QAM can be easily extended to include diversity reception and thereby provide greater robustness to fading. It is found from computer simulations that Equal Gain Correlation Metric Combining (EGCMC) is best suited for SSDD-M and MSDDVA-M, whereas Predetection Selection Diversity (Pre-SD) is best suited for QSVA. It is also found that for second-order diversity, MSDDVA-M for differentially encoded circular 8-QAM, gives a better performance than the conventional symbol-by-symbol differential detector for 8-PSK, by about 2.0 dB, for a symbol-error-rate of 10^{-4}. It has been found from computer simulations that the QSVA does not perform as well as MSDDVA-M, especially in the presence of diversity. The QSVA however, performs as well as the MSDDVA-M in AWGN channels and Rician fading channels with a large ratio of specular-to-diffuse power.

Nearly all the simulations of the various detectors assume a continuous transmission (and reception) model, where the fade process is assumed to be correlated. If instead, an explicit Time Division Multiple Access (TDMA) model is considered, uncorrelated fade variables from burst-to-burst can be assumed, provided the interval between bursts is sufficiently large. Under this TDMA scheme, we

find that if the Rayleigh fade variable can be assumed constant over a single burst (frame of 1000 bits), the SNVA-M can still be used. Note that this model implies a very slow Rayleigh fading channel. In fact, with first-order diversity, the SNVA-M yields a symbol-error-rate (SER) performance similar to the coherent detector, and two-times better than MSDDVA-M, for the same SNR. For second-order diversity, the SNVA-M is again as good as the coherent detector, while its SER performance is four times better than MSDDVA-M, for the same SNR.

In the Appendices, we provide some useful insights on linear prediction-based (LP-based) detectors which have been originally proposed by other researchers for frequency-nonselective fading channels. We show that with a small modification in the derivation of the LP-based detector, we can avoid estimation of the prediction error variance. The resulting detector is only slightly inferior to the one which estimates the prediction error variance. We also show that a first-order LP-based detector reduces to the conventional symbol-by-symbol differential detector, for M-ary PSK signalling. Further, we motivate why differential encoding is necessary to overcome the problem of *isometry* in LP-based detection. Though the performance of the differential detection schemes proposed in this thesis is at best comparable, or inferior, to the LP-based detectors at high SNR, their complexity is much lower than the LP-based detectors. Moreover, the complexity of the proposed detectors is independent of the fade statistics, unlike the LP-based detectors, whose complexity increases exponentially with the order of the prediction filter required to whiten the fade process.

The final part of this thesis deals with a coherent *Split Trellis* VA-based (STVA) detector for M-ary signals in Intersymbol Interference (ISI) channels encountered in voiceband modem communications. The STVA approach significantly reduces the number of real multiplications in the trellis. In particular, for a channel of length Q symbols, the number of real multiplications in the conventional Whitened Matched Filter (WMF) approach is approximately $2M^Q$ per symbol duration, for M-ary signalling. However, the Split Trellis VA requires only about $2M$ real multiplications per symbol duration. The number of real additions is also reduced

nearly by a factor of two in the Split Trellis approach, compared to the WMF approach. In the derivation of the STVA, we assume the channel to be known *a priori* at the receiver.

It is expected that the proposed low-complexity, differential detectors (especially the MSDDVA-M) will find interesting applications in the emerging Third Generation (3G) cellular and personal communications systems which are required to efficiently support high bit-rate data services. The FSNVA-M detector could find application in wireless LANs based on TDMA, e.g., the IEEE 802.11 standard. The STVA may find useful applications in high bit-rate wireline communications, especially subscriber loop applications where the channel impulse response may not vary significantly over time.

TABLE OF CONTENTS

LIST OF TABLES

LIST OF FIGURES

CHAPTER 1

INTRODUCTION

1.1 A Brief Review of Fading Channels

Communications through a wireless fading channel is an old research area [Kai60]. A typical fading channel has a time-variant impulse response, and the *Doppler spread* characterizes the rate-of-change of the impulse response. The Doppler spread is defined [Mon80, Cox87, Pro95, Skl97] as the bandwidth of the signal received through a fading channel, when the transmitted signal is a single tone (a sinusoid at a particular frequency). Unless explicitly mentioned, we define the "bandwidth" as the 3-dB-down bandwidth. It may be recalled that in the case of a nonfading channel whose impulse response is time-invariant, the Doppler spread is zero, since the received signal is also a tone at the same frequency as the transmitted signal. Fading channels can be frequency-nonselective (flat) or frequency-selective. We now discuss briefly the two types of channel characterizations.

1.1.1 Frequency-Nonselective (Flat) Fading Channels

Theoretically, a frequency-nonselective fading channel has a flat magnitude response that is time-varying, and a linear phase response that is time-invariant, over the bandwidth of the transmitted signal. In other words, the bandwidth of the transmitted signal is much smaller than the *coherence bandwidth* [Pro95] of the channel. For mathematical convenience, assuming that the bandwidth of the channel is infinity, the complex lowpass equivalent impulse response of a flat-fading channel is given by

$$\tilde{h}(t,\tau) = \tilde{G}(t)\delta(\tau - \tau_d) \tag{1.1}$$

where $\tilde{G}(t)$ represents the complex time-varying channel gain and τ_d denotes the time-invariant (constant) channel delay and $\delta(\cdot)$ denotes the Dirac-Delta function.

Observe that in $\tilde{h}(t,\tau)$, t denotes the time-variant component. In other words, according to our notation, a time-invariant channel would be denoted by $\tilde{h}(\tau)$. The time-varying frequency response of the channel is given by

$$\tilde{H}(t,f) = \tilde{G}(t) \int_{-\infty}^{\infty} \delta(\tau - \tau_d) \exp\left(-\mathrm{j}2\pi f\tau\right) \, \mathrm{d}\tau \tag{1.2}$$

which reduces to

$$\tilde{H}(t,f) = \tilde{G}(t) \exp\left(-\mathrm{j}2\pi f\tau_d\right). \tag{1.3}$$

In the above equations $\mathrm{j} \triangleq \sqrt{-1}$. At the receiver, if the received signal is bandlimited by an ideal lowpass filter having a bandwidth $F_s/2$, and sampled at Nyquist-rate (F_s) [PM92], the frequency response of the overall, discrete-time, flat-fading channel model can be written as

$$\tilde{H}(kT_s, \mathrm{e}^{\mathrm{j}\,\omega}) = \tilde{G}(kT_s) \exp\left(-\mathrm{j}\,\omega n_d\right) \qquad \text{for } -\pi < \omega \leq \pi \tag{1.4}$$

where $T_s = 1/F_s$, $\omega = 2\pi f/F_s$ is the discrete-time frequency in radians and the sampling frequency F_s is such that $n_d = \tau_d F_s$ is an integer delay. Hence, the discrete-time impulse response is given by

$$\tilde{h}(kT_s, lT_s) = \tilde{G}(kT_s)\delta\left((l - n_d)T_s\right) \tag{1.5}$$

where l denotes the l^{th} tap of the impulse response and $\delta(\cdot)$ is the Kronecker delta function [PM92].

Thus, when the transmitted signal is $\sin(2\pi F_c t)$, where F_c is the carrier frequency, the discrete-time received signal for sampling-rate $F_s > 2F_c$ is given by

$$\tilde{r}(kT_s) = \tilde{G}(kT_s) \sin\left(\Omega_c(k - n_d)\right) \tag{1.6}$$

where $\Omega_c = 2\pi F_c/F_s$. The above is just the discrete-time representation for a Double Sideband-Suppressed Carrier (DSB-SC) modulation. Hence, the Doppler spread of the channel is the bandwidth defined from the power spectral density (psd) of $\tilde{G}(kT_s)$. In most practical situations, $\tilde{G}(kT_s)$ is nearly constant over at least one symbol duration and varies slowly from one symbol to next [YP95]. We refer to such channels as *slow* [YP95, MK97] flat-fading channels. This implies

that the symbol duration is much smaller than the *coherence time* [Pro95] of the channel. When $\tilde{G}(kT_s)$ is constant over several symbol durations, we refer to it as a *very slow* flat-fading situation. When $\tilde{G}(kT_s)$ varies significantly over one symbol duration, we have a *fast* flat-fading channel, which implies that the symbol duration is of the order of, or larger than, the coherence time of the channel. The terminology used in this thesis for flat-fading channels is summarized in Table 1.1.

Table 1.1: Summary of the terminology used for flat-fading channels.

Terminology	Explanation
Very slow fading	$\tilde{G}_k$ is nearly constant over many symbols
Slow fading	$\tilde{G}_k$ is nearly constant over one symbol and varies slowly from one symbol to next
Fast fading	$\tilde{G}_k$ varies over one symbol

In a typical radio channel, $\tilde{G}(kT_s)$ is well approximated by a correlated complex Gaussian random variable. The autocovariance of $\tilde{G}(kT_s)$ is usually modelled as the zeroth-order Bessel function of the first kind [DS94]. The other popular and mathematically simpler model for the autocovariance of $\tilde{G}(kT_s)$, is the exponential function [Kam91b]. We have used the exponential autocovariance in most of our simulations. The bandwidth defined from the psd of a fast flat-fading channel is larger than that of a slow flat-fading channel. If $\tilde{G}(kT_s)$ has zero-mean, it is a Rayleigh flat-fading channel; otherwise it is a Rician flat-fading channel.

The signal received through a slow flat-fading channel, after matched filtering and symbol-rate sampling, can be written as [YP95, Kam91b, Kam91a, SF95]

$$\tilde{r}(kT) = \tilde{G}(kT)I(kT) + \tilde{w}(kT) \tag{1.7}$$

where T denotes the symbol duration, $I(kT)$ denotes complex symbols drawn from an M-ary QAM constellation, and $\tilde{w}(kT)$ denotes samples of a zero-mean, complex white Gaussian noise process. As mentioned earlier, the time-varying gain $\tilde{G}(kT)$

is assumed to be a complex, correlated Gaussian process. The symbols may be correlated (due to convolutional encoding at the transmitter) or uncorrelated.

The above equation can be written more compactly as

$$\tilde{r}_k = \tilde{G}_k I_k + \tilde{w}_k \tag{1.8}$$

and this is the notation that we will use to represent flat-fading channels throughout this thesis.

1.1.2 Frequency-Selective Fading Channels

Though we deal only with flat-fading channels in this thesis, for the sake of completeness, we now briefly review frequency-selective fading. The magnitude response of a frequency-selective channel is not flat and the phase response is not linear over the bandwidth of the transmitted signal. Moreover if the channel is fading, both the magnitude and the phase response are in general time-variant. Thus, in a frequency-selective fading channel, the bandwidth of the transmitted signal is of the order of or larger than the *coherence bandwidth* of the physical channel. In order to determine the Doppler spread of a frequency-selective fading channel, it is convenient to adopt the discrete-time approach. Let us denote the *effective* complex lowpass equivalent impulse response [Hay83] of the channel by $\tilde{h}(t, \tau)$. Observe that the effective channel is the convolution of the transmit filter with the physical channel, and is thus bandlimited. Henceforth, in the case of frequency-selective fading, when we refer to the channel, we mean the effective channel.

We now obtain the discrete-time channel by sampling [PM92] $\tilde{h}(t, \tau)$ at a sufficiently high rate such that aliasing effects are negligible. We denote the discrete, time-varying channel taps as $\tilde{h}(kT_s, lT_s)$, where l denotes the l^{th} tap and k denotes the time-varying component.

When the transmitted signal is a tone, the discrete-time signal received through a bandlimited frequency-selective fading channel is given by

$$\tilde{r}(kT_s) = \sum_l \tilde{h}(kT_s, lT_s) \sin\left(\Omega_c(k-l)\right). \tag{1.9}$$

However, the above is just a summation of scaled, time-delayed DSB-SC modulated waveforms in discrete-time. Note that for the case of a flat-fading channel, (1.9) reduces to (1.6), since the summation in the above equation has only one term. The Doppler spread of a frequency-selective channel is given by

$$\text{Doppler spread } = \text{3-dB bandwidth of } \left[\sum_l \text{ (psd of the } l^{th} \text{ tap)}\right] \tag{1.10}$$

which reduces to

$$\text{Doppler spread } = \text{3-dB bandwidth of } \left[\sum_l \left|\tilde{H}(\mathrm{e}^{\mathrm{j}\,\omega}, lT_s)\right|^2\right] \tag{1.11}$$

where

$$\tilde{H}(\mathrm{e}^{\mathrm{j}\,\omega}, lT_s) = \sum_k \tilde{h}(kT_s, lT_s) \exp(\mathrm{j}\,\omega k)\,. \tag{1.12}$$

At this point, it is interesting to distinguish between the psd of the l^{th} tap given above and the time-varying frequency response of the frequency-selective channel, which is given by

$$\tilde{H}(kT_s, \mathrm{e}^{\mathrm{j}\,\omega}) = \sum_l \tilde{h}(kT_s, lT_s) \exp(\mathrm{j}\,\omega l)\,. \tag{1.13}$$

When the channel taps can be assumed to be constant over several samples, we refer to this as slow frequency-selective fading. This implies that the sample duration ($T_s = 1/F_s$) is much smaller than the coherence time of the channel. When the taps vary from one sample to next, we have fast frequency-selective fading, which implies that the sample duration is of the order of or greater than the coherence time of the channel.

The discrete-time signal received through a fast frequency-selective fading channel can be written as

$$\tilde{r}(kT_s) = \sum_l I(lT)\tilde{h}(kT_s, kT_s - lT) + \tilde{w}(kT_s) \tag{1.14}$$

where the above equation is obtained from the continuous-time signal $r(t)$, which is given by

$$\tilde{r}(t) = \sum_l I(lT)\tilde{h}(t, t - lT) + \tilde{w}(t). \tag{1.15}$$

and replacing t by kT_s. Observe that unlike the flat-fading channel case in (1.8) where the received samples are symbol-spaced, the samples received through a

frequency-selective channel are in general fractionally-spaced. Figure 1.1 gives the summary of the classification of fading channels.

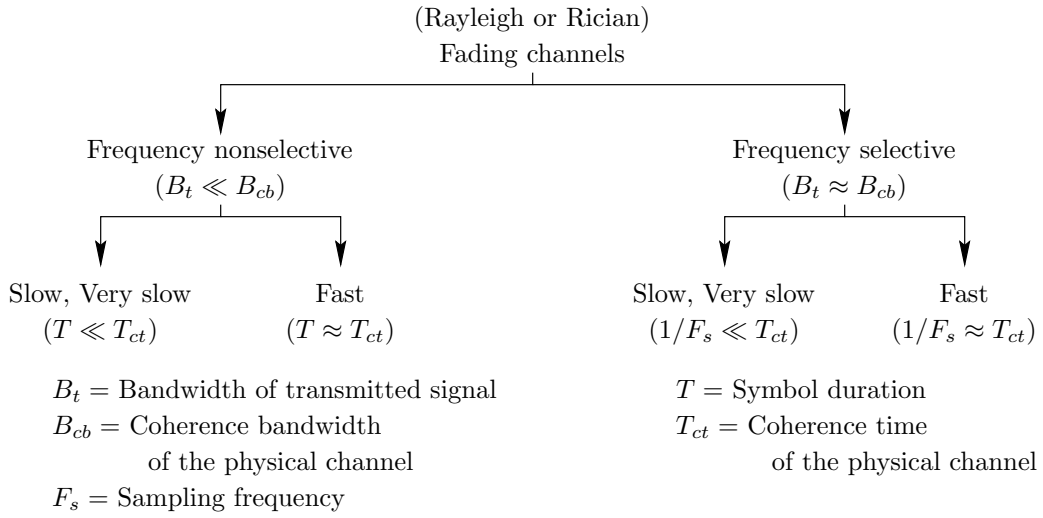

Figure 1.1: Summary of fading channels.

1.2 Literature Survey - Overview

The major part of this thesis is devoted to the detection of multilevel signals transmitted through frequency-nonselective fading channels (both Rayleigh and Rician, slow and very slow fading). In this section, we briefly discuss the published literature on frequency-nonselective fading channel communications. In Chapter 2, we give a detailed review of the literature.

The optimum detector for multilevel signals transmitted through flat-fading channels is a coherent detector, which has perfect knowledge of the fade process [Pro95]. Practically, such a detector is not feasible [Kam91b] since it is not possible to have perfect knowledge of the fade process, especially for Rayleigh fading channels. However, it is possible in practice for the detector to know the autocovariance of the fade process, which can be assumed to be wide sense stationary (WSS). Such a detector has a symbol-error-rate performance that is inferior compared to the coherent detector, even when the autocovariance is perfectly known, and is hence suboptimum.

This suboptimum detector for multilevel signals transmitted through a flat-

fading channel, can be implemented as a bank of prediction filters [Kai60]. We refer to this strategy as Linear Prediction-based (LP-based) detection. This detector is also the Maximum Likelihood (ML) detector when all symbol sequences are equally likely. This will be shown in Chapter 2. However, the complexity of the LP-based detector depends exponentially on the length of the transmitted symbol sequence. When the fade process can be modeled as an Autoregressive (AR) process of a finite order, the Viterbi Algorithm (VA) (whose complexity depends exponentially on the order of the AR process [MS79]), can be used to efficiently decode the data.

Linear prediction-based (LP-based) detection of constant envelope signals over flat-fading channels is discussed in [LM90]. The LP-based detector in [YP95, LM90] is found to be superior than conventional two-symbol differential detectors for M-ary PSK in flat-fading channels. In [VT95], Reduced State Sequence Estimation (RSSE) is employed to reduce the complexity of LP-based detection for constant envelope signalling. In [YP95], LP-based detectors for multilevel signals transmitted through both frequency-nonselective as well as frequency-selective Rayleigh fading channels are derived. The detectors in [YP95, LM90, VT95] can be implemented using the VA.

1.3 Motivation and New Contributions

All the LP-based detectors for flat-fading channels mentioned in Section 1.2 require *a priori* knowledge of the autocovariance of the fade process, which is difficult to estimate in real-time. In practice, the LP-based detectors have to use some standard autocovariance functions [MK97] to detect the data. Moreover, the LP-based detectors implemented using the Viterbi Algorithm (VA) have a complexity that increases exponentially with the order of the prediction filter used to whiten the fade process. In contrast, an important feature of the noncoherent detectors proposed in this thesis is that they do not require any knowledge of the fade statistics. Though the error-rate performance of the noncoherent detectors proposed in this thesis is comparable or inferior to the LP-based detectors at high

SNR in Rayleigh fading channels, their complexity is much lower. Moreover, the complexity of the proposed detectors is independent of the fade statistics. They are easy to implement on a DSP and can be readily extended to include diversity reception, which greatly enhances their performance.

Since the primary focus of this thesis is on efficient detectors for flat-fading channels, it is useful to quantify fade-rates with respect to existing wireless communication standards. We model the fade variable $\tilde{G}_k$ in (1.8), as a 1^{st}-order or 3^{rd}-order AR process, which is characterized by a fade parameter $0 < \rho < 1$. For a first-order IIR filter, the in-phase and quadrature components of $\tilde{G}_k$ are given by

$$G_{k,\,I\{Q\}} = \rho\, G_{k-1,\,I\{Q\}} + \sqrt{1-\rho^2}\, g_{k,\,I\{Q\}} \tag{1.16}$$

where $0 < \rho < 1$ and $g_{k,\,I}$ and $g_{k,\,Q}$ are real, self and mutually uncorrelated, zero-mean white Gaussian noise processes, each with a variance equal to σ_g^2. Note that $G_{k,\,I}$ and $G_{k,\,Q}$ are each real, zero-mean Gaussian with variance $\mu_0 = \sigma_g^2$, since the IIR filter in (1.16) has unit energy. We have considered $\rho = 0.9995$ and $\rho = 0.995$ in the computer simulations given in this thesis.

For a third-order IIR filter, we have assumed that the in-phase and quadrature components of $\tilde{G}_k$ are given by

$$G_{k,\,I\{Q\}} = 3\rho\, G_{k-1,\,I\{Q\}} - 3\rho^2 G_{k-2,\,I\{Q\}} + \rho^3 G_{k-3,\,I\{Q\}} + C_0 g_{k,\,I\{Q\}} \tag{1.17}$$

where again $0 < \rho < 1$, C_0 is a constant chosen such that the filter has a dc gain of unity, and $g_{k,\,I}$ and $g_{k,\,Q}$ are defined in (1.16). In this case $\mu_0 = E_{\rm IIR}\sigma_g^2$, where $E_{\rm IIR}$ is the energy of the IIR filter. We have considered $\rho = 0.8$ and $C_0 = 0.008$ in the computer simulations given in this thesis.

Now, to understand the significance of this parameter ρ, we find the frequency response of the corresponding all-pole filter for $\rho = 0.9995$, $\rho = 0.995$ (both 1^{st}-order, all-pole filters) and $\rho = 0.8$ (a 3^{rd}-order, all-pole filter). This is illustrated in Figure 1.2, where the frequency is normalized with respect to the baud-rate. Observe that smaller the value of ρ, greater is the 3-dB bandwidth, implying greater Doppler-spread (fade-rate).

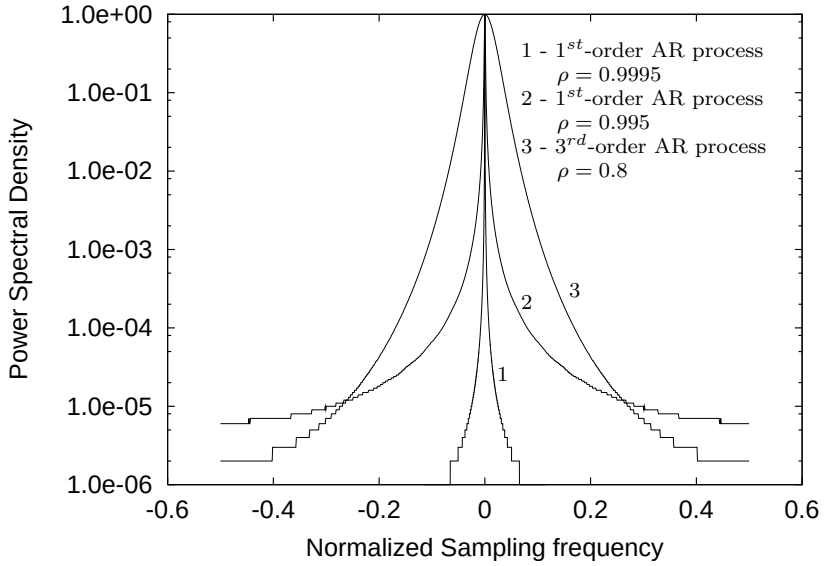

Figure 1.2: Power spectral density of $\left\{\tilde{G}_k\right\}$.

To quantify this further, we look at some existing wireless standards, namely, GSM, IS-136 and DCS-1800. The baud-rate and frequency of operation of these

Table 1.2: Values of ρ obtained for a vehicle moving at 100 kmph, when $\tilde{G}_k$ is a 1^{st}-order AR process.

Standard	Carrier Freq. (MHz)	Baud rate (kbauds)	ρ for 1^{st}-order all-pole model
IS-136	900	24.3	0.9966
GSM	900	277	0.9997
DCS-1800	1800	277	0.9994

standards are provided in Table 1.2. The one-sided 3-dB Doppler-spread is given by

$$B_d = vF_c/c \tag{1.18}$$

where v denotes the velocity of the mobile in m/s, F_c denotes the carrier frequency in Hz, and c denotes the speed of light in m/s. The Doppler-spread normalized with respect to the baud-rate is given by $\Omega_{3-\mathrm{dB}} = B_d T$, where T denotes the symbol duration. This normalized Doppler-spread is equated to the one-sided 3-dB

bandwidth of the filter used to generate $\tilde{G}_k$. In Table 1.2, we have considered a 1^{st}-order IIR filter as an example (this implies that $\tilde{G}_k$ has an exponential auto-covariance function [Kam91b]) and the corresponding value of ρ is obtained by solving the following equation:

$$\rho^2 - \rho\left(4 - 2\cos\left(\Omega_{3-\mathrm{dB}}\right)\right) + 1 = 0. \tag{1.19}$$

The values of ρ in Table 1.2 are given for a vehicle speed of 100 kmph. Note that the values of ρ given in the above table closely match the values used in our simulations, namely, $\rho = 0.9995$ and $\rho = 0.995$, for a 1^{st}-order fade process.

We now briefly summarize the important contributions of this thesis. First, an approximate ML detector is derived for frequency-nonselective, very slow fading channels, where the channel gain and phase remain constant over several symbol durations. We refer to this as the ML-UAP detector, where a metric suitable for multilevel signals is proposed. Next, we describe a suboptimal VA-based approach whose complexity increases linearly with the sequence length to be detected, as opposed to the exponential complexity of the ML-UAP detector. We call this approach the Suboptimal Noncoherent VA for Multilevel signals (SNVA-M) [VGR98b, VGR98a]. The SNVA-M can be viewed as a generalization of the earlier work on noncoherent detection of constant envelope signals [AAS86, AS89, DMV94, SK97, VGR97]. We also propose a forgetting-factor-based SNVA-M (FSNVA-M), to deal with slow variations in the gain and phase.

To deal with frequency-nonselective *slow* fading channels where the channel gain and phase vary from symbol to symbol, the ML-UAP detector is modified to accommodate differential encoding, and a VA-based detector for differentially encoded circular QAM signals is proposed. This VA-based Multiple Symbol Differential Detector for Multilevel signals (MSDDVA-M) has a better symbol-error-rate performance when compared to the Symbol-by-Symbol Differential Detector for circular M-ary QAM (SSDD-M) and incidentally, is also superior to the conventional differential detectors for M-ary PSK.

In [WHS91], a *quotient-space* symbol-by-symbol detector is proposed for differentially encoded star-QAM constellations over slow Rayleigh fading channels.

That is, the quotient of two successive symbol-spaced samples is taken to determine whether an amplitude change has taken place. Further, oversampling and interpolation techniques are adopted to mitigate the effects of fading. However, the inherent correlation in the quotient magnitudes is not exploited. Similar approaches based on computing the quotient of successive symbol-spaced received samples are also discussed in [Sve95]. In this thesis, we propose a Viterbi Algorithm-based detector in the quotient-space, for differentially encoded, circular-QAM signals. This Quotient Space VA (QSVA) technique exploits the fact that not all quotient sequences are valid, and hence is expected to perform better than the simple two-symbol quotient space approach in [WHS91].

Computer simulation results, comparing the symbol-error-rate performance of the proposed noncoherent detectors for 8-QAM and 8-PSK signals transmitted through AWGN, Rayleigh and Rician fading channels, are presented. The simulation results indicate that while the FSNVA-M detector is best-suited for AWGN, very slow Rayleigh fading, and slow Rician fading channels, the MSDDVA-M and the QSVA detectors are best-suited for slow Rayleigh fading channels.

All the three differential detectors proposed, namely, SSDD-M, MSDDVA-M and the QSVA, can be easily extended to include diversity reception, which greatly enhances their performance in slow Rayleigh fading channels, where the channel gain and phase vary from one symbol to next [VGR99a]. It has been found from computer simulations that Equal Gain Correlation Metric Combining (EGCMC) is best suited for SSDD-M and MSDDVA-M, whereas Pre-detection Selection Diversity (Pre-SD) is best suited for QSVA. Moreover, we find that MSDDVA-M for differential 8-QAM performs better than the conventional differential detector for 8-PSK, especially for high fade-rates. However, QSVA does not perform as well as MSDDVA-M for the same number of diversity channels.

Finally, we propose the *Split Trellis* VA for Intersymbol Interference (ISI) channels. Since a typical application we have in mind for this technique is wireline modems, we refer to the channel as an ISI channel (rather than a frequency selective channel as in the case with wireless channels). Moreover, in wireline ban-

dlimited communications, fading or time-variation of the channel is typically very small. Unlike the other detectors proposed in this thesis, which are noncoherent, the Split trellis VA is a coherent detector, requiring estimation of channel, carrier phase and timing. In this thesis, however, we assume that the channel, carrier phase and timing are known at the receiver. The Split Trellis approach significantly reduces the number of real multiplications in the trellis. In particular, for a channel of length Q symbols, the number of real multiplications in the conventional VA (Whitened Matched Filter (WMF) approach) in [Pro95, For72] is approximately $2M^Q$ per symbol duration, for M-ary signalling. However, the Split Trellis VA requires only about $2M$ real multiplications per symbol duration. The number of real additions is also reduced by nearly a factor of two, in the Split Trellis approach, compared to the WMF approach.

1.4 Summary

In this chapter we briefly discussed the characterization of fading channels. In particular, we described how the Doppler spread of both frequency-selective as well as frequency-nonselective fading channels can be evaluated, if the autocovariance of the fade process is known. Following this, a brief overview of the literature on communications through flat-fading channels was provided. The next section dealt with the motivation behind this thesis and its main contributions, including a Split Trellis approach which is proposed to reduce the complexity of the Viterbi detector for ISI channels.

CHAPTER 2

REVIEW OF LITERATURE

2.1 Introduction

In this chapter, we give a detailed review of the literature on detectors for multilevel signalling in slow flat-fading channels. Detectors for slow flat-fading channels may be broadly classified into three types: (i) the detector that has perfect knowledge of the fade process, (ii) the detector that has perfect knowledge of the statistics of the fade process, and (iii) the detector that has no knowledge of either the fade process or the statistics of the fade process. The first type of detector is called the coherent detector. The second type is referred to as a Maximum Likelihood (ML) detector, when the autocovariance of the fade process is known and all symbol sequences are equally likely. Detectors based on the Maximum *a posteriori* (MAP) rule have also been proposed in the literature, when all the symbol sequences are not equally likely. This is especially true for Pilot Symbol Assisted Modulation (PSAM) [SF95, GL97], where known (pilot) symbols are used to estimate the fade statistics. The third type constitute the conventional symbol-by-symbol differential detectors, which do not require any knowledge of the fade process or its statistics. The first type of detector is the optimal detector, whereas the next two types are successively more suboptimal, with respect to the symbol-error-rate performance. The second and third type of detectors are also "noncoherent" detectors, in the sense that they do not require any direct knowledge of the fade process itself.

Finally, we review the published literature on Multiple Symbol Differential Detectors (MSDD), which are basically noncoherent detectors proposed for AWGN channels, and recently have been extended to flat-fading channels. These multiple symbol detectors proposed in the literature assume that the channel gain is known (though the channel phase is assumed to be unknown). In this thesis, we propose

the Maximum Likelihood detector in Unknown Amplitude and Phase (ML-UAP), where the detector assumes that both the channel phase as well as gain is unknown. Thus, the ML-UAP detector is a generalization of the MSDD detectors proposed in the literature.

In Section 2.2, we derive the coherent detector. It is not possible to implement a coherent detector for Rayleigh flat-fading channels, since the rate-of-change of the fade process, $\tilde{G}_k$ in (1.8), increases as the magnitude of $\tilde{G}_k$ approaches zero, thus making it impossible to track the fade process. This is referred to in the literature as the "FM-effect" [DS94, Kam91b, Kam91a], due to which the suboptimal detectors exhibit an error-floor even at infinite Signal-to-Noise Ratio (SNR). However, it is possible to implement a near optimal detector for Rician flat-fading channels having large specular-to-diffuse power.

Section 2.3 covers the literature on linear prediction-based (LP-based) detectors, which require knowledge of the autocovariance of the fade process. We also briefly describe two Suboptimal LP-based detectors referred to as SLP-I and SLP-II. The concept of SLP-I and SLP-II has been discussed earlier in [YP95], but the major difference between SLP-I and SLP-II has not been clearly highlighted. We point out that the vital difference lies in the fact that SLP-I requires knowledge of the *conditional* prediction error variance whereas SLP-II does not require this knowledge. Computer simulations for 8-QAM indicate that SLP-I gives a slightly better symbol-error-rate performance compared to SLP-II, when SLP-I has perfect knowledge of the conditional prediction error variance.

Section 2.4 deals with differential detection strategies which do not require any knowledge of the fade process or its statistics. Finally, in Section 2.5, we review the literature on Multiple Symbol Differential Detection.

We assume that the received signal is given by (1.8), which is repeated here with a small modification

$$\tilde{r}_k = \tilde{G}_k I_k^{(i)} + \tilde{w}_k \tag{2.1}$$

where the superscript i refers to the i^{th} possible transmitted sequence. We assume that L symbols have been transmitted, that is, $0 \leq k \leq L-1$, hence the superscript

i lies in the range $0 \leq i \leq M^L - 1$. The complex fade variable $\tilde{G}_k$ is usually a correlated Gaussian process. The complex noise samples, $\tilde{w}_k$, are uncorrelated with variance given by $E\left[|\tilde{w}_k|^2\right] = 2\sigma_w^2$. We rewrite (2.1) in matrix notation as

$$\tilde{\mathbf{r}} = \tilde{\mathbf{S}}^{(i)}\tilde{\mathbf{G}} + \tilde{\mathbf{w}} \tag{2.2}$$

where $\tilde{\mathbf{r}}$ is an $L \times 1$ column vector of the received samples, $\tilde{\mathbf{S}}^{(i)}$ is an $L \times L$ diagonal matrix of symbols corresponding to the i^{th} possible transmitted sequence, $\tilde{\mathbf{G}}$ is an $L \times 1$ column vector of the fade variables, and $\tilde{\mathbf{w}}$ is an $L \times 1$ column vector of white Gaussian noise samples.

2.2 The Coherent Detector

Assuming that all symbol sequences are equally likely and $\tilde{\mathbf{G}}$ is known perfectly, the Maximum Likelihood detection rule maximizes the joint conditional pdf

$$\max_j f\left(\tilde{\mathbf{r}}|\tilde{\mathbf{S}}^{(j)}, \tilde{\mathbf{G}}\right) \tag{2.3}$$

where $f(\cdot)$ denotes the probability density function. The conditional mean of $\tilde{\mathbf{r}}$ is given by

$$E\left[\tilde{\mathbf{r}}|\tilde{\mathbf{S}}^{(j)}, \tilde{\mathbf{G}}\right] \triangleq \tilde{\mathbf{m}} = \tilde{\mathbf{S}}^{(j)}\tilde{\mathbf{G}} \tag{2.4}$$

which is an $L \times 1$ column vector. Note that $\tilde{\mathbf{m}}$ depends on the data matrix $\tilde{\mathbf{S}}^{(j)}$, though it is not explicitly stated for the sake of notational convenience. The conditional covariance matrix is given by [DS94]

$$\frac{1}{2}E\left[\left(\tilde{\mathbf{r}} - \tilde{\mathbf{m}}\right)\left(\tilde{\mathbf{r}} - \tilde{\mathbf{m}}\right)^H\right] \triangleq \tilde{\mathbf{R}} = \frac{1}{2}E\left[\tilde{\mathbf{w}}\tilde{\mathbf{w}}^H\right] = \sigma_w^2\mathbf{I} \tag{2.5}$$

where the superscript H denotes the conjugate transpose and $\mathbf{I}$ denotes the $L \times L$ identity matrix. Since the elements of $\tilde{\mathbf{r}}$ in (2.2) are jointly Gaussian, (2.3) reduces to

$$\max_j \frac{1}{(2\pi)^L \det\left(\tilde{\mathbf{R}}\right)} \exp\left[-\frac{1}{2}\left(\tilde{\mathbf{r}} - \tilde{\mathbf{m}}\right)^H \tilde{\mathbf{R}}^{-1}\left(\tilde{\mathbf{r}} - \tilde{\mathbf{m}}\right)\right] \tag{2.6}$$

where $\det(\cdot)$ denotes the determinant and $\tilde{\mathbf{R}}^{-1}$ denotes the inverse of $\tilde{\mathbf{R}}$. Since $\tilde{\mathbf{R}}$ is a diagonal matrix, (2.6) reduces to

$$\max_j \frac{1}{(2\pi\sigma_w^2)^L} \exp\left[-\frac{\sum_{k=0}^{L-1}\left|\tilde{r}_k - I_k^{(j)}\tilde{G}_k\right|^2}{2\sigma_w^2}\right]. \tag{2.7}$$

When $I_k^{(j)}$ is uncorrelated, the above rule reduces to symbol-by-symbol detection. When the symbols are correlated (say, due to convolutional coding), the Viterbi Algorithm (VA) is used. The number of trellis states (which determines the complexity of the VA), depends on the memory of the convolutional encoder.

2.3 Detectors Based on Linear Prediction

Assuming that all symbol sequences are equally likely, the Maximum Likelihood (ML) detector based on linear prediction maximizes the joint conditional pdf [BMM93, MMB94, DS94]

$$\max_j f\left(\tilde{\mathbf{r}}|\tilde{\mathbf{S}}^{(j)}\right). \tag{2.8}$$

The conditional mean of $\tilde{\mathbf{r}}$ is given by

$$E\left[\tilde{\mathbf{r}}|\tilde{\mathbf{S}}^{(j)}\right] = \tilde{\mathbf{S}}^{(j)} E\left[\tilde{\mathbf{G}}\right] + E\left[\tilde{\mathbf{w}}\right] = \mathbf{0} \tag{2.9}$$

where we have assumed that $\tilde{\mathbf{G}}$ has zero-mean (Rayleigh flat-fading) and $\mathbf{0}$ is an $L \times 1$ null vector. For mathematical convenience, we consider only a Rayleigh flat-fading channel. The result can be easily extended to a Rician flat-fading channel. The conditional covariance matrix is given by

$$\frac{1}{2} E\left[\tilde{\mathbf{r}}\tilde{\mathbf{r}}^H|\tilde{\mathbf{S}}^{(j)}\right] \triangleq \tilde{\mathbf{R}}_1 = \frac{1}{2}\tilde{\mathbf{S}}^{(j)} E\left[\tilde{\mathbf{G}}\tilde{\mathbf{G}}^H\right]\left(\tilde{\mathbf{S}}^{(j)}\right)^H + \sigma_w^2 \mathbf{I} \tag{2.10}$$

where we have assumed that $\tilde{\mathbf{G}}$ and $\tilde{\mathbf{w}}$ are statistically independent. We have used the notation $\tilde{\mathbf{R}}_1$ to distinguish from the covariance matrix $\tilde{\mathbf{R}}$ described in the previous section. Note that $\tilde{\mathbf{R}}_1$ is dependent on the data sequence $\tilde{\mathbf{S}}^{(j)}$, though, for the sake of notational convenience, it has not been explicitly stated. From (2.10), it can be shown that an element $\tilde{R}_{p,q}$ corresponding to the p^{th} row and q^{th} column of $\tilde{\mathbf{R}}_1$ is given by

$$\tilde{R}_{p,\,q} = I_p^{(j)}\left(I_q^{(j)}\right)^* \mu_{p-q} + \sigma_w^2 \delta(p-q) \tag{2.11}$$

where "*" denotes complex-conjugation, $\delta(\cdot)$ is a Kronecker delta function and

$$\mu_{p-q} = \frac{1}{2} E\left[\tilde{G}_p \tilde{G}_q^*\right]. \tag{2.12}$$

Note that μ_{p-q} is real when the in-phase and quadrature components of $\tilde{G}_k$ in (2.1) are statistically independent. Hence, $\mu_{p-q} = \mu_{q-p}$.

Now, maximizing the joint conditional pdf in (2.8) is equivalent to

$$\max_j \frac{1}{(2\pi)^L \det\left(\tilde{\mathbf{R}}_1\right)} \exp\left[-\frac{1}{2}\tilde{\mathbf{r}}^H \tilde{\mathbf{R}}_1^{-1} \tilde{\mathbf{r}}\right]. \tag{2.13}$$

However, since $\tilde{\mathbf{R}}_1$ is not a diagonal matrix, the above maximization cannot be implemented recursively. In fact, it is easy to see that its complexity increases exponentially with the sequence length, L. This problem can be overcome by using a linear-predictor-based approach which decorrelates the vector $\tilde{\mathbf{r}}$. Let $\tilde{y}_k^{(j)}$ denote the *conditional* prediction error corresponding to the optimum k^{th}-order predictor at time k, *given* that the j^{th} sequence has been transmitted. We then have

$$\tilde{y}_k^{(j)} = \sum_{p=0}^{k} \tilde{a}_{k,\,p}^{(j)}\, \tilde{r}_{k-p} \qquad \text{for } 0 \le k \le L-1, \tag{2.14}$$

where $\tilde{a}_{k,\,p}^{(j)}$ denotes the p^{th} coefficient of the optimal k^{th}-order predictor, *given* that $\tilde{\mathbf{S}}^{(j)}$ is transmitted. Note that both $\tilde{y}_k^{(j)}$ and $\tilde{a}_{k,\,p}^{(j)}$ depend on the data sequence $\tilde{\mathbf{S}}^{(j)}$. The Yule-Walker equations for obtaining the optimal k^{th}-order predictor coefficients at time k are given by [PM92]

$$\begin{bmatrix} \tilde{R}_{k-1,\,k-1} & \dots & \tilde{R}_{0,\,k-1} \\ \vdots & \vdots & \vdots \\ \tilde{R}_{k-1,\,0} & \dots & \tilde{R}_{0,\,0} \end{bmatrix} \begin{bmatrix} \tilde{a}_{k,\,1}^{(j)} \\ \vdots \\ \tilde{a}_{k,\,k}^{(j)} \end{bmatrix} = -\tilde{a}_{k,\,0}^{(j)} \begin{bmatrix} \tilde{R}_{k,\,k-1} \\ \vdots \\ \tilde{R}_{k,\,0} \end{bmatrix} \tag{2.15}$$

where $\tilde{R}_{p,\,q}$ is given by (2.11). It is easy to see from the above equation that the coefficients of the optimal p^{th}-order predictor depend upon the noise variance, σ_w^2, as well as the autocovariance of the fade process $\tilde{G}_k$. However, estimating the noise variance is not an easy task, and hence we describe suboptimal LP-based predictors. The first practical solution is to assume that the product of the average energy of the constellation and the variance of the fade process is much greater than the noise variance [BMM93], that is

$$E_{av}\mu_0 \gg \sigma_w^2 \tag{2.16}$$

where $E\left[|I|^2\right] = E_{av}$ and I denotes a symbol in the M-ary signal constellation. Thus, we can now neglect the effects of noise and derive two suboptimal LP-based receivers, referred to as SLP-I and SLP-II. The approximate Yule-Walker equations can now be written as

$$\begin{bmatrix} \left|I_{k-1}^{(j)}\right|^2 \mu_0 & \dots & \tilde{R}_{0,\,k-1} \\ \vdots & \vdots & \vdots \\ \tilde{R}_{k-1,\,0} & \dots & \left|I_0^{(j)}\right|^2 \mu_0 \end{bmatrix} \begin{bmatrix} \tilde{a}_{k,\,1}^{(j)} \\ \vdots \\ \tilde{a}_{k,\,k}^{(j)} \end{bmatrix} = -\tilde{a}_{k,\,0}^{(j)} \begin{bmatrix} \tilde{R}_{k,\,k-1} \\ \vdots \\ \tilde{R}_{k,\,0} \end{bmatrix}. \tag{2.17}$$

Note that the $k \times k$ square matrix in (2.15) and (2.17) are identical excepting for the diagonal elements. Based on the above equation, two suboptimal detectors, referred to as the Suboptimal LP-based detector-I (SLP-I) and the Suboptimal LP-based detector-II (SLP-II) can be derived. The basic difference between SLP-I and SLP-II lies in the choice of $\tilde{a}_{k,\,0}^{(j)}$ in (2.17). This has been discussed in detail in Appendices A and B.

It has been shown in Appendix A that the SLP-I detection rule is given by

$$\min_j \sum_{k=\mathcal{P}}^{L-1} \frac{\left|\tilde{y}_k^{(j)}\right|^2}{2\left|I_k^{(j)}\right|^2 \sigma_{e,\,\mathcal{P}}^2} + \ln\left[\left|I_k^{(j)}\right|^2 \sigma_{e,\,\mathcal{P}}^2\right] \tag{2.18}$$

where $\mathcal{P}$ is the predictor order required to whiten $\{\tilde{G}_k\}$ and $\sigma_{e,\mathcal{P}}^2$ is the corresponding prediction error variance. The above equation is similar to equation (16) in [YP95]. Note that the above equation has an additional factor of $1/2$ since we have defined the prediction error variance as in (A.4) in Appendix A, which inherently has a factor of $1/2$, whereas the prediction error variance defined in [YP95] does not have this factor.

Similarly, in Appendix B we show that the SLP-II detector is given by

$$\min_j \sum_{k=\mathcal{P}}^{L-1} \left|\tilde{z}_k^{(j)}\right|^2 \tag{2.19}$$

where $\tilde{z}_k^{(j)}$ denotes the modified prediction error. The above is similar to equation (31) in [YP95].

In Appendix C we explore the property of *isometry* in SLP-I and SLP-II detection, which has not been explicitly described in the literature. This property

of isometry can be used to significantly reduce the computational complexity of SLP-I and SLP-II detection, for M-ary PSK signalling. This is discussed in Appendix D.

The concept of LP-based detection for Continuous Phase Modulated (CPM) signals transmitted over Rayleigh flat-fading channels is discussed in [LM90]. The SLP-II detector has also been derived earlier in [BMM93, MMB94], though the equations seem much more complicated. This is simply because $\tilde{z}_k^{(j)}$ in (2.19) has been expanded. In [MMB94], The SLP-II detection strategy has been termed as a combined envelope, multiple differential and coherent detection approach. In [BMM93], the sensitivity of the SLP-II detector to the employed fading spectral model has been investigated. In particular, a rectangular fading filter is used, whereas the regular land-mobile characteristic [Jr.74] is assumed by the receiver. In other words, the receiver assumes a different fading spectral model, instead of the actual spectral model. The degradation in symbol-error-rate (SER) performance is found to be less than 0.7 dB. In another case, a Gaussian fading filter is used, with the receiver again assuming the land-mobile fading characteristic. Here the degradation in SER is found to be less than 2 dB. The amount of degradation is dependent on the "dissimilarity" between the actual and the assumed fading spectral model.

The SLP-II detector is also found to be quite insensitive to the actual and assumed Doppler-spread [BMM93]. The performance of the SLP-II detector in Rician fading channels is also investigated in [BMM93], for situations when the actual and assumed values of the K-factor (ratio of specular-to-diffuse power) are different. It is found that as long as the estimated value of the K-factor lies within ± 15 dB range of the actual value, the performance degradation is less than 1 dB. In [BMM93, MMB94], bit-error-rate simulation results are given for $\pi/4$-shift Differential Quadrature Phase Shift Keying (DQPSK), $\pi/4$-shift Differential Quadrature Amplitude Modulation (DQAM) and 8-DPSK (Differential Phase Shift Keying).

Recall that the SLP detectors require *a priori* knowledge of the autocovariance of the fade process. In [Ada96b], an adaptive Viterbi detection of MPSK signals

is proposed, which does not require any *a priori* information of the fade statistics. In fact, the prediction filter taps are adapted according to the LMS algorithm, and the Per Survivor Processing (PSP) [RPT95] principle. However, this approach is much more complex than the SLP detectors described in this thesis, since each survivor path in the trellis has to maintain a set of prediction filter coefficients. In [Ada98], Recursive Least Squares (RLS) is used instead of LMS, to update the predictor coefficients.

The computational complexity of the SLP-I and SLP-II detectors increases exponentially with the order of the prediction filter used to whiten the fade process. In particular, for a predictor of order $\mathcal{P}$ and for M-ary signalling, the number of trellis states is $M^{\mathcal{P}}$, when the modulator is memoryless. For the case of CPM described in [LM90], the number of trellis states is given by $M^{\mathcal{P}+\alpha}$, where the CPM modulator has a memory of α symbols. In [VT95], an idea similar to Reduced State Sequence Estimation (RSSE) [EQ88] is used to reduce the number of trellis states, and the detection of differentially encoded M-ary PSK is considered for both trellis coded and uncoded systems.

It has been shown in [LM90], that the optimal LP-based detector does not possess an irreducible error floor for a class of Rayleigh fading channels frequently used to model terrestrial mobile channels.

There is yet another kind of detection strategy for Rayleigh flat-fading channels, which is based on symbol-by-symbol detection by optimally estimating the fade process [Kam91b, KT84]. It is easy to see that this detector is also based on linear prediction, since the optimal predictor yields the minimum mean-square prediction error of the fade process. However, this is only a symbol-by-symbol detector, and hence its symbol-error-rate performance is inferior to the SLP-I and SLP-II detectors, which are based on Maximum Likelihood Sequence Estimation (MLSE).

Finally, Maximum Likelihood two-symbol differential detection strategy is presented in [Chu97]. This detector is identical to (2.13), excepting that the detection is performed over two successive samples ($\tilde{\mathbf{R}}_1$ is a 2×2 matrix). This detector thus

optimally detects two consecutive symbols and estimates the transmitted symbol from the differential encoding rules.

2.4 Two-Symbol Differential Detectors

As mentioned in Section 2.1, the two-symbol differential detectors do not require any knowledge of the fade process or its statistics. They have a low computational complexity compared to the LP-based detectors and the MAP detectors, and are simple to implement on a Digital Signal Processor (DSP). The conventional two-symbol differential detector for M-ary PSK is well known [Pro95]. Two-symbol differential detectors for multilevel signalling has been studied extensively in the literature. In particular, the star 16-QAM constellation has gained much attention for Personal Communication Network (PCN) applications where high bit-rate services are required.

In [WHS91], a *quotient-space* symbol-by-symbol detector is proposed for differentially encoded star-QAM constellations over Rayleigh flat-fading channels. That is, the quotient of two successive symbol-spaced samples is taken to determine whether an amplitude change has taken place. Further, oversampling and interpolation techniques are adopted to mitigate the effects of fading. However, the inherent correlation in the quotient magnitudes is not fully exploited. Similar approaches based on computing the quotient of successive symbol-spaced received samples are discussed in [Sve95]. In this thesis, we propose a Viterbi Algorithm-based detection in the quotient-space, for differentially encoded, circular-QAM signals. This Quotient Space VA (QSVA) technique exploits the fact that not all quotient sequences are valid, and hence is expected to perform better than the simple two-symbol quotient space approach in [WHS91].

The detector proposed in [Sve95] is similar to [WHS91]. That is, the transmitted symbol is estimated by computing the quotient and the phase-difference of two successive symbol-spaced received samples. However in [Sve95], the diversity combining is based on the Received Signal Strength (RSS). This RSS-based diversity combining detector is found to perform as well as the the two-symbol Maximum

Likelihood differential detector which uses Equal Gain Diversity Combining.

The bit-error-probability of star 16-QAM in Rayleigh fading channels is analyzed in [AS92a, CNM92]. An improved differential detector that employs decision feedback to improve the reference signal is proposed and analyzed in [AS93] for star 16-QAM signalling over AWGN channels.

In Rayleigh flat-fading channels, diversity reception is necessary for attaining acceptable performance levels for differential detection. There are two kinds of diversity combiners: (i) the predetection type and (ii) the postdetection type. The predetection diversity combiner cophases, weights and combines all signals received on the different branches before signal detection. Well known predetection combiners are the Selection Diversity (SD), Equal Gain Diversity Combiner (EGDC) and the Maximal-Ratio Combiner (MRC). On the other hand, postdetection diversity combiners weight and combine all branches *after* signal detection and do not require the difficult-to-implement cophasing function. Since the postdetection combiner has a simpler structure, it is more practically attractive for mobile radio.

Postdetection combining has been analyzed and simulated for differential 16-APSK over flat Rayleigh fading channels in [CNM93], where square-law and postdetection maximal-ratio combining have been proposed for detecting amplitude and phase changes respectively. A postdetection optimal diversity combiner has been proposed in [Ada93], for DPSK differential detection, which takes into account unequal average powers among diversity branches. It has also been shown in the same paper that postdetection MRC is suboptimal when the average signal power in the diversity branches are not identical. It may be noted that unequal average powers are produced by differences in the gain of each diversity antenna. In particular, for hand-held portable transceivers, the built-in diversity antenna scheme produces an antenna gain difference of about 1 dB [Ada93].

Postdetection phase combining for two branch diversity reception of differential phase shift keying (DPSK) over Rayleigh flat-fading channels is discussed in [IA94]. The receiver in [IA94] has a Differential Phase Detector (DPD) in each diversity

arm and the combiner weights each detector output in proportion to the n^{th} power of the signal envelope at the detector's input. It has been found via computer simulations in [IA94], that for $\pi/4$-shift DQPSK over Rayleigh flat-fading channels, the optimum value of $n = 2$. The detection strategy in [IA94] is summarized below. Each of the DPD outputs is given by

$$\Delta\psi_{k,\,l} = \arg\left\{\tilde{r}_{k,\,l}\tilde{r}^{*}_{k-1,\,l}\right\} \qquad \text{for } l = 1, 2, \tag{2.20}$$

where $\tilde{r}_{k,\,l}$ denotes the received sample at time k in the l^{th} diversity branch (see also (1.8)). The DPD outputs are combined as follows:

$$\Delta\psi_k = w_{k,\,1}\Delta\psi_{k,\,1} + w_{k,\,2}\Delta\psi_{k,\,2}, \tag{2.21}$$

where the weights $w_{k,\,l}$ are given by

$$w_{k,\,l} = \frac{r^{n}_{k,\,l}}{r^{n}_{k,\,1} + r^{n}_{k,\,2}}, \tag{2.22}$$

where the optimum value of n was found to be 2. The decision rule is given by

$$\widehat{\Delta\phi}_k = \min_{\Delta\phi} \left|\Delta\psi - \Delta\phi\right|, \tag{2.23}$$

where $\Delta\phi$ is one of $2\pi m/M$ and $\Delta\psi$ is given by (2.21).

An error rate analysis of M-ary differential PSK and coherent PSK with selection diversity reception under very slow frequency nonselective Rayleigh fading and cochannel interference has been carried out in [AS94].

In [AI94], postdetection diversity that uses $\mathcal{D}$ ($\mathcal{D}$ denotes the number of diversity branches) Differential Phase Detector (DPD) outputs for data decision is described for M-ary DPSK. The data decision is based on minimizing the weighted sum of errors of $\mathcal{D}$ DPD detector outputs. The squared geometric mean of the two consecutively received samples is used as the branch weight. In other words, the decision rule in [AI94] is to choose the phase symbol that minimizes the weighted sum of phase errors as follows:

$$\widehat{\Delta\phi}_k = \min_{\Delta\phi} \sum_{l=1}^{\mathcal{D}} w_{k,\,l} \left|\Delta\psi_{k,\,l} - \Delta\phi\right|^{\beta}, \tag{2.24}$$

where $w_{k,l}$ is the weight for the l^{th} diversity branch at time k, $\Delta\psi_{k,l}$ is the l^{th} DPD output, $\Delta\phi$ is one of $2\pi m/M$ and β is a parameter to be optimized. Observe that $\Delta\psi_{k,l}$ is given by (2.20). In [AI94], it was found from computer simulations that when the squared geometric mean of two consecutive received samples, given by

$$w_{k,l} = |\tilde{r}_{k,l}\tilde{r}_{k-1,l}| \tag{2.25}$$

is used as the weight, the bit-error-rate is minimized. Moreover, the optimum value of β in (2.24), in terms of minimizing the bit-error-rate, was found to be equal to unity.

In [Ada96a], an adaptive differential detection of M-ary DPSK is proposed in which the phase reference for differential detection is estimated using the least-mean-square algorithm with step-size optimally adapted to changing channel conditions. The VA and decision feedback are applied to effectively perform ML detection of the transmitted phase sequence. The BER performance of the detector proposed in [Ada96a] was found to be close to coherent detection with differential decoding, in AWGN channels. In Rayleigh flat-fading channels, it was found that the BER can be reduced almost by half, compared to the conventional differential detector.

In [Ada96c], a theoretical analysis of BER is presented for the differential detection of differentially encoded star 16-QAM (16DAPSK), under Rician fading, Rayleigh faded co-channel interference (CCI) and AWGN. The differential detection involves eight-level differential phase detection (DPD) and two-level amplitude ratio detection. It is shown in [Ada96c] that 16DAPSK is superior to 16DPSK, and requires 1.7 dB less SNR at BER $= 10^{-3}$ in Rician fading channels with specular-to-diffuse power ratio, $K = 5$ dB. It has also been shown that 16DAPSK requires 1.6 dB less Signal-to-Interference Ratio (SIR) compared to 16DPSK, for the same BER and K-factor.

2.5 Multiple Symbol Differential Detectors

MLSE-based Multiple Symbol Differential Detector (MSDD) for AWGN chan-

nels has been discussed extensively in the literature. These detectors are essentially noncoherent detectors which do not require estimation of the carrier phase. However, the MSDD requires the amplitude of the symbols to be known for QAM-type multilevel signals. In this thesis, we derive a noncoherent detector for multilevel signals, referred to as the Maximum Likelihood detector in Unknown Amplitude and Phase (ML-UAP), which does not require estimation of either the carrier phase or the symbol amplitudes. The symbol-error-rate performance of MSDD approaches that of the coherent detector in AWGN channels. The computational complexity of the MSDD however increases exponentially with the length of the symbol sequence to be detected.

The concept of the MSDD was perhaps first introduced in [AAS86] for Continuous Phase Modulated (CPM) signals in AWGN channels. MSDD for uncoded PSK is discussed in [DS90] and that for coded PSK is described in [DMV94]. In [LP92], suboptimal, reduced-complexity, noncoherent detection strategies are discussed for Minimum Shift Keyed signals, whose performance is close to the MSDD. In [DMV94], the MSDD is implemented using the VA for coded PSK. In fact, the MSDD along with per-survivor processing is used in [DMV94] to estimate the unknown phase of the carrier, and its performance, in terms of the "mean time to slip" and "acquisition behaviour", is found to be better than the conventional PLL-based tracking of the carrier phase. In [SK97], the VA is used to implement the MSDD detector for CPM signals, whose computational complexity and symbol-error-rate performance is comparable to that of a coherent detector. In [AS92b], simulation results are presented for 2DPSK in AWGN channels. The trellis in [AS92b] for 2DPSK has only two states. Recall that number of states theoretically required by the MSDD increases exponentially with the total number of symbols to be detected [DS90]. Bit-error-rate analysis for VA-based MSDD for M-ary DPSK has been carried out in [Ada95a] for AWGN channels.

Differential detection can be done in two ways. The conventional differential detector uses a delayed version of the noisy received signal as a phase reference. The other approach is to implement the differential detector using a phase de-

tector. Here, the phase of the received signal is detected and the phase difference is output for decision. This method is called Differential Phase Detection (DPD). In [Ada94], a multiple-symbol approach to differential phase detection is employed to improve the performance over two-symbol differential phase detection. In [AS95, AS96], decision feedback is also employed to further improve the performance of the detector proposed in [Ada94].

The MSDD has also been extended to fading channels. For Rayleigh fading channels, the MSDD is equivalent to a linear prediction-based receiver [LM90]. In [Ada95b], linear prediction is used for phase reference estimation for M-ary DPSK signals transmitted through Rayleigh fading channels.

The performance of MSDD in both AWGN and frequency-nonselective fading channels is discussed in [DS94]. For Rayleigh fading channels, the MSDD is similar to the SLP-I and SLP-II detectors, though in [DS94], no attempt is made to whiten the fade process. In other words, the MSDD in [DS94] is directly given by (2.13), whose expansion results in a very complicated detector equation. The bit-error-rate performance of MSDD for PSK signals in correlated Rayleigh fading channels is described in [HF92].

2.6 Summary

In this chapter, we have given an extensive literature survey on detectors for flat-fading and AWGN channels. The detectors based on linear prediction (LP-based detectors) have been found to perform much better than the conventional two-symbol differential detectors, in Rayleigh flat-fading channels. However, the LP-based detectors have a much higher computational complexity compared to the two-symbol differential detectors, especially for M-ary signalling. There has been some effort towards improving the performance of two-symbol differential detectors using different types of diversity techniques.

CHAPTER 3

NONCOHERENT MAXIMUM LIKELIHOOD DETECTORS

3.1 Introduction

In this chapter, we formulate a low-complexity, approximate noncoherent ML detection strategy for multilevel signals in frequency-nonselective very slow fading channels. We assume that the channel gain and phase remain constant over many symbol intervals. In many high bit-rate, low-range indoor wireless applications like the wireless LAN (e.g. the IEEE 802.11 standard) or wireless EPABX based on TDMA technology, this assumption of very slow and flat-fading may be simultaneously satisfied, especially over one slot duration. Our receiver is noncoherent in the sense that no knowledge is required about the channel gain as well as phase. In this respect, our problem is more general than in [DS94, LP92], which describe ML detectors for channels with unknown phase, but known gain.

3.2 Approximate Maximum Likelihood Detector in Unknown Amplitude and Phase (ML-UAP)

The received signal given by (2.1), is repeated here in a slightly different form as

$$\tilde{r}_k = G_1 I_k^{(i)} \mathrm{e}^{\mathrm{j}\phi_1} + \tilde{w}_k \tag{3.1}$$

where $G_1 > 0$ denotes the unknown gain (G_1 is real), $\phi_1 \in [0, 2\pi)$ denotes the unknown phase and $\mathrm{j} \triangleq \sqrt{-1}$. In the above equation, G_1 and ϕ_1 denote particular values taken by the random variables G and ϕ respectively. Note that $\tilde{G} \triangleq G\mathrm{e}^{\mathrm{j}\phi}$ where $\tilde{G}$ in (2.1) is assumed to be constant over the data length to be detected and hence is independent of time index k. The probability density functions (pdfs)

of G and ϕ are denoted by $f_G(G)$ and $f_\Phi(\phi)$, respectively. We define the average SNR as

$$\frac{E\left[G^2\right]E\left[|I_k|^2\right]}{E\left[|\tilde{w}_k|^2\right]} = \frac{E\left[G^2\right]E\left[|I_k|^2\right]}{2\sigma_w^2} \tag{3.2}$$

whereas the received SNR for a particular instance of the channel is given by

$$\frac{G_1^2 E\left[|I_k|^2\right]}{2\sigma_w^2} \tag{3.3}$$

where G_1 is given in (3.1). The complex mean value of the fade process is given by

$$\tilde{m} \triangleq E\left[\tilde{G}\right]. \tag{3.4}$$

The ratio of the specular-to-diffuse power is defined by [DS94]

$$K \triangleq \frac{|\tilde{m}|^2}{2\mu_0} \tag{3.5}$$

where

$$\mu_0 \triangleq \frac{1}{2}E\left[\left|\tilde{G}-\tilde{m}\right|^2\right]. \tag{3.6}$$

Observe that we have used the notation μ_{p-q} in (2.12) to denote the autocovariance of a Rayleigh flat-fading process ($\tilde{m}=0$). Note that the average SNR can also be given by

$$\frac{E\left[G^2\right]E\left[|I_k|^2\right]}{E\left[|\tilde{w}_k|^2\right]} = \frac{\left(2\mu_0+|\tilde{m}|^2\right)E\left[|I_k|^2\right]}{2\sigma_w^2} \tag{3.7}$$

The noncoherent ML receiver [Pro95] is given by

$$\max_j \mathcal{M}^{(j)} = \int_G\int_\phi \exp\left(-\frac{\Lambda^{(j)}(G,\phi)}{2\sigma_w^2}\right) f_\Phi(\phi) f_G(G)\,\mathrm{d}G\,\mathrm{d}\phi \tag{3.8}$$

where

$$\Lambda^{(j)}(G,\phi) \triangleq \sum_{k=0}^{L-1}\left|\tilde{r}_k - GI_k^{(j)}\mathrm{e}^{\mathrm{j}\phi}\right|^2. \tag{3.9}$$

Note that i and j mentioned in (3.1) and (3.8) lie in the range $0 \le i,j \le M^L-1$. Assuming that the unknown phase is uniformly distributed over $[0,2\pi)$, averaging over ϕ results in [DS94]

$$\max_j \mathcal{M}^{(j)} = \int_G \exp\left(-\frac{G^2\left(B^{(j)}\right)^2}{2\sigma_w^2}\right) I_0\left(\frac{2GA^{(j)}}{2\sigma_w^2}\right) f_G(G)\,\mathrm{d}G \tag{3.10}$$

where $I_0(\cdot)$ is the modified zeroth-order Bessel function of the first kind, and $A^{(j)}$ and $\left(B^{(j)}\right)^2$ are defined by

$$A^{(j)} \triangleq \left|\sum_{k=0}^{L-1} \tilde{r}_k \left(I_k^{(j)}\right)^*\right| \qquad \text{and} \qquad \left(B^{(j)}\right)^2 \triangleq \sum_{k=0}^{L-1} \left|I_k^{(j)}\right|^2. \tag{3.11}$$

At this point we need to substitute the appropriate pdf for G depending on the channel model, to derive the approximate noncoherent ML receiver. In the following subsections, we derive the ML-UAP receiver for Rician, Rayleigh and uniform pdfs, and show that for all the three pdfs the expression for the approximate ML-UAP detection rule remains the same, and is given by

$$\max_j \eta_L^{(j)} = \left(\frac{A^{(j)}}{B^{(j)}}\right)^2. \tag{3.12}$$

3.2.1 Approximate ML-UAP for a Rician pdf

For a Rician pdf, (3.10) becomes

$$\begin{aligned}\max_j \mathcal{M}^{(j)} &= \int_{G=0}^{\infty} \exp\left(-\frac{G^2\left(B^{(j)}\right)^2}{2\sigma_w^2}\right) I_0\left(\frac{2GA^{(j)}}{2\sigma_w^2}\right) \frac{G}{\mu_0} \exp\left(-\frac{(G^2+|\tilde{m}|^2)}{2\mu_0}\right) \\ &\quad \times I_0\left(\frac{|\tilde{m}|G}{\mu_0}\right) \mathrm{d}G. \end{aligned} \tag{3.13}$$

We now make use of the result [GR94, pp. 739]

$$\int_0^{\infty} x \exp(-\alpha x^2) I_\nu(\beta x) J_\nu(\gamma x)\, \mathrm{d}x = \frac{1}{2\alpha} \exp\left(\frac{\beta^2-\gamma^2}{4\alpha}\right) J_\nu\left(\frac{\beta\gamma}{2\alpha}\right) \tag{3.14}$$

where $\alpha > 0$, $\nu > -1$, $J_\nu(\cdot)$ is the Bessel function of the first kind, of order ν and $I_\nu(\cdot)$ is the modified Bessel function of the first kind, of order ν. In order to solve (3.13), we need to substitute the following into (3.14):

$$\begin{aligned}\alpha &= \frac{\left(B^{(j)}\right)^2}{2\sigma_w^2} + \frac{1}{2\mu_0} \\ \beta &= \frac{A^{(j)}}{\sigma_w^2} \\ \gamma &= \frac{\mathrm{j}\,|\tilde{m}|}{\mu_0} \\ \nu &= 0. \end{aligned} \tag{3.15}$$

In the above substitutions, we note that γ must be complex, since $I_0(x) = J_0(\mathrm{j}\, x)$ [Hay83]. For large average signal-to-noise ratio (SNR), $\mu_0 \gg \sigma_w^2$ (see also (3.7)), and we obtain the following approximation:

$$\frac{1}{2\alpha} \approx \frac{\sigma_w^2}{\left(B^{(j)}\right)^2}. \tag{3.16}$$

Using the above approximation we obtain

$$\frac{\beta^2 - \gamma^2}{4\alpha} \approx \frac{\left(A^{(j)}\right)^2}{2\sigma_w^2 \left(B^{(j)}\right)^2} \tag{3.17}$$

where we have assumed $\beta^2 \gg \gamma^2$ (large average SNR), and

$$\frac{\beta\gamma}{2\alpha} \approx \frac{\mathrm{j}\, A^{(j)} |\tilde{m}|}{\left(B^{(j)}\right)^2 \mu_0}. \tag{3.18}$$

Thus, using the approximations in (3.16), (3.17) and (3.18), the maximization in (3.13) reduces to (after ignoring constants and noting that $J_0(\mathrm{j}\, x) = I_0(x)$):

$$\max_j \mathcal{M}^{(j)} = \frac{1}{\left(B^{(j)}\right)^2} \exp\left(\frac{\left(A^{(j)}\right)^2}{2\sigma_w^2 \left(B^{(j)}\right)^2}\right) I_0\left(\frac{A^{(j)}|\tilde{m}|}{\left(B^{(j)}\right)^2 \mu_0}\right). \tag{3.19}$$

Let us now consider the argument of $I_0(\cdot)$ in the above equation. From (3.11), we note that at large received SNR (see (3.3)) and for the correct sequence

$$\frac{A^{(j)}}{\left(B^{(j)}\right)^2} \approx G_1 \tag{3.20}$$

where G_1 is given in (3.1). Thus G_1 is approximately the upper bound on $A^{(j)} / \left(B^{(j)}\right)^2$. When two sequences are orthogonal, we have:

$$\frac{A^{(j)}}{\left(B^{(j)}\right)^2} \approx 0 \tag{3.21}$$

since $A^{(j)} \approx 0$. Next, we consider the term $|\tilde{m}|/\mu_0$ in $I_0(\cdot)$. Observe that when the factor K defined in (3.5) is large, e.g. equal to 10, $|\tilde{m}|/\mu_0$ is much greater than zero. Thus, for the correct sequence and its nearest neighbours, for large enough SNR (both average as well as received SNR), and for large specular-to-diffuse power, we make the approximation [Hay83]

$$I_0(x) \approx \frac{\exp(x)}{\sqrt{2\pi x}} \tag{3.22}$$

which is valid for medium to large values of x. Thus the maximization in (3.19) reduces to (again, after ignoring constant terms)

$$\max_j \mathcal{M}^{(j)} = \frac{1}{B^{(j)}\sqrt{A^{(j)}}} \exp\left(\frac{\left(A^{(j)}\right)^2}{2\sigma_w^2 \left(B^{(j)}\right)^2} + \frac{A^{(j)}|\tilde{m}|}{\left(B^{(j)}\right)^2 \mu_0}\right). \tag{3.23}$$

It is easy to see that the above maximization is dominated by the exponential term for large received SNR, hence we ignore the denominator term outside the exponent. Moreover, we also observe that the first term in the exponent is much larger than the second term, since for large average SNR, $\mu_0 \gg \sigma_w^2$ (see (3.7)), hence we ignore the second term. With these approximations, and taking the natural logarithm on both sides, we obtain the maximization

$$\max_j \eta_L^{(j)} = \left(\frac{A^{(j)}}{B^{(j)}}\right)^2$$

which is the same as (3.12).

Note that we need not separately consider the situation when $A^{(j)} \approx 0$, since such sequences are straightaway eliminated by the rule in (3.12). However, when $A^{(j)}$ is large and the specular-to-diffuse power is very small (this happens when $|\tilde{m}|$ is close to zero) such that the entire argument of $I_0(\cdot)$ in (3.19) tends to zero, we need to make the approximation [DS94]

$$I_0(x) \approx \exp(x^2/4) \tag{3.24}$$

which is valid for values of x close to zero. Substituting this approximation in (3.19) we get

$$\max_j \mathcal{M}^{(j)} = \frac{1}{\left(B^{(j)}\right)^2} \exp\left(\frac{\left(A^{(j)}\right)^2}{2\sigma_w^2 \left(B^{(j)}\right)^2} + \frac{\left(A^{(j)}\right)^2 |\tilde{m}|^2}{4\left(B^{(j)}\right)^4 \mu_0^2}\right). \tag{3.25}$$

Once again we see that when the received SNR is large (G_1 is large), the exponential term dominates, and moreover, the first term in the exponent is much larger than the second term (since the second term tends to zero, due to our assumption). Hence, we need to consider only the first term in the exponent. With these approximations, and taking the natural logarithm on both sides, we get the detection rule in (3.12).

It may be noted that when the ratio of the specular-to-diffuse power is very small, the probability that the received SNR is small (G_1 is small) becomes significant, and the Rician channel behaves almost like a Rayleigh channel. Thus, when the received SNR is small (G_1 is small), it is not possible to simplify the detection rule in (3.25) any further, and moreover, the detector requires knowledge of the noise variance, which is not practical. The only practical solution is to make the approximations to (3.25) (even though they may not be valid), and arrive at the detection rule in (3.12).

It is interesting to note that the same detection rule given in (3.12), was obtained in [VGR99b] by approximating $I_0(x) = \mathrm{e}^x$ for all values of x in (3.13), even though it is clear from Figure 3.1 that "mathematically" this is not a good approximation for large values of x. However, $I_0(x) = \mathrm{e}^x$ seems to be a good approximation for the *maximization* problem, since, for large values of x, the exponential term dominates over the term $1/\sqrt{x}$. This approximation ($I_0(x) \approx \mathrm{e}^x$ for large values of x) has also been used in [DS94]. The squared normalized ap-

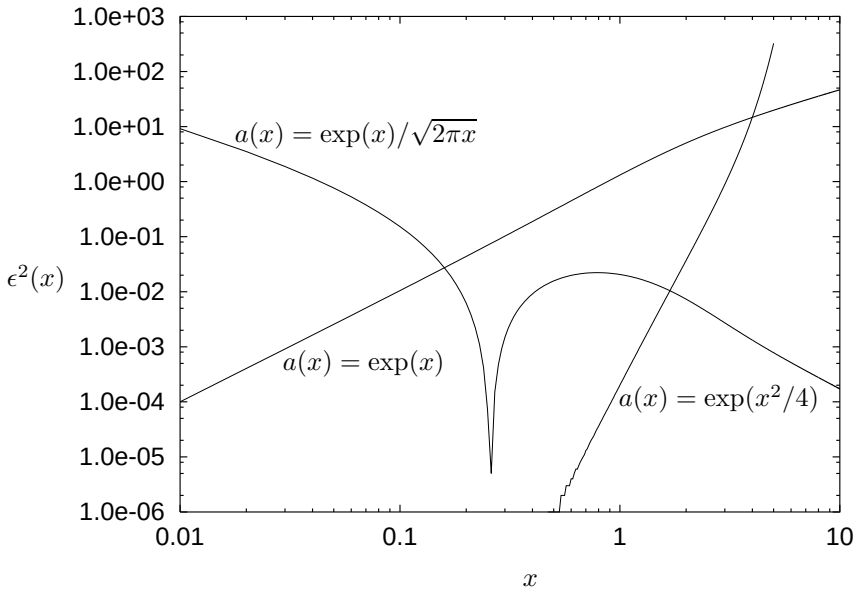

Figure 3.1: Plots showing errors for various approximations of $I_0(x)$.

proximation error plotted in Figure 3.1, is obtained as follows:

$$\epsilon^2(x) = \frac{\left(I_0(x) - a(x)\right)^2}{I_0^2(x)} \tag{3.26}$$

where $a(x)$ denotes the approximation of $I_0(x)$.

3.2.2 Approximate ML-UAP for a Rayleigh pdf

For a Rayleigh pdf, (3.10) becomes

$$\max_j \mathcal{M}^{(j)} = \int_{G=0}^{\infty} \exp\left(-\frac{G^2\left(B^{(j)}\right)^2}{2\sigma_w^2}\right) I_0\left(\frac{2GA^{(j)}}{2\sigma_w^2}\right) \frac{G}{\mu_0} \exp\left(-\frac{G^2}{2\mu_0}\right) \mathrm{d}G. \quad (3.27)$$

Observe that the above integral is identical to (3.13) with $\tilde{m} = 0$. To solve the above integral, we make use of the result [GR94, pp. 738]

$$\int_0^{\infty} x^{\nu+1} \exp(-\alpha x^2) J_\nu(\gamma x)\, \mathrm{d}x = \frac{\gamma^{\,\nu}}{(2\alpha)^{\nu+1}} \exp\left(-\frac{\gamma^{\,2}}{4\alpha}\right) \quad (3.28)$$

where $\alpha > 0$, $\nu > -1$, and $J_\nu(\cdot)$ is the Bessel function of the first kind, of order ν. Once again, to solve for (3.27), we need to substitute the following into (3.28):

$$\begin{aligned} \alpha &= \frac{\left(B^{(j)}\right)^2}{2\sigma_w^2} + \frac{1}{2\mu_0} \\ \gamma &= \frac{\mathrm{j}\, A^{(j)}}{\sigma_w^2} \\ \nu &= 0. \end{aligned} \quad (3.29)$$

For large average SNR, we use the approximation in (3.16). Thus, the maximization in (3.27) reduces to (after ignoring constants)

$$\max_j \mathcal{M}^{(j)} = \frac{1}{\left(B^{(j)}\right)^2} \exp\left(\frac{\left(A^{(j)}\right)^2}{2\sigma_w^2 \left(B^{(j)}\right)^2}\right). \quad (3.30)$$

When the received SNR is large (G_1 is large) and when $A^{(j)}$ is large (this is true for the correct sequence and its nearest neighbours), the exponential term dominates. With this approximation, taking the natural logarithm on both sides of (3.30), we again get the detection rule in (3.12).

It may be noted that for a Rayleigh fading channel, the probability that the received SNR is small (G_1 is small), is significant. Hence, at low received SNR, it may not be appropriate to ignore the denominator term outside the exponential. However, the maximization in (3.30) requires knowledge of the noise variance, which is not feasible in practice. Hence (3.12) is a practical implementation of the noncoherent detector.

It may be noted that the same detection rule given in (3.12), was obtained in [VGR99b] by approximating $I_0(x) = \mathrm{e}^x$ for all values of x in (3.27).

3.2.3 Approximate ML-UAP for a Uniform pdf

Here we assume that $f_G(G)$ is uniform between 0 and $\mathcal{G}_1$, where $\mathcal{G}_1$ is a large value. Thus (3.10) becomes

$$\max_j \mathcal{M}^{(j)} = \frac{1}{\mathcal{G}_1} \int_{G=0}^{\mathcal{G}_1} \exp\left(-\frac{G^2\left(B^{(j)}\right)^2}{2\sigma_w^2}\right) I_0\left(\frac{2GA^{(j)}}{2\sigma_w^2}\right) \mathrm{d}G. \tag{3.31}$$

For mathematical convenience, we allow $\mathcal{G}_1$ to tend to infinity, and use the result [GR94, pp. 737]

$$\begin{aligned}\int_0^\infty x^\mu \exp(-\alpha x^2) J_\nu(\gamma x)\,\mathrm{d}x &= \frac{\Gamma(\nu/2+\mu/2+1/2)}{\gamma\alpha^{\mu/2}\Gamma(\nu+1)} \exp\left(-\frac{\gamma^2}{8\alpha}\right) \\ &\quad \times M_{\mu/2,\,\nu/2}\left(\frac{\gamma^2}{4\alpha}\right)\end{aligned} \tag{3.32}$$

for $\alpha > 0$, $\mu + \nu > -1$, $\Gamma(\cdot)$ is the Gamma function and $M_{p,q}(\cdot)$ is the Whittaker's function. The Whittaker's function is in turn given by

$$M_{p,\,q}(z) = \exp(-z/2) z^{1/2+q} M\left(\frac{1}{2}+q-p, 1+2q, z\right) \tag{3.33}$$

where $z = \gamma^2/(4\alpha)$, $p = \mu/2$, $q = \nu/2$ and $M(\cdot)$ is the Kummer's function [AS65, pp. 504]. Now, to solve (3.31), we need to substitute the following in (3.32):

$$\begin{aligned}\alpha &= \frac{\left(B^{(j)}\right)^2}{2\sigma_w^2} \\ \gamma &= \frac{\mathrm{j}\,A^{(j)}}{\sigma_w^2} \\ \mu &= 0 \\ \nu &= 0\end{aligned} \tag{3.34}$$

and use the fact that the Kummer's function [AS65, pp. 509]

$$M\left(\frac{1}{2}, 1, z\right) = \Gamma(1)\exp(z) I_0(z). \tag{3.35}$$

Substituting (3.33), (3.34) and (3.35) in (3.32) and using the fact that [AS65]

$$\begin{aligned}\Gamma(1/2) &= \sqrt{\pi} \\ \Gamma(1) &= 1\end{aligned} \tag{3.36}$$

the maximization in (3.31) reduces to (after ignoring constants)

$$\max_j \mathcal{M}^{(j)} = \lim_{\mathcal{G}_1 \to \infty} \frac{1}{\mathcal{G}_1 B^{(j)}} I_0 \left(- \frac{\left(A^{(j)}\right)^2}{2\sigma_w^2 \left(B^{(j)}\right)^2} \right). \tag{3.37}$$

However, in the limit $\mathcal{G}_1 \to \infty$, $\mathcal{M}^{(j)} \to 0$ for all j, and we do not get any useful result. Hence, we first perform the maximization and ignore the limit. Finally, using the relation $I_0(-x) = I_0(x)$ [Hay83], the above maximization reduces to

$$\max_j \mathcal{M}^{(j)} = \frac{1}{B^{(j)}} I_0 \left(\frac{\left(A^{(j)}\right)^2}{2\sigma_w^2 \left(B^{(j)}\right)^2} \right). \tag{3.38}$$

When the received SNR (given by (3.3)) is large, the approximation in (3.22) can be used. However, we again note that for large received SNR, the exponential term dominates and the other terms can be ignored, as far as the maximization is concerned. Hence, the above maximization again reduces to

$$\max_j \mathcal{M}^{(j)} = \exp \left(\frac{\left(A^{(j)}\right)^2}{2\sigma_w^2 \left(B^{(j)}\right)^2} \right). \tag{3.39}$$

Taking the natural logarithm on both sides and ignoring the terms independent of j, we again get the detection rule in (3.12).

It is interesting to note that the detection rule in (3.12) was also obtained in [VGR99b] by using the approximation $I_0(x) \approx \mathrm{e}^x$ for all values of x in (3.31).

3.3 Summary of the ML-UAP Detector

Therefore, independent of whether the fade statistics for the gain is Rician, Rayleigh or Uniform, the approximate ML rule is given by (3.12). Using (3.11), we restate the approximate ML-UAP decision rule as follows:

$$\max_j \eta_L^{(j)} = \frac{\left| \sum_{k=0}^{L-1} \tilde{r}_k \left(I_k^{(j)}\right)^* \right|^2}{\sum_{k=0}^{L-1} \left| I_k^{(j)} \right|^2} \tag{3.40}$$

where $\eta_L^{(j)}$ is the *correlation metric* of the j^{th} possible transmitted sequence after L symbols. It can be shown using the Schwartz inequality that, when the i^{th} sequence is transmitted, $\eta_L^{(j)} \leq \eta_L^{(j)}$ for $j \neq i$, in the absence of noise. In other

words, an incorrect sequence cannot yield a larger correlation metric than the correct sequence, in the absence of noise. In the next section, we study some of the important properties of this correlation metric.

For constant envelope signals, (3.40) reduces to the Multiple Symbol Differential Detector (MSDD) for AWGN channels in [DS94, DS90, LP92]. The MSDD for multilevel signals in AWGN channels when G_1 in (3.1) is known [DS94], is given by the integrand of (3.10) with G replaced by G_1:

$$\max_j \mathcal{N}^{(j)} = \exp\left(-\frac{G_1^2\left(B^{(j)}\right)^2}{2\sigma_w^2}\right) I_0\left(\frac{2G_1A^{(j)}}{2\sigma_w^2}\right). \tag{3.41}$$

For large SNR, $I_0(x) \approx \mathrm{e}^x$ (since the other terms in (3.22) can be ignored). Taking the natural logarithm on both sides we obtain the metric for the MSDD for multilevel signals [DS94] as

$$\max_j \zeta^{(j)} = 2G_1A^{(j)} - G_1^2\left(B^{(j)}\right)^2. \tag{3.42}$$

3.4 Properties of the Correlation Metric $\eta(\cdot)$

Property 1 If two sequences $\left\{I_k^{(i)}\right\}$ and $\left\{I_k^{(j)}\right\}$ are related by $I_k^{(i)} = G\mathrm{e}^{\mathrm{j}\phi}I_k^{(j)}$ for $0 \le k \le N-1$, where G and ϕ are real constants, then $\eta_N^{(i)} = \eta_N^{(j)}$.

The proof follows directly from (3.40). Henceforth we will refer to sequences related as above, as *isometric sequences*, since they yield the same correlation metric. We now discuss the implications of the above property. We explain using

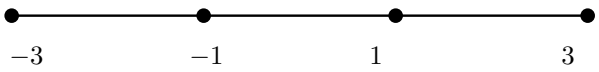

Figure 3.2: The 4-PAM constellation.

the 4-PAM constellation shown in Figure 3.2. Property 1 implies that the ML-UAP detector cannot distinguish between, for example, an all 1 and an all 3 sequence, since both these sequences yield the same correlation metric. Hence the ML-UAP detector by itself is not very useful, in terms of detecting an entire sequence. Therefore, we adopt a different strategy, and instead of detecting an

entire sequence at one go, we detect one symbol at a time, very much like the regular Viterbi Algorithm (VA) with finite decoding delay (truncation). Note that detecting one symbol at a time does not imply a symbol-by-symbol detector. The ambiguity caused due to isometry is removed by properly initializing the detector using a few known training symbols. In the next property, we show that when the ML-UAP detector estimates a large number of symbols in a sequence correctly, the noncoherent squared distance between subsequent symbols constituting an "error-event", approaches the coherent squared distance.

Property 2 Given that the i^{th} sequence is transmitted, the difference between the correlation metrics $\eta_{N+D}^{(i)}$ and $\eta_{N+D}^{(j)}$, is approximately equal to the coherent squared distance between sequences i and j in the absence of noise, provided $I_k^{(i)} = I_k^{(j)}$ for $0 \leq k \leq N-1$ and $1 \leq D \ll N$. The difference between the correlation metrics, in general, is denoted by the noncoherent squared distance.

Here, the symbol sequence $\left\{I_k^{(j)}\right\}$ constitutes an error event over D symbol durations, which diverges from the sequence $\left\{I_k^{(i)}\right\}$ at time N and remerges back at time $N+D-1$. Such error events extending over more than symbol duration occur when the symbols are correlated, due to convolutional encoding at the transmitter. In this case, the valid symbol sequences can be represented by a trellis, the number of trellis states depending on the memory of the convolutional encoder. When the symbols are uncorrelated, we have a single-state trellis with M parallel transitions, for M-ary signalling and the length of the error event is $D = 1$. In what follows, we consider only noiseless signals, since distances between valid sequences are computed in the absence of noise. We have

$$\eta_{N+D}^{(i)} = G^2 \sum_{k=0}^{N+D-1} \left|I_k^{(i)}\right|^2 \tag{3.43}$$

and

$$\eta_{N+D}^{(j)} = G^2 \frac{\left|\sum_{k=0}^{N-1} \left|I_k^{(i)}\right|^2 + \sum_{k=N}^{N+D-1} I_k^{(i)} \left(I_k^{(j)}\right)^*\right|^2}{\sum_{k=0}^{N-1} \left|I_k^{(i)}\right|^2 + \sum_{k=N}^{N+D-1} \left|I_j^{(j)}\right|^2} \tag{3.44}$$

Let

$$\begin{aligned} S^{(i)} &= \textstyle\sum_{k=0}^{N-1} \left|I_k^{(i)}\right|^2 \quad \text{and} \quad X^{(ij)} + \mathrm{j}\, Y^{(ij)} = \textstyle\sum_{k=N}^{N+D-1} I_k^{(i)} \left(I_k^{(j)}\right)^* \\ E^{(j)} &= \textstyle\sum_{k=N}^{N+D-1} \left|I_k^{(j)}\right|^2 \quad \text{and} \qquad\qquad E^{(i)} = \textstyle\sum_{k=N}^{N+D-1} \left|I_k^{(i)}\right|^2 . \end{aligned} \tag{3.45}$$

Note that $S^{(i)} \gg |X^{(ij)} + \mathrm{j}\, Y^{(ij)}|$ and $S^{(i)} \gg E^{(j)}$ for $N \gg D$. Therefore $\eta_{N+D}^{(j)}$ can be approximated as

$$\eta_{N+D}^{(j)} \approx G^2 S^{(i)} \frac{1 + (2X^{(ij)}/S^{(i)})}{1 + (E^{(j)}/S^{(i)})} \approx G^2 \left(S^{(i)} + 2X^{(ij)} - E^{(j)} \right) \tag{3.46}$$

and the noncoherent squared distance between $\eta_{N+D}^{(i)}$ and $\eta_{N+D}^{(j)}$ is then given by

$$d_{nc,a}^2(i,j) = \eta_{N+D}^{(i)} - \eta_{N+D}^{(j)} = G^2 \left(E^{(i)} + E^{(j)} - 2X^{(ij)} \right) \tag{3.47}$$

where the subscript a denotes the asymptotic distance ($N \to \infty$).

On the other hand, the coherent squared distance between sequences i and j is given by

$$\begin{aligned} d_c^2(i,j) &= \sum_{k=N}^{N+D-1} \left| G\mathrm{e}^{\mathrm{j}\phi} I_k^{(i)} - G\mathrm{e}^{\mathrm{j}\phi} I_k^{(j)} \right|^2 \\ &= G^2 \left(E^{(i)} + E^{(j)} - 2X^{(ij)} \right) = d_{nc,a}^2(i,j). \end{aligned} \tag{3.48}$$

Thus, we see that the noncoherent squared distance asymptotically tends to the coherent squared distance. At high SNR, it can be shown that the probability of deciding in favour of sequence j given that sequence i was transmitted, is equal to that of a coherent detector. This proof is given in Appendix E.

Property 3 If the transmitted sequence is $\left\{ I_k^{(i)} \right\}$ and there exists an isometric sequence $\left\{ I_k^{(j)} \right\}$, then at high SNR the ML-UAP estimator will correctly decide in favour of $\left\{ I_k^{(i)} \right\}$ provided it has been "initialized" by $I_k^{(i)}$ upto N symbols, where $N \gg 0$.

This property follows directly from Property 2, since the noncoherent squared distance between the correlation metrics is nearly equal to the coherent squared distance, and at high SNR the estimator has no difficulty in distinguishing between the two. From our computer simulations, it was found that $N = 10$ is sufficient for the noncoherent squared distance to tend to the coherent squared distance. We now explain Property 3 with an example.

Let us assume 4-PAM signalling shown in Figure 3.2 and that the symbols are uncorrelated. Hence we have a single-state trellis with four parallel transitions.

We also assume for convenience that the channel gain $G = 1$. Let the transmitted sequence be the all-3 sequence. Assume that the ML-UAP detector is initialized by 3s upto the first 10 symbols. This is possible in practice when the first 10 symbols constitute a known preamble. Now, *given* that the ML-UAP has estimated correctly upto the first 10 symbols, we wish to find out the noncoherent squared distance between two symbols (say 1 and 3) occurring at the 11^{th} symbol instant. We denote $\eta_{11}^{(1)}$ as the correlation metric due the symbol 1 at the 11^{th} symbol instant and $\eta_{11}^{(3)}$ that due to symbol 3. We have

$$\eta_{11}^{(3)} = \frac{\left|\sum_{k=0}^{10} 3^2\right|^2}{\sum_{k=0}^{10} 3^2} = 99 \tag{3.49}$$

and

$$\eta_{11}^{(1)} = \frac{\left|\left(\sum_{k=0}^{9} 3^2\right) + 1 \times 3\right|^2}{\left(\sum_{k=0}^{9} 3^2\right) + 1^2} = 95.04. \tag{3.50}$$

Hence the noncoherent squared distance between symbol 3 and 1 at the 11^{th} symbol instant is

$$\eta_{11}^{(3)} - \eta_{11}^{(1)} = 3.96 \tag{3.51}$$

which is close to the coherent squared distance of 4 for $G = 1$. Hence the ML-UAP detector will correctly decide in favour of symbol 3 at the 11^{th} symbol instant at high SNR. In other words, *given* that the ML-UAP detector has detected correctly upto the first 10 symbols, it will detect the 11^{th} symbol with a symbol-error-probability that is close to that of a coherent detector. This property is now recursively used in successive symbol intervals and finally, the ML-UAP detector detects the entire sequence with a symbol-error-rate that is close to that of a coherent detector. Had the ML-UAP detector been used to detect the entire sequence in one go (block detection), it would not have been possible (due to isometry) to differentiate between an all-1 sequence and an all-3 sequence, or for that matter, any sequence with identical symbols.

We now propose a VA-based approach to the ML-UAP estimator given in (3.40), which detects one symbol at a time as explained in the above example, and takes advantage of Property 2 and 3.

3.5 Suboptimal Noncoherent Viterbi Algorithm for Multilevel Signals (SNVA-M)

The noncoherent sequence estimator given by (3.40) has a complexity that increases exponentially with L, and is therefore impractical. We now describe a Suboptimal Noncoherent VA-based estimator for Multilevel signals (SNVA-M), whose complexity is only linear in L. This estimator is similar to the SNVA proposed by us in [VGR97] for constant envelope signals, and also to the schemes discussed in [AS89, DMV94, SK97], but with the transition metrics computed differently, reflecting the underlying multilevel modulation. The primary aim of the

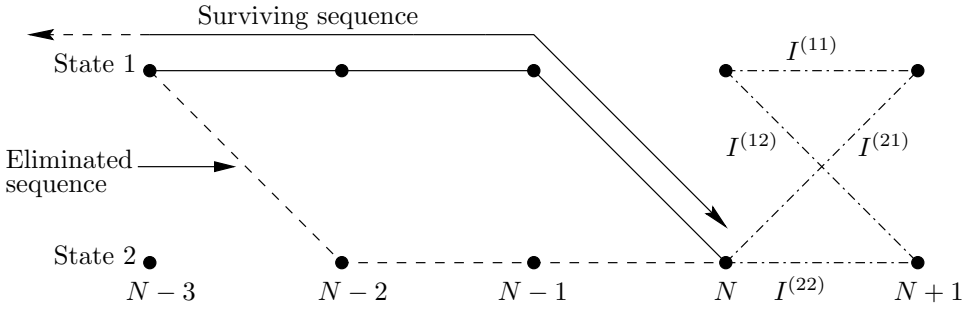

Figure 3.3: Surviving and eliminated sequences at state 2 after N symbols.

SNVA-M detector is to reduce the complexity of the ML-UAP to that of a coherent detector, even while ensuring through proper initialization that the noncoherent squared distance tends to the coherent squared distance. Note that in a coherent detector, G and ϕ are known. The complexity of the coherent detector depends on whether the symbols $I_k^{(i)}$ are correlated or not. When the symbols are uncorrelated, symbol-by-symbol detection is optimum, which is equivalent to a single-state trellis. When the symbols are correlated, for example due to convolutional coding [Pro95], then obviously the optimum detection strategy is Maximum Likelihood Sequence Estimation (MLSE) using the Viterbi Algorithm (VA). The number of trellis states depends on the constraint-length of the convolutional encoder. We now assume without any loss of generality that the symbols are correlated and the trellis has more than one state.

Let $\tilde{A}_N^{(j)}$ denote the surviving complex cross-correlation (the summation term

in the numerator of (3.40)) and $\left(B_N^{(j)}\right)^2$ denote the surviving autocorrelation (denominator of (3.40)) at the j^{th} state at time N. The surviving path at state # 2 is illustrated in Figure 3.3 by a solid line, for a 2-state trellis. Note that $\tilde{A}_N^{(j)}$ is different from $A^{(j)}$ defined in (3.11). The recursions for the Forgetting-factor-based SNVA-M (FSNVA-M) at time $N+1$ are given by

$$\begin{aligned} \tilde{A}_{N+1}^{(ji)} &= \gamma \tilde{A}_N^{(j)} + \tilde{r}_N \left(I^{(ji)}\right)^* \\ \left(B_{N+1}^{(ji)}\right)^2 &= \gamma \left(B_N^{(j)}\right)^2 + \left|I^{(ji)}\right|^2 \end{aligned} \tag{3.52}$$

where $I^{(ji)}$ denotes the symbol due to the transition from state j to state i and $0 \leq \gamma \leq 1$ is the forgetting-factor. Observe that the above equations are similar to the recursions of a first-order IIR filter. All the possible trellis transitions are shown in Figure 3.3 by dot-dashed lines. The forgetting-factor is necessary to deal with slow variations in G and ϕ. Thus, explicit carrier phase estimation and received signal gain estimation procedures are not required. The forgetting-factor also prevents build-up of the metrics in (3.52) as the VA progresses in time, thus preventing overflow errors, especially in fixed-point DSP implementations. When $\gamma = 1$, we obtain the SNVA-M detector. The survivor at the i^{th} state is given by

$$\eta_{N+1}^{(i)} = \max_j \frac{\left|\tilde{A}_{N+1}^{(ji)}\right|^2}{\left(B_{N+1}^{(ji)}\right)^2} \tag{3.53}$$

where the maximization is done over all states j that lead to state i.

Observe that the survivor computation based on (3.53) is suboptimal in general. For example, let $\tilde{A}$ and B^2 correspond to the survivor sequence at state j. Let $\tilde{C}$ and D^2 correspond to the eliminated sequence at state j. This implies that

$$\frac{|\tilde{A}|^2}{B^2} > \frac{|\tilde{C}|^2}{D^2}. \tag{3.54}$$

Now, if $\tilde{x}$ and y^2 correspond to the branch metrics emerging from state j to some other state i then (3.54) does not imply that

$$\frac{|\tilde{A}+\tilde{x}|^2}{B^2+y^2} > \frac{|\tilde{C}+\tilde{x}|^2}{D^2+y^2}. \tag{3.55}$$

Thus in general, an eliminated sequence could have a higher correlation metric than the surviving sequence, at a later point of time.

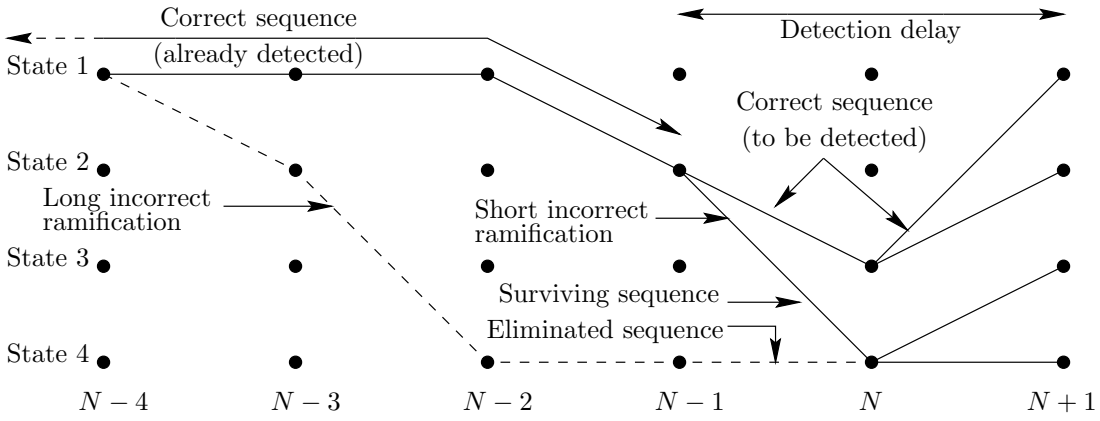

Figure 3.4: Surviving sequences after $N+1$ symbols.

However, it can be shown that the survivor computation based on (3.53) is nearly optimal at high SNR and when the accumulated metric is sufficiently large. Consider Figure 3.4, where we show the surviving sequences at time $N+1$. For the purpose of illustration, we have considered a 4-state trellis. Note that the survivor sequence at each state are those that maximize the correlation metric. Hence, the survivor sequence at each state is actually a ramification of the "correct" sequence. We refer to the "correct" sequence as the one that has the minimum number of errors with respect to the transmitted sequence. Observe that only one of the survivor sequences is the correct sequence, but at time $N+1$, the detector can make reliable decisions only on symbols that had occurred at time $N-1$, since all the survivor sequences have diverged from the correct sequence at this point of time. Thus, in this example, the detection delay of the VA is two symbols. In practice, the detection delay is usually five times the memory of the convolutional encoder [Pro95]. It is also important to note that an incorrect ramification cannot survive indefinitely. This is also illustrated in Figure 3.4. In fact, a long incorrect ramification will eventually be eliminated by a correct/incorrect shorter ramification from the correct path due to two reasons:

(i) The trellis is periodic. This ensures that at every symbol interval the correlation metric corresponding to the longer incorrect ramification must compete with that of a shorter correct/incorrect ramification.

(ii) Since a shorter ramification has more correct symbols than a longer incor-

rect ramification, it has a larger correlation metric than a longer incorrect ramification.

Thus, the error events cannot be infinitely long, and the condition $N \gg D$ required in Property 2 is valid. Now, it is easy to see that the accumulated metric upto time $N-1$ is large when N is large, since it corresponds to the correct sequence. Further, it has been shown in Appendix E, that when the accumulated metric of the correct sequence is large, the error events are short and the SNR is high, the correlation metric is nearly equal to the metric corresponding to a coherent VA. In other words, the SNVA-M behaves just like a coherent VA. However, it is well known that in the case of a coherent VA, an eliminated sequence cannot have a higher metric than a surviving sequence at a later point in time, since the metrics are additive. Thus, even in the case of the SNVA-M, an eliminated sequence cannot have a larger metric than a surviving sequence. Thus at high SNR, the SNVA-M is expected to yield nearly the same Maximum Likelihood survivor sequence, as the coherent VA. At low SNR however, the high SNR approximation in (E.3) in Appendix E, is not valid and the correlation metric cannot be approximated by the coherent metric. Hence at low SNR, the SNVA-M cannot be expected to yield the same surviving sequence as the coherent VA, and is suboptimal. This has been confirmed by computer simulations given in Table E.1 in Appendix E.

At this point, the performance of the ML-UAP detector needs some discussion. We have not carried out any computer simulations with the ML-UAP detector, mainly due to its exponential complexity. Moreover, as mentioned in the earlier section, the ML-UAP cannot distinguish between isometric sequences. Barring this drawback of isometry, we anticipate that the symbol-error-rate performance of the ML-UAP will also be as good as a coherent detector, at high SNR. However, the survivor sequence of the ML-UAP may not be identical to a coherent VA, even at high SNR.

A note on the choice of γ (in (3.52)) as a function of the fade-rate (which determines how rapidly G_k and ϕ_k vary with k) is now in order. Firstly, it must be noted that the value of γ needs to close to unity to ensure that the memory

of the IIR filter is large and hence the accumulated metric is large. By doing this, the noncoherent squared distance better approximates the coherent squared distance. However, if γ is close to unity, G_k and ϕ_k may vary significantly over the memory of the IIR filter, and Property 2 will not be valid. Thus we have two conflicting requirements, and γ needs to be optimized, depending on the fade-rate. At present, it seems that optimization of γ for a given fade-rate can only be done by trial-and-error based on the symbol-error-rate performance. It is however clear from computer simulations that the FSNVA-M performs as well as the coherent detector, only for very slow Rayleigh fading channels (G_k and ϕ_k are constant over many symbols) and slow Rician fading channels with a large specular-to-diffuse power ratio (G_k and ϕ_k vary slowly).

It is important to note that in the case of SNVA-M and FSNVA-M detection, the current symbol cannot be detected independently of the previously detected symbols. In fact, their performance depends on the correctness of the previously detected symbols. Moreover, since the accumulated correlation metric plays a vital role (assuming that most of the prior decisions are correct so that Property 2 holds), metric computations using the recursions given by (3.52) along with (3.53) are required, to estimate the current symbol. *Note that when the symbols are i.i.d and drawn from an M-ary constellation, it is necessary to have a single-state trellis with M parallel transitions.* This is in contrast to the coherent detector, where the current symbol can be detected independently of the previously detected symbols using the nearest neighbour rule, when the symbols are i.i.d.

However, if the symbols are correlated, for example, due to convolutional coding [Pro95], then the number of states depends upon the constraint-length of the convolutional encoder.

3.5.1 SNVA-M with Diversity

In the presence of diversity of order $\mathcal{D}$, the survivor at the i^{th} state is obtained

by

$$\eta_{N+1}^{(i)} = \max_{j} \sum_{l=1}^{\mathcal{D}} \frac{\left|\tilde{A}_{N+1,l}^{(ji)}\right|^2}{\left(B_{N+1}^{(ji)}\right)^2} \tag{3.56}$$

where $B_{N+1}^{(ji)}$ is given in (3.52) and $\tilde{A}_{N+1,l}^{(ji)}$ is the cross-correlation term obtained from the l^{th} diversity arm and is given by

$$\tilde{A}_{N+1,l}^{(ji)} = \gamma \tilde{A}_{N,l}^{(j)} + \tilde{r}_{N,l} \left(I^{(ji)}\right)^* . \tag{3.57}$$

In the above equation, $\tilde{A}_{N,l}^{(j)}$ denotes the surviving cross-correlation term at the j^{th} state at time N, in the l^{th} diversity arm and $\tilde{r}_{N,l}$ denotes the received sample at time N in the l^{th} diversity arm. Observe that the denominator in (3.56) is independent of the diversity arm. Though other diversity techniques like selection diversity are possible, we have not investigated these approaches.

3.6 Summary

In this chapter, we have derived the approximate noncoherent Maximum Likelihood detector in Unknown Amplitude and Phase (ML-UAP). The ML-UAP metric (correlation metric) for Rician, Rayleigh and uniform pdfs are found to be identical. Three important properties of the correlation metric are discussed. The computational complexity of the ML-UAP increases exponentially with the length of the data sequence to be detected. We have proposed a suboptimal detection strategy, referred to as the Suboptimal Noncoherent Viterbi Algorithm for Multilevel signals (SNVA-M) whose computational complexity is comparable to a coherent detector. A Forgetting-factor-based SNVA-M is also proposed to deal with small variations in the gain and the phase of the received signal. Thus, explicit carrier phase estimation and received signal gain estimation procedures are not required. We have also shown that at high SNR, the SNVA-M can be expected to yield nearly the same survivor sequence as the coherent VA.

CHAPTER 4

DIFFERENTIAL DETECTORS

4.1 Introduction

In the previous chapter, we had described noncoherent receivers for slow fading channels, where the channel gain G and phase ϕ are constant over several symbols. Although the FSNVA-M can be useful for frequency-selective fading channels, it may not be well suited for slow, Rayleigh flat-fading channels, where G and ϕ vary from symbol to symbol. We now consider three differential detection techniques which are suitable for slow, Rayleigh flat-fading channels. For the purpose of describing the differential detection schemes, we use as an example, the circular 8-QAM constellation shown in Figure 4.1. The detection strategies can be easily extended to higher-order circular QAM constellations. Though this constellation is optimum for coherent detection, in the sense of minimizing the symbol-error-rate, it may not be optimum for the differential detection strategies discussed here. In particular, there may exist other values of the inner and outer radii in Figure 4.1, which yields a better symbol-error-rate performance. Moreover, it is not necessary that the optimum constellation must have only two radii; the optimum constellation could have more than two radii. We have not attempted to optimize the constellation in this work.

4.2 Symbol-by-Symbol Differential Detector for Multilevel Signals (SSDD-M)

Consider the differentially encoded circular 8-QAM signal, whose encoding rules are provided in Table 4.1. The symbol-by-symbol differential detector for the differentially-encoded circular 8-QAM signal requires twelve correlators, each correlator consisting of a sequence of two symbols denoted by $\left\{I_0^{(j)}, I_1^{(j)}\right\}$ for $0 \leq$

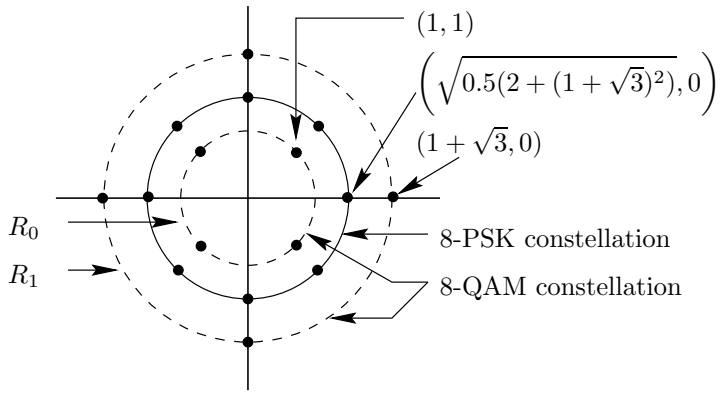

Figure 4.1: 8-QAM and 8-PSK constellations with the same average energy.

Table 4.1: Encoding rules for differential 8-QAM.

Input Symbol	Encoding rule	
	Radius change	Phase change (deg)
0	No	0
1	No	90
2	No	180
3	No	270
4	Yes	45
5	Yes	45+90
6	Yes	45+180
7	Yes	45+270

$j \leq 11$. Note that there are in fact $8^2 = 64$ correlators, but due to isometry, there exist only twelve distinct correlators. These twelve correlators are given in Table 4.2. The symbol-by-symbol decision rule is given by

$$\max_j \eta_{k+1}^{(j)} = \frac{\left|\sum_{n=0}^{1} \tilde{r}_{k+n} \left(I_n^{(j)}\right)^*\right|^2}{\sum_{n=0}^{1} \left|I_n^{(j)}\right|^2} \tag{4.1}$$

for $0 \leq j \leq 11$. Observe that this detection rule can be obtained from the ML-UAP rule by substituting $L = 2$ in (3.40). The estimated input symbol is then given by the mapping in Table 4.2. For example, if $\eta_{k+1}^{(j)}$ is maximum for $j = 10$, then the estimated symbol is 6 according to Table 4.2. Note that (4.1) is a *sliding window* detector over two symbols and *not a block detector*. That is, the same input sample $\tilde{r}_k$ is used in computing the correlation metrics $\eta_k^{(j)}$ and $\eta_{k+1}^{(j)}$.

Observe from Table 4.1 that for symbols 0 to 3 corresponding to a phase change,

Table 4.2: SSDD-M detection rules.

	Correlator		Detected
j	$I_0^{(j)}$	$I_1^{(j)}$	Symbol
0	R_0	R_0	0
1	R_0	$R_0 e^{j\pi/2}$	1
2	R_0	$R_0 e^{j\pi}$	2
3	R_0	$R_0 e^{j3\pi/2}$	3
4	R_0	$R_1 e^{j\pi/4}$	4
5	R_0	$R_1 e^{j3\pi/4}$	5
6	R_0	$R_1 e^{j5\pi/4}$	6
7	R_0	$R_1 e^{j7\pi/4}$	7
8	R_1	$R_0 e^{j\pi/4}$	4
9	R_1	$R_0 e^{j3\pi/4}$	5
10	R_1	$R_0 e^{j5\pi/4}$	6
11	R_1	$R_0 e^{j7\pi/4}$	7

but no radius change, only one correlator is required to represent each of the symbols. These four correlators, reckoned with radius R_0, (R_1 could also have been used) are provided as the first four entries in Table 4.2. To see why, let us assume that the transmitted input symbol is 1. The second row in Table 4.2 represents a 90^o phase change in the inner radius (R_0). But the same input symbol could also cause a phase change of 90^o in the outer radius (R_1). Apparently, we need another correlator of the form $\left\{R_1, R_1 e^{j\pi/2}\right\}$, to represent a 90^o phase change in the outer radius. However, we get one correlator from the other by multiplying with a constant. But from Property 1 in Section 3.4, we know that when two sequences are related by a complex constant, they yield the same correlation metric. Thus, we require only a single correlator to represent symbols 0 to 3. This is, however, not the case for symbols 4 to 7, since the correlators corresponding to a transition from the inner radius to the outer radius are not related by a complex constant to the correlators corresponding to a transition from the outer radius to the inner.

When all the symbols in the constellation have equal energy (e.g., 8-ary PSK), (4.1) reduces to the familiar detection rule for differentially-encoded 8-ary PSK

as expected. Moreover, the number of correlators required is only eight. In fact, the j^{th} correlator for the differentially encoded 8-PSK is given by the sequence $\left\{1, \mathrm{e}^{\mathrm{j}2\pi j/8}\right\}$ for $0 \leq j \leq 7$. The 8-PSK constellation with the same average energy as the 8-QAM constellation is also shown in Figure 4.1.

For this particular example, it turns out that SSDD-M is not optimum. In fact, the minimum noncoherent squared distance between the correlators in Table 4.2 is equal to 0.8453. For example, let us assume that two consecutive transmitted (differentially encoded) symbols are $\left\{R_0\,\mathrm{e}^{\mathrm{j}\pi/4}, R_0\,\mathrm{e}^{\mathrm{j}\pi/4}\right\}$, corresponding to an input symbol 0 (see Table 4.1). Then the correlator corresponding to $j = 0$ in Table 4.2 gives the maximum metric equal to 4, in the absence of noise and fading (for $G = 1$). However, the correlator corresponding to $j = 7$ in Table 4.2 gives a metric of 3.1547, which is closest to 4. Therefore, the worst-case noise margin for SSDD-M is only $4 - 3.1547 = 0.8453$. In the next section we show that the minimum distance can be doubled by using a trellis. We refer to this as the Multiple Symbol Differential Detector using the VA for Multilevel signals (MSDDVA-M).

4.3 Multiple Symbol Differential Detector using Viterbi Algorithm for Multilevel Signals (MSDDVA-M)

Consider the trellis diagram in Figure 4.2. Note that the trellis is representative of all possible transitions of the differential encoder. All transitions are not shown for the sake of clarity, and for ease of representation, we number the states from 0 to 7. The input symbols that cause the transitions are also shown. The VA propagates the metrics given by (4.1) over various paths in the trellis. We now show that some of the states in the trellis in Figure 4.2 are redundant. That is, some of the states have identical metrics and can be merged into a single state. In particular, we show that the first four states can be merged into a single state and similarly the last four states can be merged into another state.

Let us start from time zero and assume that symbol 4 was transmitted. Let us also assume that the differential encoder makes a transition from the inner radius

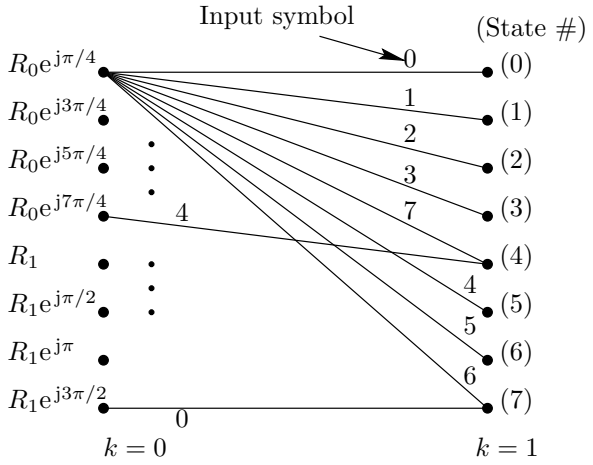

Figure 4.2: Trellis diagram for differential 8-QAM.

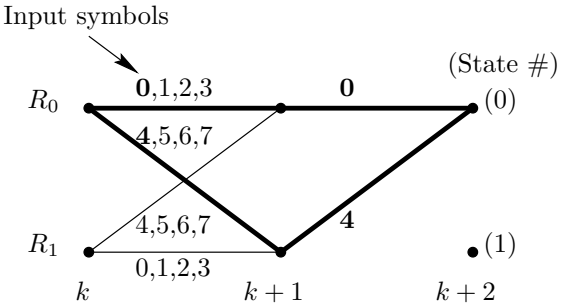

Figure 4.3: Reduced trellis for MSDDVA-M detection. Each transition actually consists of four parallel transitions.

to the outer radius. According to the encoding rules in Table 4.1, the corresponding phase change is 45^o. Hence in the absence of any errors, the *surviving* metric at state # 4 at time $k = 1$ is due to the transition from state 3 at time zero. The value of the surviving (maximum) metric is equal to

$$\eta_1^{\text{max, state 4}} = \frac{\left|\tilde{r}_0 R_0 e^{-j7\pi/4} + \tilde{r}_1 R_1\right|^2}{R_0^2 + R_1^2} \tag{4.2}$$

where the negative sign in the exponent is due to complex conjugation. Similarly, the surviving metric at state # 5 at time $k = 1$ is due to the transition from state # 0 at time zero. Note that since the two transitions are isometric, the surviving metric at state # 4 and 5 are identical, i.e.,

$$\begin{aligned} \eta_1^{\text{max, state 5}} &= \frac{\left|\tilde{r}_0 R_0 e^{-j\pi/4} + \tilde{r}_1 R_1 e^{-j\pi/2}\right|^2}{R_0^2 + R_1^2} \\ &= \eta_1^{\text{max, state 4}}. \end{aligned} \tag{4.3}$$

Proceeding as above, it is easy to see that state # 4, 5, 6 and 7 have identical

metrics at time $k = 1$. Similarly, it can be shown that the surviving metrics in the first four states at time $k = 1$ are identical, though they are different from the surviving metrics in the last four states. Even in the presence of errors, it can be easily verified that the surviving metrics in the first four and last four states are identical; the only difference is that the surviving metrics are different from the error-free case.

Note that when the transmitted symbol does not result in a radius change, e.g., for symbols zero to three, the surviving metrics at all states are identical, since the transitions that yield the surviving metric are all isometric. It is interesting to note that since M-ary PSK has only a single radius, all the M states can be merged into a single state, which reduces to the conventional two-symbol differential detector.

By proceeding recursively in time, it is possible to show that for the 8-QAM constellation considered, the first four states have identical surviving metrics and can be merged into a single state. Similarly, the last four states can be merged into a single state. Thus, the resulting trellis has only two states as shown in Figure 4.3, where each transition actually consists of four parallel transitions. The input symbols that cause the transitions are also shown. The recursion for MSDDVA-M can be written as

$$\eta_{k+1}^{(i)} = \max_{j} \left(\eta_{k}^{(j)} + \eta_{k+1}^{(ji)} \right) \tag{4.4}$$

where $\eta_{k+1}^{(i)}$ denotes the surviving correlation metric at the i^{th} state at time $k+1$ and $\eta_{k+1}^{(ji)}$ denotes the branch metric from state j to state i at time $k+1$. The maximization in the above equation is done over all transitions that converge to state i. The branch metric is computed as

$$\eta_{k+1}^{(ji)} = \frac{\left| \sum_{n=0}^{1} \tilde{r}_{k+n} \left(I_n^{(ji)} \right)^* \right|^2}{\sum_{n=0}^{1} \left| I_n^{(ji)} \right|^2} \tag{4.5}$$

where $I_n^{(ji)}$ denotes a symbol in the appropriate correlator in Table 4.2, corresponding to a transition from state j to state i. For example, the four parallel transitions from state # 0 to state # 0 and also those from state # 1 to state # 1 in Figure 4.3, correspond to the correlators $j = 0, 1, 2, 3$ in Table 4.2.

By searching through the trellis, it can be established that the minimum distance between paths is equal to 1.6906 which is twice of 0.8453. Therefore we expect the MSDDVA-M to have 3 dB better performance than SSDD-M in AWGN channels. The minimum-distance path and the corresponding input symbols that cause the transitions are shown in boldface in Figure 4.3.

4.4 Quotient Space Viterbi Algorithm (QSVA)

The rationale behind the quotient-space approach is simple. If the fade process can be considered to be a constant over two symbol durations, then computing the quotient of two consecutive received samples results in the elimination of the unknown fade process (in the absence of additive noise). We explain this approach

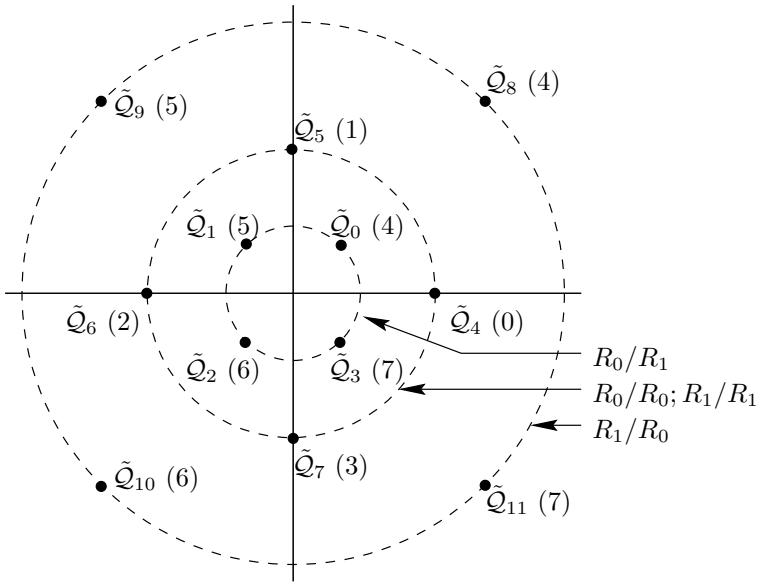

Figure 4.4: Quotient space for 8-QAM.

for the circular 8-QAM constellation shown in Figure 4.1. The differential encoding rules are as shown in Table 4.1. The receiver computes

$$\tilde{q}_{k+1} = \tilde{r}_{k+1}/\tilde{r}_k \tag{4.6}$$

and decides in favour of that point, $\tilde{\mathcal{Q}}_i$, in the quotient-space which is nearest to $\tilde{q}_{k+1}$. The points $\tilde{\mathcal{Q}}_i$ in Figure 4.4 constitute all possible distinct quotients of the 8-QAM symbols in Figure 4.1. The number in brackets denotes the detected symbol.

In [WHS91], an approach that uses oversampling in time combined with a quotient operation between the adjacent samples on either side of the symbol boundary is proposed. However this is only a symbol-by-symbol detector which is suboptimal. We now propose a VA-based quotient-space (QSVA) approach, which exploits the inherent memory in the quotient variables $\tilde{\mathcal{Q}}_i$.

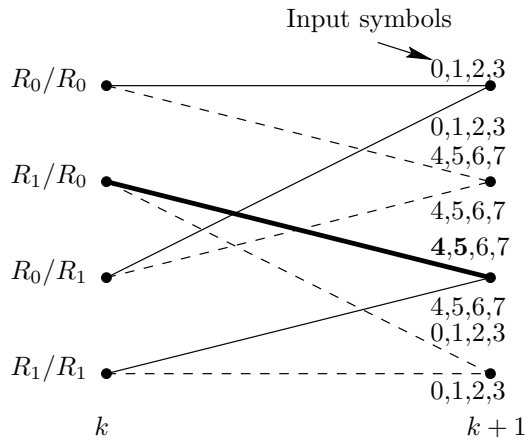

Figure 4.5: Trellis diagram for QSVA detection. Each transition actually consists of four parallel transitions.

Figure 4.5 shows the trellis diagram, where the transitions due to the input symbol having a magnitude of R_0 are indicated by solid lines and those due to the input symbol having a magnitude of R_1 are indicated by dashed lines. Note that there are actually four parallel transitions between any two states, since there are four symbols in each radius in Figure 4.1. The parallel transitions are not shown in the figure for the sake of clarity. The recursion for the QSVA is given by

$$\varepsilon_{k+1}^{(i)} = \min_j \left(\varepsilon_k^{(j)} + \varepsilon_{k+1}^{(ji)} \right) \tag{4.7}$$

where $\varepsilon_{k+1}^{(i)}$ denotes the surviving squared error in the i^{th} state at time $k+1$ and $\varepsilon_{k+1}^{(ji)}$ denotes the branch metric from state j to state i at time $k+1$. The minimization is done over all transitions that converge to state i. The branch metric is computed as

$$\varepsilon_{k+1}^{(ji)} = \left| \tilde{\mathcal{Q}}^{(ji)} - \tilde{q}_{k+1} \right|^2 \tag{4.8}$$

where $\tilde{q}_{k+1}$ is given by (4.6) and $\mathcal{Q}^{(ji)}$ denotes the point in the quotient space corresponding to the transition from state j to state i. For example, the four

parallel transitions from state R_0/R_0 to R_0/R_0 and state R_1/R_1 to R_1/R_1 in Figure 4.5, correspond to the four points $\tilde{\mathcal{Q}}_4$, $\tilde{\mathcal{Q}}_5$, $\tilde{\mathcal{Q}}_6$ and $\tilde{\mathcal{Q}}_7$ in the quotient space in Figure 4.4.

By searching through the trellis, the minimum distance between paths is found to be equal to 0.5359 (this is basically the minimum squared Euclidean distance between points $\mathcal{Q}_0$, $\mathcal{Q}_1$, $\mathcal{Q}_2$ and $\mathcal{Q}_3$ in Figure 4.4). The minimum-distance parallel transition and the corresponding input symbols are shown in boldface in Figure 4.5. Recall that the minimum distance between paths for the MSDDVA-M is equal to 1.6906. However, the performance of the QSVA is not governed purely by the minimum distance since the corresponding transition *cannot* occur every symbol interval. It can occur only every alternate symbol interval. Hence, we can expect the error-rate performance of the QSVA to be better than that predicted by minimum distance considerations. Simulation results show that this is indeed the case.

4.5 Differential Detectors with Diversity

We now discuss diversity techniques for the proposed differential detectors. These diversity techniques greatly enhance the symbol-error-rate performance of the differential detectors in Rayleigh flat-fading channels. The signal received through a flat-fading channel for the l^{th} diversity arm is given by [Kam91b]

$$\tilde{r}_{k,l} = \tilde{G}_{k,l} I_k + \tilde{w}_{k,l} \qquad \text{for } 1 \leq l \leq \mathcal{D} \tag{4.9}$$

where $\tilde{G}_{k,l}$ denotes samples of a complex fade process, $\tilde{w}_{k,l}$ denotes samples of a zero-mean, white Gaussian noise process in the l^{th} diversity arm, and $\mathcal{D}$ denotes the number of diversity arms. We assume that the fade process in the diversity arms are self-correlated and mutually uncorrelated:

$$\frac{1}{2} E\left[\left(\tilde{G}_{k,l} - \tilde{m}_l\right)\left(\tilde{G}_{j,i} - \tilde{m}_i\right)^*\right] = \begin{cases} \mu_{k-j} & \text{for } l = i,\ 1 \leq l, i \leq \mathcal{D} \\ 0 & \text{for } l \neq i \end{cases} \tag{4.10}$$

where

$$\tilde{m}_l = E\left[\tilde{G}_{k,l}\right] \qquad \text{for } 1 \leq l \leq \mathcal{D}. \tag{4.11}$$

In the above equation, we have assumed that the fade process in all the diversity arms are Wide Sense Stationary (WSS), and hence the mean value of the fade process in independent of the time index k. We have also assumed that the autocovariance of the fade process in each diversity arm are identical, hence μ_{k-j} is independent of l. Finally, we also assume that the noise process is self and mutually uncorrelated, that is:

$$\frac{1}{2}E\left[\tilde{w}_{k,\,l}\tilde{w}^{*}_{j,\,i}\right] = \begin{cases} \sigma_w^2 & \text{for } l = i,\ k = j \\ 0 & \text{for } l \neq i,\ k \neq j. \end{cases} \tag{4.12}$$

4.5.1 SSDD-M with Diversity

Diversity combining for SSDD-M can be done in three different ways. The first method is to add the correlation metrics obtained from each diversity arm as follows:

$$\max_{j} \eta_{k+1}^{(j)} = \sum_{l=1}^{\mathcal{D}} \frac{\left|\sum_{n=0}^{1} \tilde{r}_{k+n,\,l}\left(I_n^{(j)}\right)^{*}\right|^2}{\sum_{n=0}^{1}\left|I_n^{(j)}\right|^2} \qquad \text{for } 0 \leq j \leq 11 \tag{4.13}$$

where $\mathcal{D}$ denotes the number of diversity arms and $\tilde{r}_{k,\,l}$ denotes the received signal at time k for the l^{th} diversity arm. We refer to the above method as Equal Gain Correlation Metric Combining (EGCMC), since the correlation metric from each diversity arm is weighted equally.

In the next approach, the SSDD-M first selects the diversity branch having the maximum energy as follows:

$$|\tilde{r}_{k+1,\,\max}|^2 = \max_{l} |\tilde{r}_{k+1,\,l}|^2 \qquad \text{for } 1 \leq l \leq \mathcal{D} \tag{4.14}$$

and computes the correlation metric

$$\max_{j} \eta_{k+1}^{(j)} = \frac{\left|\sum_{n=0}^{1} \tilde{r}_{k+n,\,\max}\left(I_n^{(j)}\right)^{*}\right|^2}{\sum_{n=0}^{1}\left|I_n^{(j)}\right|^2} \qquad \text{for } 0 \leq j \leq 11. \tag{4.15}$$

We refer to the above method as Pre-detection Selection Diversity (Pre-SD), since the diversity arm is selected before detection.

It is also possible to do Post-detection Selection Diversity (Post-SD), where selection is done after detection:

$$\max_{j,\,l} \eta_{k+1,\,l}^{(j)} = \frac{\left|\sum_{n=0}^{1} \tilde{r}_{k+n,\,l}\left(I_n^{(j)}\right)^{*}\right|^2}{\sum_{n=0}^{1}\left|I_n^{(j)}\right|^2} \qquad \text{for } 0 \leq j \leq 11,\ 1 \leq l \leq \mathcal{D}. \tag{4.16}$$

The Post-SD decides in favour of the j^{th} correlator that maximizes the above correlation metric.

From computer simulations we have found that EGCMC gives the best symbol-error-rate performance compared to Pre-SD and Post-SD, though the difference in performance is not very significant at medium and low SNR (< 30 dB). At high SNR, the symbol-error-rate performance of EGCMC is better than both Pre-SD and Post-SD by a factor of 2. This is because, the correlation metric is non-negative and since we are maximizing the correlation metric, adding the correlation metrics from the lower energy diversity arms does not reduce the correlation metric from the diversity arm having the largest received signal energy. Secondly, the correlation metric is directly proportional to the received signal energy, which is clear from (4.13). Hence, the correlation metrics from the diversity arms having lower signal strength are inherently given a lower weightage, and do not have a significant influence on the decision making process.

Diversity combining based on the Received Signal Strength (RSS) has been suggested in [Sve95], which can be extended to the detection schemes proposed here. In the RSS approach, the correlation metric from each diversity arm is weighted by the instantaneous received signal strength in each diversity arm as follows:

$$\max_{j} \eta_{k+1}^{(j)} = \sum_{l=1}^{\mathcal{D}} \left|\tilde{r}_{k+1,\,l}\right|^{\beta} \frac{\left|\sum_{n=0}^{1} \tilde{r}_{k+n,\,l} \left(I_n^{(j)}\right)^*\right|^2}{\sum_{n=0}^{1} \left|I_n^{(j)}\right|^2} \tag{4.17}$$

where β is a parameter that needs to be optimized. We have not investigated the RSS combining approach.

Observe that a simple addition of the received signal in the diversity arms does not lead to any diversity improvement for Rayleigh flat-fading channels, since the average SNR remains unchanged. The modified received signal can be written as

$$\tilde{r}'_k = I_k \sum_{l=1}^{\mathcal{D}} \tilde{G}_k + \sum_{l=1}^{\mathcal{D}} \tilde{w}_{k,\,l}. \tag{4.18}$$

For Rayleigh flat-fading channels, the mean value of the fade process is zero. Hence the SNR in each diversity arm is given by

$$\mathrm{SNR}_{\text{Each arm}} = \frac{2\mu_0 E\left[|I_k|^2\right]}{2\sigma_w^2}. \tag{4.19}$$

The average SNR of the signal in (4.18) is given by

$$\mathrm{SNR}_{\mathrm{av}} = \frac{2\mathcal{D}\mu_0 E\left[|I_k|^2\right]}{2\mathcal{D}\sigma_w^2} \tag{4.20}$$

which is exactly identical to the SNR in each diversity arm. Hence, a simple addition of the received signal is equivalent to a diversity of one for Rayleigh flat-fading channels. This is also confirmed from computer simulations. This is however not true for Rician flat-fading channels. To show this, we assume that the mean value of the fade process in each diversity arm is the same and is denoted by $\tilde{m}$. The average SNR for a single diversity channel is given by

$$\mathrm{SNR}_{\text{Each arm}} = \frac{\left(2\mu_0 + |\tilde{m}|^2\right) E\left[|I_k|^2\right]}{2\sigma_w^2}. \tag{4.21}$$

The average SNR of the signal in (4.18) is given by

$$\mathrm{SNR}_{\mathrm{av}} = \frac{\left(2\mathcal{D}\mu_0 + \mathcal{D}^2 |\tilde{m}|^2\right) E\left[|I_k|^2\right]}{2\mathcal{D}\sigma_w^2} \tag{4.22}$$

which is greater than the the average SNR per diversity channel in (4.21). Hence, even simple addition of the received signal in each diversity arm is expected to give a better performance for Rician fading channels compared to a diversity of one.

4.5.2 MSDDVA-M with Diversity

Diversity reception in the case of MSDDVA-M is similar to SSDD-M excepting that the correlation metrics are propagated over the trellis. The recursion for EGCMC is given by (4.4) and the branch is computed as

$$\eta_{k+1}^{(ji)} = \sum_{l=1}^{\mathcal{D}} \frac{\left|\sum_{n=0}^{1} \tilde{r}_{k+n,l} \left(I_n^{(ji)}\right)^*\right|^2}{\sum_{n=0}^{1} \left|I_n^{(ji)}\right|^2} \tag{4.23}$$

where $I_n^{(ji)}$ denotes a symbol in the appropriate correlator in Table 4.2, corresponding to a transition from state j to state i. Observe that the correlation metric from each diversity arm is weighted equally, hence we refer to this strategy as EGCMC.

In the case of Pre-SD, the diversity arm with the maximum instantaneous energy is first selected as in (4.14). Next, the branch metric is computed as

$$\eta_{k+1}^{(ji)} = \frac{\left|\sum_{n=0}^{1} \tilde{r}_{k+n,\,\max} \left(I_n^{(ji)}\right)^*\right|^2}{\sum_{n=0}^{1} \left|I_n^{(ji)}\right|^2}. \tag{4.24}$$

The above branch metric is then substituted in the recursion in (4.4).

In the case of Post-SD, all the diversity arms are used in the computation of the branch metric corresponding to a transition from state j to state i. The branch metric is given as

$$\eta_{k+1,\,l}^{(ji)} = \frac{\left|\sum_{n=0}^{1} \tilde{r}_{k+n,\,l} \left(I_n^{(ji)}\right)^*\right|^2}{\sum_{n=0}^{1} \left|I_n^{(ji)}\right|^2} \qquad \text{for } 1 \le l \le \mathcal{D}. \tag{4.25}$$

The modified recursion for the VA is given by

$$\eta_{k+1}^{(i)} = \max_{j,\,l} \left(\eta_k^{(j)} + \eta_{k+1,\,l}^{(ji)}\right). \tag{4.26}$$

From computer simulations, we have found that EGCMC gives a better symbol-error-rate performance compared to Pre-SD and Post-SD, though the difference in performance is not very significant at medium and low SNR (< 30 dB). At high SNR, the symbol-error-rate performance of EGCMC is better than both Pre-SD and Post-SD by a factor of 2. The explanation for this is same as that for SSDD-M with diversity.

4.5.3 QSVA with Diversity

Diversity combining for QSVA can be done in three ways. In the first approach the QSVA detector selects

$$|\tilde{r}_{k+1,\,\max}|^2 = \max_{l} |\tilde{r}_{k+1,\,l}|^2 \qquad \text{for } 1 \le l \le \mathcal{D} \tag{4.27}$$

and then computes the quotient

$$\tilde{q}_{k+1} = \tilde{r}_{k+1,\,\max} / \tilde{r}_{k,\,\max} \tag{4.28}$$

which is then used in (4.8). Note that in this case, Pre-detection Selection Diversity (Pre-SD) is used.

It is also possible to perform Post-SD. The quotient corresponding to all the diversity arms is first computed as

$$\tilde{q}_{k+1,\,l} = \tilde{r}_{k+1,\,l}/\tilde{r}_{k,\,l} \qquad \text{for } 1 \leq l \leq \mathcal{D} \tag{4.29}$$

which is then used in branch metric computation as follows:

$$\varepsilon_{k+1,\,l}^{(ji)} = \left|\tilde{\mathcal{Q}}^{(ji)} - \tilde{q}_{k+1,\,l}\right|^2 \qquad \text{for } 1 \leq l \leq \mathcal{D}. \tag{4.30}$$

The recursion for the VA is now given as:

$$\varepsilon_{k+1}^{(i)} = \min_{j,\,l} \left(\varepsilon_{k}^{(j)} + \varepsilon_{k+1,\,l}^{(ji)}\right). \tag{4.31}$$

In the third approach, we considered Equal Gain Quotient Error Combining (EGQEC). Here again the quotient corresponding to all the diversity arms is first computed as in (4.29). Next, the branch metric is computed by summing the squared errors of all the diversity arms as follows

$$\varepsilon_{k+1}^{(ji)} = \sum_{l=1}^{\mathcal{D}} \left|\tilde{\mathcal{Q}}^{(ji)} - \tilde{q}_{k+1,\,l}\right|^2 \tag{4.32}$$

which is then substituted in (4.7). Observe that the squared error from each diversity arm is weighted equally. Hence we refer to this method as EGQEC.

From computer simulations it is found that Pre-SD gives a much better symbol-error-rate performance compared to Post-SD and EGQEC. This is because both Post-SD and EGQEC compute the quotients $\tilde{q}_{k+1,\,l}$ from all the diversity arms. For diversity arms having low signal strength, it is quite possible the the quotient $\tilde{q}_{k+1,\,l}$ is close an incorrect point in the quotient space $\tilde{\mathcal{Q}}^{(ji)}$ instead of the correct point. Moreover, the corresponding error $\epsilon_{k+1}^{(ji)}$ from a diversity arm with a lower signal strength could be less than the error from even the largest energy diversity arm. Hence, the error in the quotient space from lower energy diversity arms has an adverse effect on the performance of the QSVA approach. This is in contrast to SSDD-M and MSDDVA-M with diversity, where the diversity arms having a lower signal strength do not have an adverse effect on the diversity arm having the maximum signal strength. As explained earlier, this is because firstly, the correlation metric is non-negative. Hence the addition of correlation metrics in

EGCMC, from lower energy diversity arms does not adversely affect the correlation metric from the diversity arm having the maximum signal strength. Secondly, the correlation metrics are inherently weighted by the received signal strength in that diversity arm, and hence the correlation metric from lower energy diversity arms have a lesser influence on the decisions.

4.6 Summary

In this chapter, we have proposed three differential detection strategies that are suitable for slow, Rayleigh flat-fading channels, where the fade process $\tilde{G}_k$ varies from symbol to next. The proposed detection strategies, namely the Symbol-by-Symbol Differential Detector for Multilevel signals (SSDD-M), the Multiple Symbol Differential Detector using the Viterbi Algorithm for Multilevel Signals (MSDDVA-M) and the Quotient Space Viterbi Algorithm (QSVA), are computationally inexpensive and can be readily implemented on DSP platforms. While the SSDD-M and MSDDVA-M are extensions of the ML-UAP detector discussed in the previous chapter, the QSVA is a different approach that takes advantage of the inherent memory in the quotient operation. Extensions to diversity reception have also been described.

CHAPTER 5

COMPUTER SIMULATION RESULTS

5.1 Introduction

In this chapter we present computer simulation results for flat fading channels. Firstly, we present the simulation results for slow, Rayleigh flat-fading channels, where the fade process varies from symbol-to-symbol. Next, we present results for very slow Rayleigh flat-fading channels, where the fade process is nearly constant over a frame containing a large number of symbols. Next we present the results for slow Rician flat-fading channels. Finally, for the sake of completeness, we present some results for AWGN channels.

5.2 Results for Slow Rayleigh Flat-Fading Channels

The communication model used for a slow Rayleigh flat-fading channel is given by (1.8), which is repeated here for convenience

$$\tilde{r}_k = \tilde{G}_k I_k + \tilde{w}_k \tag{5.1}$$

where I_k is an uncoded or a differentially encoded symbol sequence drawn from an M-ary constellation. The in-phase and quadrature components of the complex fade process, $\tilde{G}_k$, are obtained by passing zero-mean, white Gaussian noise through an IIR filter. As mentioned in Section 1.3, we have considered a first-order and a third-order IIR filter, which is again repeated here for convenience.

For a first-order IIR filter, the in-phase and quadrature components of $\tilde{G}_k$ are given by

$$G_{k,\,I\{Q\}} = \rho\, G_{k-1,\,I\{Q\}} + \sqrt{1-\rho^2}\, g_{k,\,I\{Q\}} \tag{5.2}$$

where $0 < \rho < 1$ and $g_{k,\,I}$ and $g_{k,\,Q}$ are real, self and mutually uncorrelated, zero-mean white Gaussian noise processes, each with a variance equal to σ_g^2. The

value of ρ determines the Doppler spread or the Doppler bandwidth of the fade process. Values of ρ close to unity imply a smaller Doppler bandwidth and smaller values imply a larger Doppler bandwidth. Note that $G_{k,\,I}$ and $G_{k,\,Q}$ are each real, zero-mean Gaussian, with variance, $\mu_0 = \sigma_g^2$, since the IIR filter in (5.2) has unit energy.

For a third-order IIR filter, we have assumed that the in-phase and quadrature components of $\tilde{G}_k$ are given by

$$G_{k,\,I\{Q\}} = 3\rho\, G_{k-1,\,I\{Q\}} - 3\rho^2 G_{k-2,\,I\{Q\}} + \rho^3 G_{k-3,\,I\{Q\}} + C_0 g_{k,\,I\{Q\}} \tag{5.3}$$

where again $0 < \rho < 1$, C_0 is a constant chosen such that the filter has a dc gain of unity, and $g_{k,\,I}$ and $g_{k,\,Q}$ are defined in (5.2). The Doppler bandwidth is once again determined by the value of ρ. In this case $\mu_0 = E_{\rm IIR}\sigma_g^2$, where $E_{\rm IIR}$ is the energy of the IIR filter.

We have not considered the regular land-mobile fade model, which is characterized by an autocovariance of the form $J_0(2\pi B_d T)$ [DS94], where $J_0(\cdot)$ denotes the zeroth-order Bessel function of the first kind, B_d is the Doppler bandwidth (see (1.18)) and T is the symbol duration. This is because, it is computationally difficult to obtain the Bessel autocovariance function. Moreover, the performance of the differential detectors discussed in this thesis does not depend on the type of autocovariance function used. In fact, since the differential detectors process only two consecutive symbols at-a-time, their performance depends only on the ratio μ_1/μ_0 [Kam91a], where μ_p denotes the p^{th}-lag autocovariance of $\tilde{G}_k$, as defined in (2.12). Note that the MSDDVA-M also processes only two symbols at-a-time; it is only the correlation metrics (obtained *after* processing) that are propagated. However in the case of the FSNVA-M detector, since the detection is done over many symbols, we expect its performance to be affected by the type of autocovariance function. In particular, if the autocovariance function decays faster (signifying a large variation in $\tilde{G}_k$), the performance of the FSNVA-M becomes poorer.

It also needs to be mentioned at this point that the 3^{rd}-order fade process given by (5.3) was considered merely to indicate the effectiveness of the SLP detectors for higher-order fade processes. In particular, the land-mobile fade model, whose

autocovariance is given by $J_0(\cdot)$, can also be well approximated by a 3^{rd}-order AR process [MMB94]. Consequently, it was found in [MMB94] that a third-order prediction filter is sufficient to get most of the possible performance improvements. Thus, we can expect the SLP detectors to show a similar performance in a land-mobile fading environment.

The power spectral densities (psd) of the fade processes used in computer simulations is repeated in Figure 5.1 for convenience. The x-axis shows the frequency normalized with respect to the symbol-rate. We have considered the model given by (5.2) with $\rho = 0.995$ and $\rho = 0.9995$, and the model given by (5.3) with $\rho = 0.8$ and $C_0 = 0.008$. The model given by (5.2) with $\rho = 0.995$ and $\rho = 0.9995$ is also considered in [Kam91b] and [Kam91a]. Note that the third-order fade process

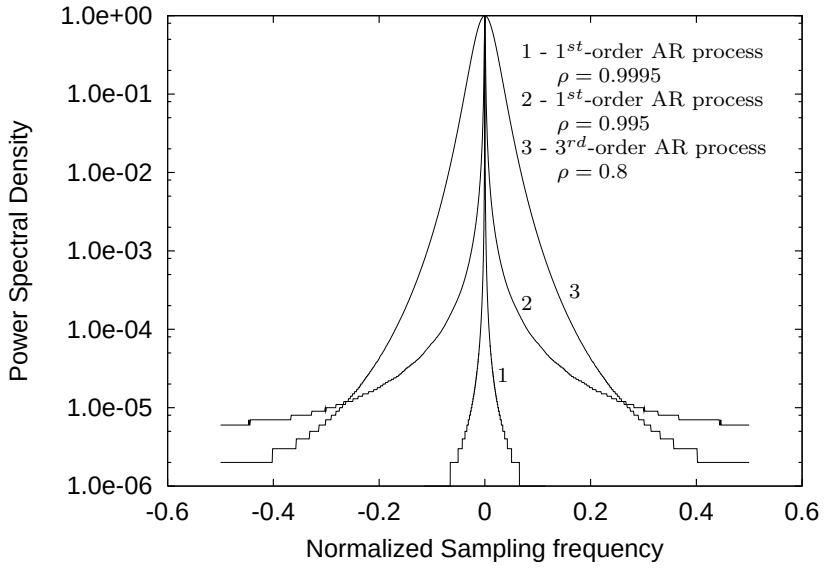

Figure 5.1: Power spectral density of $\left\{\tilde{G}_k\right\}$.

with $\rho = 0.8$ has the maximum Doppler spread, and we can expect the differential detectors to have the worst symbol-error-rate performance in this case.

The average SNR per bit over a Rayleigh fading channel is given by [Kam91b, Kam91a]

$$\mathrm{SNR}_{\mathrm{Rg}} = \frac{E\left[|\tilde{G}_k I_k|^2\right]}{2\sigma_w^2 \log_2(M)} = \frac{2E_{\mathrm{av}}\mu_0}{2\sigma_w^2 \log_2(M)} \tag{5.4}$$

where we have assumed that the fade process is wide sense stationary and statistically independent of the transmitted symbols and $E_{\mathrm{av}} = E[|I_k|^2]$ is the average

energy in the constellation.

5.2.1 Results without Diversity

In Tables 5.1, 5.2 and 5.3, we compare the symbol-error-rate performance of the SLP detectors with that of the coherent detector, for the three fade models that we have considered.

Table 5.1: Simulation results for a Rayleigh fading channel. 1^{st}-order fade process, $\rho = 0.9995$.

Average SNR per bit (dB)	Symbol-error-rate		
	Coherent detector	SLP-I	SLP-II
Infinity	0	1.8×10^{-3}	2.2×10^{-3}
49	1.2×10^{-5}	1.8×10^{-3}	2.2×10^{-3}
39	1.1×10^{-4}	2.1×10^{-3}	2.5×10^{-3}
29	1.1×10^{-3}	5.1×10^{-3}	5.9×10^{-3}
19	1.1×10^{-2}	3.7×10^{-2}	3.8×10^{-2}

Table 5.2: Simulation results for a Rayleigh fading channel. 1^{st}-order fade process, $\rho = 0.995$.

Average SNR per bit (dB)	Symbol-error-rate		
	Coherent detector	SLP-I	SLP-II
Infinity	0	1.8×10^{-2}	2.2×10^{-2}
49	1.2×10^{-5}	1.8×10^{-2}	2.2×10^{-2}
39	1.1×10^{-4}	1.9×10^{-2}	2.2×10^{-2}
29	1.1×10^{-3}	2.1×10^{-2}	2.6×10^{-2}
19	1.1×10^{-2}	5.0×10^{-2}	5.7×10^{-2}

Firstly, we note that the coherent detector (which is the optimum detector) performs better than the SLP detectors even at infinite SNR. Secondly, we find that the performance of the coherent detector is independent of the fade statistics. In fact theoretically, the performance of the coherent detector is dependent only on the pdf of the envelope of $\tilde{G}_k$ [Pro95], which is Rayleigh in all the three cases.

Table 5.3: Simulation results for a Rayleigh fading channel. 3^{rd}-order fade process, $\rho = 0.8$.

Average SNR per bit (dB)	Symbol-error-rate		
	Coherent detector	SLP-I	SLP-II
Infinity	0	9.6×10^{-4}	1.2×10^{-3}
35.2	2.7×10^{-4}	3.9×10^{-3}	4.5×10^{-3}
25.2	2.7×10^{-3}	3.5×10^{-2}	3.6×10^{-2}
15.2	2.7×10^{-2}	2.1×10^{-1}	2.1×10^{-1}
5.2	2.0×10^{-1}	5.3×10^{-1}	5.3×10^{-1}

Thirdly, there is not much performance difference between the SLP-I and SLP-II detector. In fact SLP-II is only slightly worse than the SLP-I detector. However, it must be noted that the results for the SLP-I detector are for the situation when the prediction error variance is perfectly known. In practice, we expect some degradation in the performance of the SLP-I detector due to incorrect estimation of the prediction error variance. Thus, in all the subsequent graphs, we plot only the performance of the SLP-II detector, since it does not require estimation of the prediction error variance, and is thus easier to implement.

In Figures 5.2 and 5.3, we show the simulation results for slow Rayleigh fading channels for a first-order fade process given by (5.2), with $\rho = 0.9995$ and $\rho = 0.995$ respectively. The simulations were done over 10^7 symbols for all the detectors. The detection delay of SLP-II, MSDDVA-M and QSVA was taken as 10 symbols. We have not experimented with different detection delays. We have plotted the theoretical performance of differential 8-PSK from [Kam91a]. In Figure 5.2, and in all subsequent figures, the result for SLP-II is for the situation when the autocovariance of $\tilde{G}_k$ is known perfectly. In practice, the SLP detectors suffer further performance degradation due to imperfect knowledge of the autocovariance of $\tilde{G}_k$. The differential detectors do not require any knowledge of the autocovariance of $\tilde{G}_k$. We can draw the following conclusions from Figures 5.2 and 5.3:

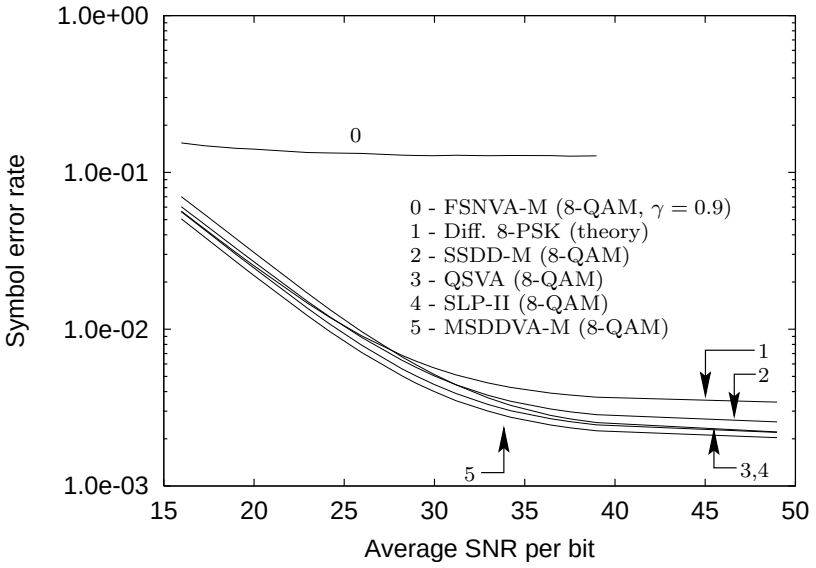

Figure 5.2: Simulation results for a Rayleigh fading channel. 1^{st}-order fade process, $\rho = 0.9995$.

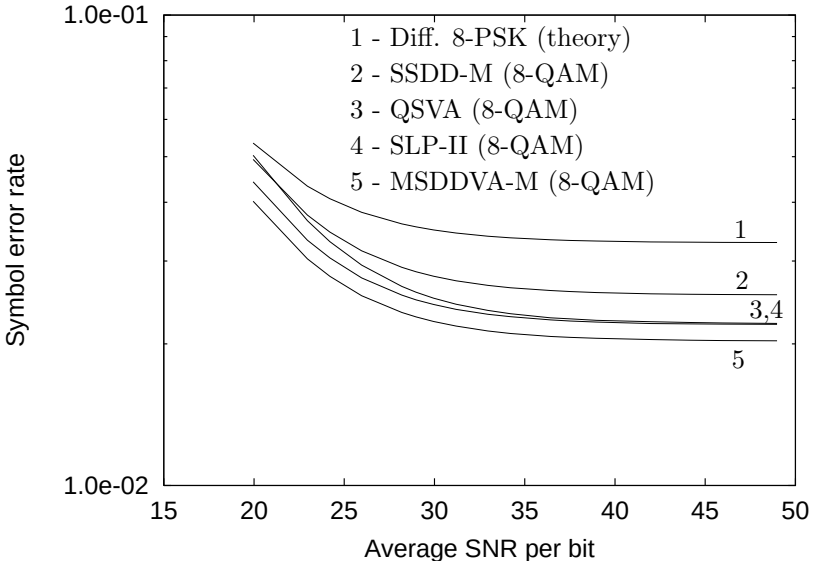

Figure 5.3: Simulation results for a Rayleigh fading channel. 1^{st}-order fade process, $\rho = 0.995$.

Conclusions-I(A):

(a) The FSNVA-M is not suitable for slow Rayleigh fading channels.

(b) MSDDVA-M gives the best performance, amongst all the differential detectors.

(c) For a 1^{st}-order fade process, MSDDVA-M performs better than the SLP-II detector. However, this result is reversed for a third-order fade process, as will be evident from Figure 5.4.

(d) The computational complexity of the proposed detectors is lower than that of the SLP detectors, but higher than the conventional differential detector for 8-PSK. Both the SLP detectors require an 8-state trellis, whereas the SSDD-M does not require a trellis, the MSDDVA-M requires a 2-state trellis and the QSVA requires a 4-state trellis.

In Figure 5.4, we show the simulation results for a third-order fade process given by (5.3) with $\rho = 0.8$ and $C_0 = 0.008$. The simulations were done over 10^6 symbols. It may be argued [MMB94] that a third-order fade process is more realistic than a first-order one to characterize many mobile radio Rayleigh fading channels. The following important observations can be made from Figure 5.4:

Conclusions-I(B):

(a) The SLP-II detector performs better than the differential detectors by an order of magnitude, at high SNR. This is because, the SLP detectors take advantage of the inherent memory in the prediction filters. It is also clear that as the memory of the prediction filter used to whiten the fade process increases, the performance difference between the SLP detectors and the differential detectors also increases.

(b) At medium and low SNR (< 25 dB) the SLP detectors perform worse than the differential detectors. This is because of noise enhancement of the prediction filter. Observe that the prediction filters corresponding to SLP-I and

SLP-II, have a squared magnitude response that is just the inverse of the power spectral densities shown in Figure 5.1. Thus, it is easy to see that the prediction filter considerably enhances high frequency noise, resulting in a low SNR at the prediction filter output even when the average SNR at its input is fairly high.

(c) The complexity of the SLP detectors increases exponentially with the memory of the prediction filter. In fact, both SLP-I and SLP-II detectors require a $8^3 = 512$ state trellis, for 8-ary signalling. However, the complexity of the proposed differential detectors remains unchanged, that is, the SSDD-M does not require any trellis, the MSDDVA-M requires a 2-state trellis, and the QSVA requires a 4-state trellis.

(d) Amongst the differential detectors, we find that the MSDDVA-M gives the best performance.

To obtain a better performance than the SLP detectors, we could use a Minimum Mean Square Error (MMSE) formulation and use the LMS algorithm to adapt the prediction filters [Ada96b]. There are two ways in which the prediction filter taps can be updated. The first approach is to use per-survivor processing [RPT95]. This approach is much more computationally expensive than the SLP approach (which is itself expensive), since a set of prediction filter taps need to be maintained by each surviving path. A cheaper alternative would be to maintain only one prediction filter using the *global survivor*. However this approach suffers from the drawback of having to use reliable data decisions, which can be obtained only after the detection delay of the VA. Hence, the global survivor approach might not work very well for fast fade-rates (large Doppler spread). Note that the per-survivor approach does not have wait for reliable decisions from the VA, since prediction filters are updated using the low-delay decisions at each state.

Perhaps data-aided adaptation for the SLP can be a better alternative than the above approaches. If we can assume that the fade process is Wide Sense Stationary (WSS) and the noise variance is constant, we can train the prediction filter using

a known preamble, and keep the filter coefficients fixed during data detection. This approach may overcome the drawbacks of the previous two approaches, and is worth investigating.

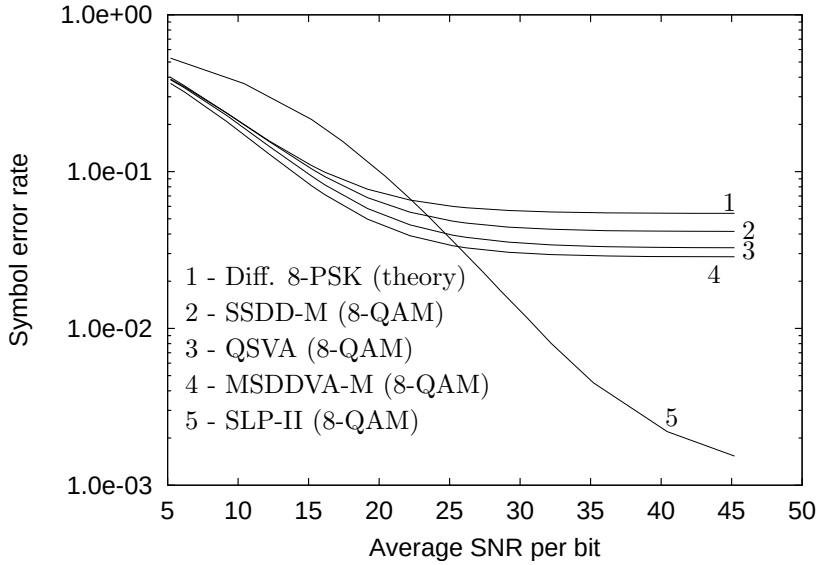

Figure 5.4: Simulation results for a Rayleigh fading channel. 3^{rd}-order fade process, $\rho = 0.8$.

Comparing the performance of the differential detectors presented in Figures 5.2, 5.3 and 5.4 we find that there is no significant performance degradation from $\rho = 0.995$ to $\rho = 0.8$, compared to the degradation from $\rho = 0.9995$ to $\rho = 0.995$. This can be explained from the fact that the performance of the differential detectors depends on the ratio μ_1/μ_0 [Kam91a], where μ_p is the auto-covariance of $\tilde{G}_k$ (see also (2.12)). For the first-order fade process given by (5.2), it can be shown that $\mu_1/\mu_0 = \rho$. Substituting this into the BER expression in [Kam91a] for $\rho = 0.9995$ and $\rho = 0.995$, we find there is a significant difference in BER. However, for the third-order fade process given by (5.3), with $\rho = 0.8$, it can be shown that $\mu_1/\mu_0 = 0.9915$, which is quite close to $\mu_1/\mu_0 = 0.995$ for the first-order fade process. Hence, the performance of the differential detectors for a third-order fade process with $\rho = 0.8$ is only slightly inferior to that of the first-order fade process with $\rho = 0.995$.

It is clear from the simulation results presented in this section that differential detectors with first-order diversity are only of academic interest in Rayleigh flat-

fading channels, since they operate at very high average SNRs (and that too, for SERs in the range $10^{-1} - 10^{-2}$). To improve the performance, we need to have at least second-order diversity, which is commonly used in practice.

5.2.2 Results with Second-Order Diversity

We now present simulation results with second-order diversity for slow Rayleigh flat-fading channels. It may be noted that second-order diversity is used in many mobile communications systems. Firstly, we compare the performance of various diversity techniques used in SSDD-M, MSDDVA-M and QSVA. Unless specified, all simulations were done over 10^7 symbols.

Table 5.4: Performance of various diversity techniques for SSDD-M. 1^{st}-order fade process, $\rho = 0.9995$, $\mathcal{D} = 2$.

Average SNR per bit for each diversity channel (dB)	Symbol-error-rate		
	EGCMC	Pre-SD	Post-SD
Infinity	6.1×10^{-6}	1.4×10^{-5}	1.2×10^{-5}
9.44	6.2×10^{-2}	9.4×10^{-2}	8.8×10^{-2}

Table 5.5: Performance of various diversity techniques for MSDDVA-M. 1^{st}-order fade process, $\rho = 0.9995$, $\mathcal{D} = 2$.

Average SNR per bit for each diversity channel (dB)	Symbol-error-rate		
	EGCMC	Pre-SD	Post-SD
Infinity	3.5×10^{-6}	5.7×10^{-6}	6.1×10^{-6}
9.44	4.5×10^{-2}	6.8×10^{-2}	6.6×10^{-2}

It may be recalled from Section 4.5.3, that Equal Gain Correlation Metric Combining (EGCMC) is best suited for SSDD-M and MSDDVA-M, whereas Pre-detection Selection Diversity (Pre-SD) is best suited for QSVA.

In Tables 5.4 and 5.5, we compare the performance of various diversity techniques for SSDD-M and MSDDVA-M respectively, for a first-order AR process

Table 5.6: Performance of various diversity techniques for QSVA. 1^{st}-order fade process, $\rho = 0.9995$, $\mathcal{D} = 2$.

Average SNR per bit for each diversity channel (dB)	Symbol-error-rate		
	EGQEC	Pre-SD	Post-SD
Infinity	1.1×10^{-3}	8.0×10^{-6}	2.3×10^{-5}
11.2	9.8×10^{-2}	4.7×10^{-2}	6.9×10^{-2}

with $\rho = 0.9995$ and diversity $\mathcal{D} = 2$. We find that Equal Gain Correlation Metric Combining (EGCMC) gives the best performance at infinite SNR as well as at very low SNR. The reason has been discussed in the Section 4.5.1.

In Table 5.6, for a similar fade process and $\mathcal{D} = 2$, we compare the performance of various diversity techniques for QSVA, where we have used Equal Gain Quotient Error Combining (EGQEC) instead of EGCMC. We find that Pre-SD gives the best performance at infinite SNR as well as at very low SNR. The reason for this has been discussed in Section 4.5.3. Henceforth, in all the simulation results with diversity, EGCMC is used for SSDD-M and MSDDVA-M, whereas Pre-SD is used for QSVA.

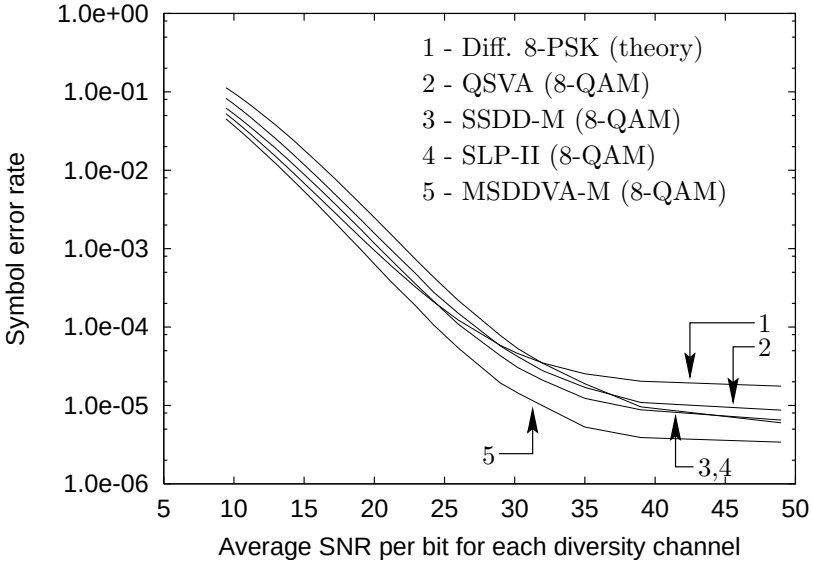

Figure 5.5: Simulation results for a Rayleigh fading channel. 1^{st}-order fade process, $\rho = 0.9995$, $\mathcal{D} = 2$.

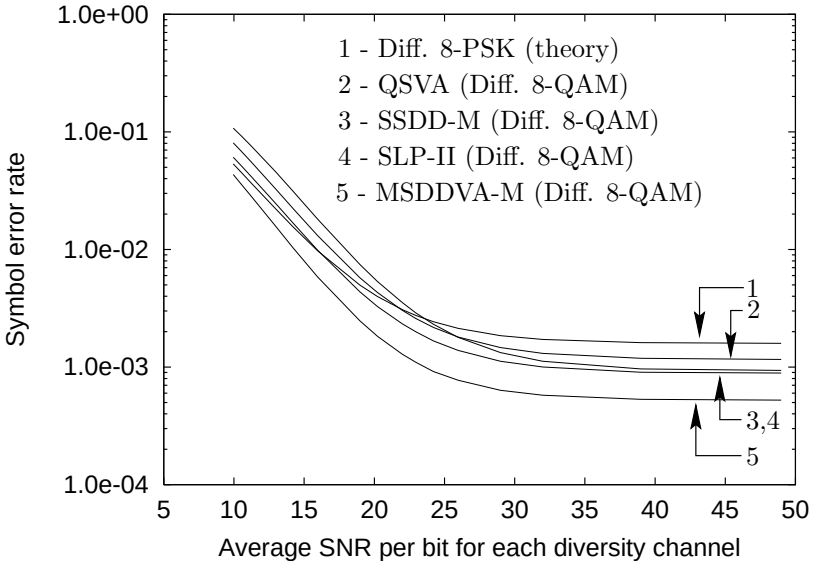

Figure 5.6: Simulation results for a Rayleigh fading channel. 1^{st}-order fade process, $\rho = 0.995$, $\mathcal{D} = 2$.

We now compare the performance of the proposed differential detection techniques with second-order diversity. Diversity for SLP-II was performed as given in (B.10) in Appendix B. Simulations were done over 10^7 symbols. In Figures 5.5 and 5.6, we present the results for a first-order fade process with $\rho = 0.9995$ and $\rho = 0.995$ respectively. The items given in Conclusions-I(A), in Section 5.2.1, are still valid. Some additional observations are given below:

Conclusions-II(A):

(a) SSDD-M performs better than QSVA. Recall that QSVA had a better performance than SSDD-M, for a first-order diversity, as shown in Figures 5.2 and 5.3.

(b) The SER performance of MSDDVA-M is better than differential PSK by a factor of two, at the error floor.

(c) For $\rho = 0.995$ and SER of 10^{-2}, the MSDDVA-M gives a better performance by about 1.6 dB compared to differential 8-PSK.

(d) For $\rho = 0.9995$ and an SER of 10^{-2}, the performance improvement of MSDDVA-M over differential 8-PSK is only about 0.67 dB. However, for

$\rho = 0.9995$, and an SER of 10^{-4}, the performance improvement is about 2 dB. Thus, we can also conclude that the performance improvement increases as we approach the error-floor.

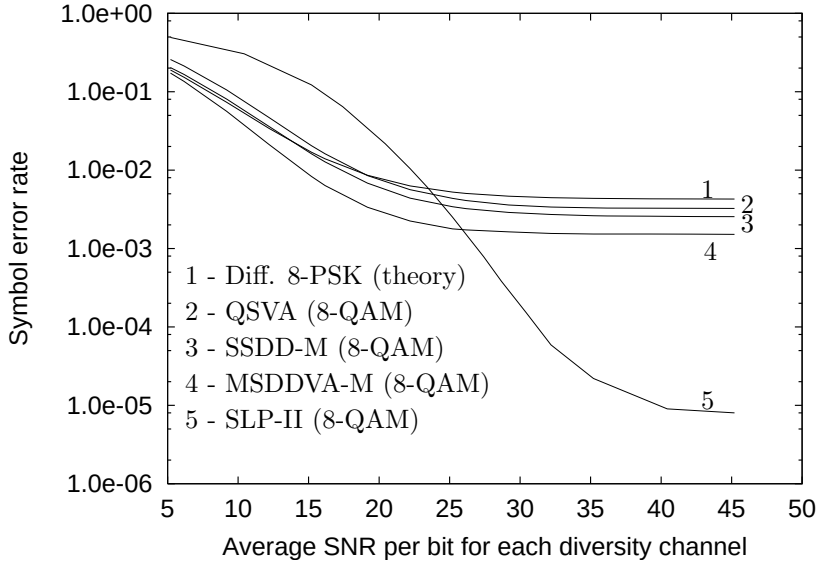

Figure 5.7: Simulation results for a Rayleigh fading channel. 3^{rd}-order fade process, $\rho = 0.8$, $\mathcal{D} = 2$.

In Figure 5.7, we compare the performance of the differential detectors with that of the SLP-II detector for the third-order fade process with $\rho = 0.8$. Simulations were done over 10^6 symbols. The following observations can be made:

Conclusions-II(B):

(a) The SSDD-M performs better than QSVA.

(b) The SER performance of MSDDVA-M is better than differential PSK by a factor of two, at the error floor.

(c) For an SER of 10^{-2}, the MSDDVA-M gives a better performance by about 2.5 dB compared to differential 8-PSK.

(d) We find that the SLP detectors perform better than the differential detectors by about two orders of magnitude at high SNR.

(e) At medium and low SNR (< 25 dB), the differential detectors perform better than SLP-II, similar to the results for $\mathcal{D} = 1$.

However, as mentioned in the previous section, the SLP detectors require a 512-state trellis. The computational time involved for simulating over 10^6 symbols, to get the SER corresponding to a particular SNR for the SLP-II in Figure 5.7, is about eight hours, on a 200 MHz Pentium PC. However, for the differential detectors it takes less than ten minutes.

5.2.3 Results with Fourth-Order Diversity

We now compare the performance of the proposed differential detection techniques with fourth-order diversity. In Figures 5.8 and 5.9, we present the results for a first-order fade process with $\rho = 0.9995$ and $\rho = 0.995$ respectively. We have not given simulation results for the SLP detectors due to the excessive computer simulation time involved.

The following observations can be made:

Conclusions-III:

(a) It is interesting to note that even differential 8-PSK performs better than QSVA. Recall that QSVA had a better performance than both SSDD-M and differential 8-PSK for first-order diversity (Section 5.2.1), and a performance in-between SSDD-M and differential 8-PSK for second-order diversity (Section 5.2.2).

(b) The MSDDVA-M gives the best performance (following the results for first and second-order diversity, we expect the performance of the SLP-II detector to be inferior to MSDDVA-M for a 1^{st}-order fade process).

(c) The simulation results for $\rho = 0.9995$ and $\rho = 0.995$ do not exhibit an error floor at high SNR. This is because from theory, the error floor for differential 8-PSK with fourth-order diversity is less than 10^{-7} [Kam91a], and since the simulations were carried out over only 10^7 symbols, the error floor cannot be observed.

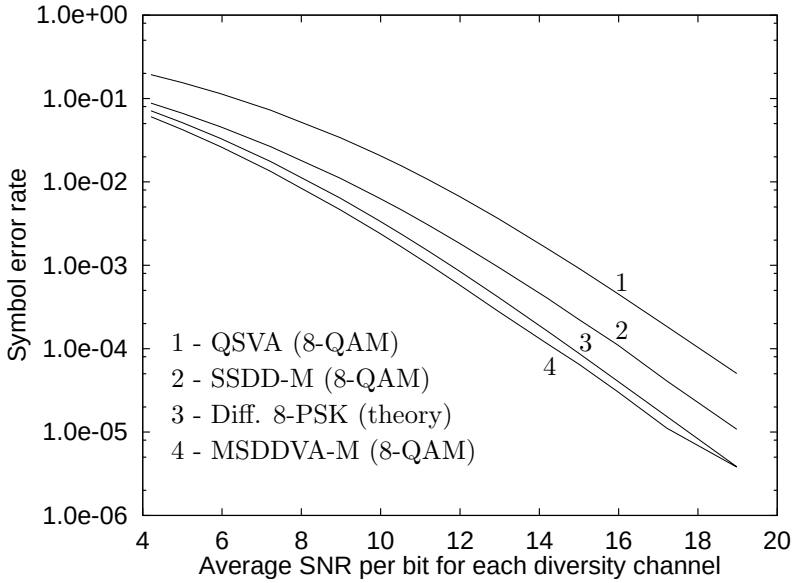

Figure 5.8: Simulation results for a Rayleigh fading channel. 1^{st}-order fade process, $\rho = 0.9995$, $\mathcal{D} = 4$.

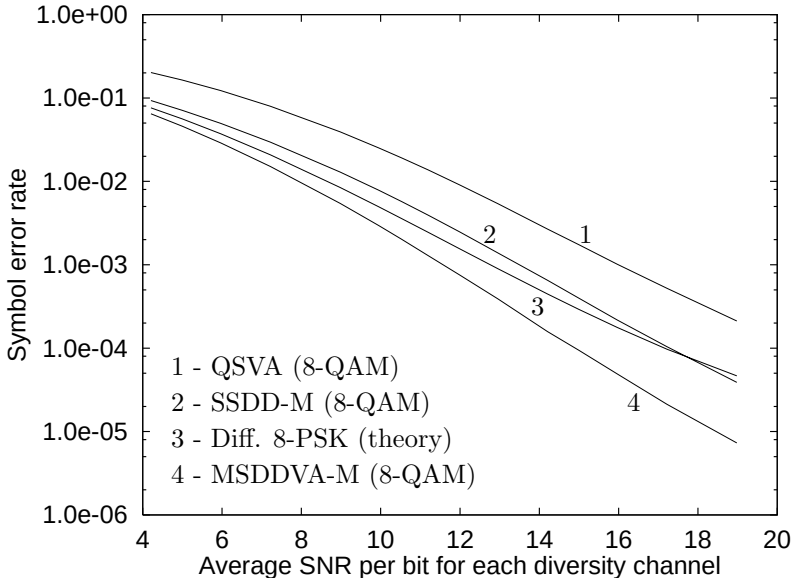

Figure 5.9: Simulation results for a Rayleigh fading channel. 1^{st}-order fade process, $\rho = 0.995$, $\mathcal{D} = 4$.

We have not performed simulations with $\mathcal{D} = 4$ for the third-order fade process with $\rho = 0.8$, but can we expect results similar to $\mathcal{D} = 1$ and $\mathcal{D} = 2$ as far as the performance of the SLP-II detector is concerned.

5.3 Results for Very Slow Rayleigh Flat-Fading Channels

In this section, we present simulation results for very slow Rayleigh flat-fading channels, where $\tilde{G}_k$ can be considered a constant over one frame duration. We assume a TDMA burst where $\tilde{G}_k = G\mathrm{e}^{\mathrm{j}\phi}$ is constant over a frame of length say L symbols. As discussed earlier in Section 3.1, this scenario arises in a wireless LAN based on TDMA.

Hence the received symbol in the α^{th} frame is given by

$$\tilde{r}_k = \tilde{G}_\alpha I_k + \tilde{w}_k, \qquad \text{for } \alpha L \leq k \leq \alpha L + L - 1, \tag{5.5}$$

where $\tilde{G}_\alpha$ is an uncorrelated, zero-mean complex Gaussian random variable with variance $2\mu_0$. Note that we have assumed $\tilde{G}_\alpha$ is uncorrelated from frame to frame. This is a valid assumption when the interval between frames is sufficiently large. The average SNR per bit is defined in (5.4).

In the simulations, frames having more than ten symbol errors are dropped. This is to emulate our data communication application, where Cyclic Redundancy Check (CRC) is employed to discard frames with more than ten errors. Each frame contains 1000 data symbols and the simulations were done over 10^5 frames (equivalent to 10^8 data symbols). The FSNVA-M requires an extra 10 symbol preamble for each frame, as discussed in Property 3 of Section 3.4. The symbol-error-rate is computed from the frames that are not dropped (valid frames), that is,

$$\text{SER} = \frac{\text{Total number of symbol errors}}{(\text{Data symbols per frame} \times \text{No. of valid frames})}. \tag{5.6}$$

The Frame Dropping Rate (FDR) is computed as

$$\text{FDR} = \frac{\text{Number of dropped frames}}{\text{Total number of frames transmitted}}. \tag{5.7}$$

Table 5.7 shows the performance of the coherent detector (uncoded 8-QAM), the SNVA-M detector ($\gamma = 1$, uncoded 8-QAM) and the MSDDVA-M detector

(differentially encoded 8-QAM) for a first-order diversity. We find that both the SER and FDR performance of FSNVA-M is as good as the coherent detector and about two times lower than MSDDVA-M. For a second-order diversity as shown in Table 5.8, the FSNVA-M again performs as well as the coherent detector and about four times better than MSDDVA-M. FSNVA-M with diversity is discussed in Section 3.5.1. We find that FSNVA-M is well suited for very slow Rayleigh fading channels, when used in a TDMA system. The assumption of uncorrelated fading from frame-to-frame may not be valid in some cases. However, if diversity is appropriately employed, long sequences of dropped frames can be avoided.

Table 5.7: Results with first-order diversity for very slow Rayleigh flat-fading. SER: Symbol-error-rate, FDR: Frame dropping rate.

Average SNR per bit for each diversity arm (dB)	Coherent		SNVA-M ($\gamma = 1$)		MSDDVA-M	
	SER	FDR	SER	FDR	SER	FDR
16	3.5×10^{-4}	13%	3.5×10^{-4}	13%	8.2×10^{-4}	27.1%
19	1.8×10^{-4}	7%	1.8×10^{-4}	7%	4.4×10^{-4}	14.7%
29	1.8×10^{-5}	0.7%	1.8×10^{-5}	0.7%	4.5×10^{-5}	1.6%

Table 5.8: Results with second-order diversity for very slow Rayleigh flat-fading. SER: Symbol-error-rate, FDR: Frame dropping rate.

Average SNR per bit for each diversity arm (dB)	Coherent		SNVA-M ($\gamma = 1$)		MSDDVA-M	
	SER	FDR	SER	FDR	SER	FDR
16	5.5×10^{-5}	1%	5.9×10^{-5}	1%	2.7×10^{-4}	4.2%
19	1.4×10^{-5}	0.2%	1.5×10^{-5}	0.2%	7.8×10^{-5}	1.2%
29**	2.8×10^{-7}	0%	3×10^{-8}	0%	1.6×10^{-6}	0.01%

** – SER and FDR measurements are not accurate

5.4 Results for Slow Rician Flat-Fading Channels

The simulation model for slow Rician fading channels is given by (5.1), with the only difference being that $\tilde{G}_k$ now has a non-zero mean denoted by $\tilde{m}$. We have considered only a first-order fade process. The in-phase and quadrature components of the first-order fade process are given by

$$G_{k,\,I\{Q\}} = \rho\,\left(G_{k-1,\,I\{Q\}} - m_{I\{Q\}}\right) + \sqrt{1-\rho^2}\,g_{k,\,I\{Q\}} + m_{I\{Q\}} \tag{5.8}$$

where $m_{I\{Q\}}$ denotes the in-phase and quadrature component of the complex mean $\tilde{m}$. We observe that the above equation can be obtained from (5.2) by replacing $G_{k,\,I\{Q\}}$ with $G_{k,\,I\{Q\}} - m_{I\{Q\}}$.

Following (5.4), the average SNR per bit is given by

$$\mathrm{SNR}_{\mathrm{Ri}} = \frac{E\left[\left|\tilde{G}_k I_k\right|^2\right]}{2\sigma_w^2 \log_2(M)} = \frac{E_{\mathrm{av}}\left(2\mu_0 + |\tilde{m}|^2\right)}{2\sigma_w^2 \log_2(M)}, \tag{5.9}$$

where we have again made use of the fact that the symbols and the fade process are statistically independent. Besides ρ and $\mathrm{SNR}_{\mathrm{Ri}}$, the performance of the proposed schemes in Rician fading channels depends also on the parameter K, which is the ratio of the specular (line-of-sight) to the diffuse power and is given by [DS94]

$$K = \frac{|\tilde{m}|^2}{2\mu_0}. \tag{5.10}$$

The simulation for the FSNVA-M detector in Rician fading channels was done as follows. The transmitted symbols are organized into frames of size 1010 symbols (1000 data symbols and a 10 symbol preamble for each frame). Note that it is necessary to organize data into frames so that even if a severe fade occurs in one frame, the FSNVA-M can recover using the preamble of the next frame. Framing is not required for the differential detectors, since they do not need to be initialized by a preamble. There is no detection delay associated with the FSNVA-M detector. The simulation was done over 10^7 data symbols (equivalent to 10^4 frames for the FSNVA-M) for all the proposed detectors. *Unless explicitly mentioned, all simulation results given in this section are for 8-QAM.*

In Figures 5.10 and 5.11, we show the performance of FSNVA-M for different forgetting factors (γ), in Rician fading channels. We have considered three different forgetting factors, $\gamma = 0.8, 0.9, 0.95$. For $\rho = 0.9995$ and $K = 10$ (Figure 5.10), there is practically no difference in performance of the FSNVA-M for $\gamma = 0.9$ and $\gamma = 0.95$. However, for $\gamma = 0.8$, there is 0.5 dB loss in performance for SNRs below 15 dB.

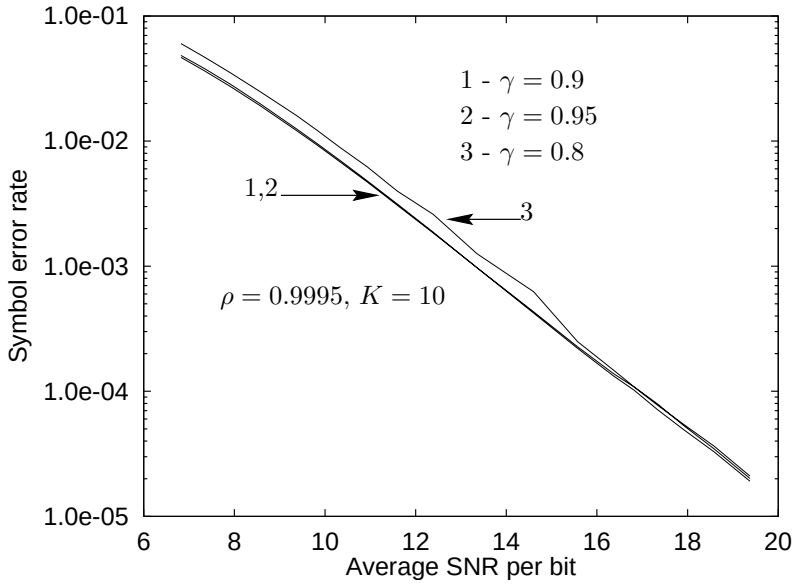

Figure 5.10: Simulation results for FSNVA-M with different forgetting factors in a Rician fading channel with $\rho = 0.9995$.

For $\rho = 0.995$ and $K = 10$ (Figure 5.11), the performance for various forgetting factors differs by nearly a factor of two, at high SNR (> 50 dB). Moreover, $\gamma = 0.8$ gives a better performance at high SNR, compared to $\gamma = 0.9$ and $\gamma = 0.95$. This is because the assumption that $\tilde{G}_k$ is nearly constant over the memory of the FSNVA-M detector is more valid for $\gamma = 0.8$, than for $\gamma = 0.9$ and $\gamma = 0.95$ (see also the discussion on the choice of the forgetting-factor, given in Section 3.5). Hence, there is no guarantee than the accumulated metric corresponding to $\gamma = 0.9$ and $\gamma = 0.95$ will be greater than that corresponding to $\gamma = 0.8$. Consequently, the noncoherent squared distance corresponding to $\gamma = 0.8$ could be closer to the coherent squared distance, compared to $\gamma = 0.9$ and $\gamma = 0.95$, resulting in a better performance. However, we also notice the sharp degradation in performance for $\gamma = 0.8$, in the SNR range of 40-50 dB, compared to other forgetting factors. This

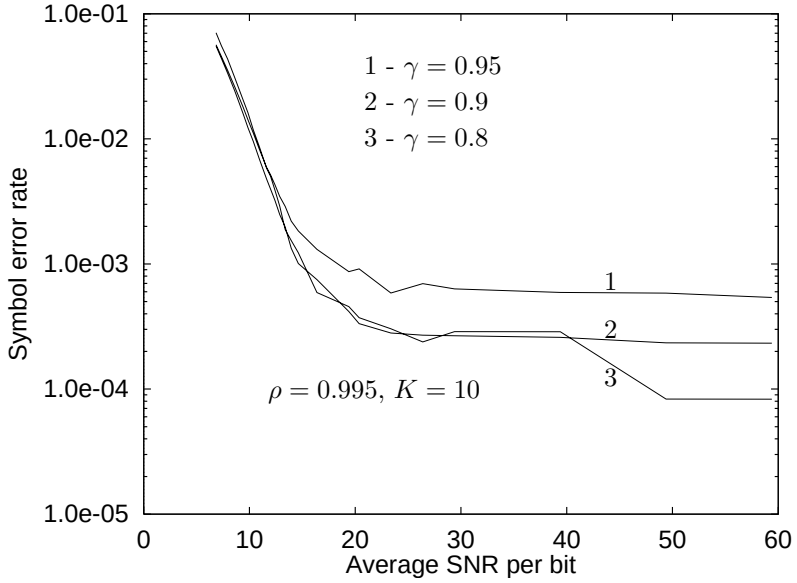

Figure 5.11: Simulation results for FSNVA-M with different forgetting factors in a Rician fading channel with $\rho = 0.995$.

could be attributed to the fact that the inherent memory corresponding to $\gamma = 0.8$ is small, which results in lower noise averaging. In fact, for SNRs less than 10 dB, $\gamma = 0.8$ gives the worst performance.

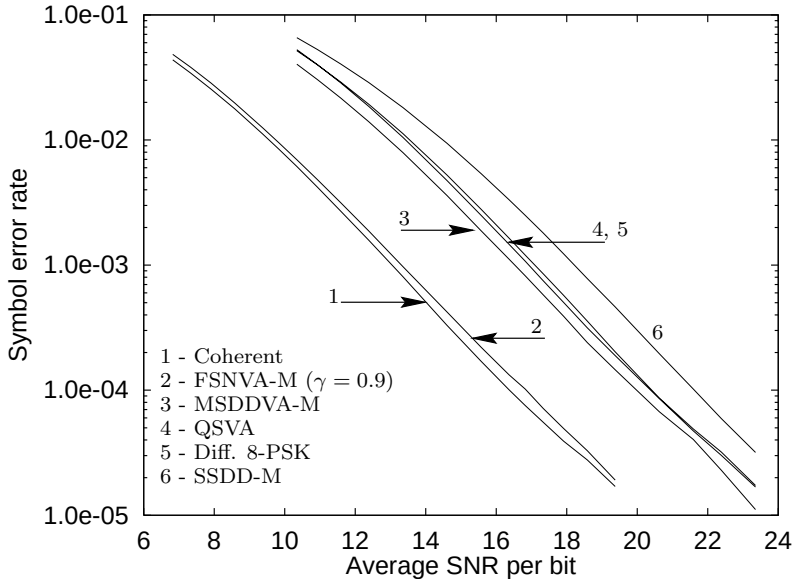

Figure 5.12: Simulation results for a Rician fading channel ($\rho = 0.9995$, $K = 10$).

In Figures 5.12 and 5.13, we show the performance of the proposed detectors in slow Rician flat-fading channels. For $\rho = 0.9995$ and $K = 10$, (Figure 5.12), we find that the FSNVA-M performs as well as the coherent detector, where $\tilde{G}_k$ and

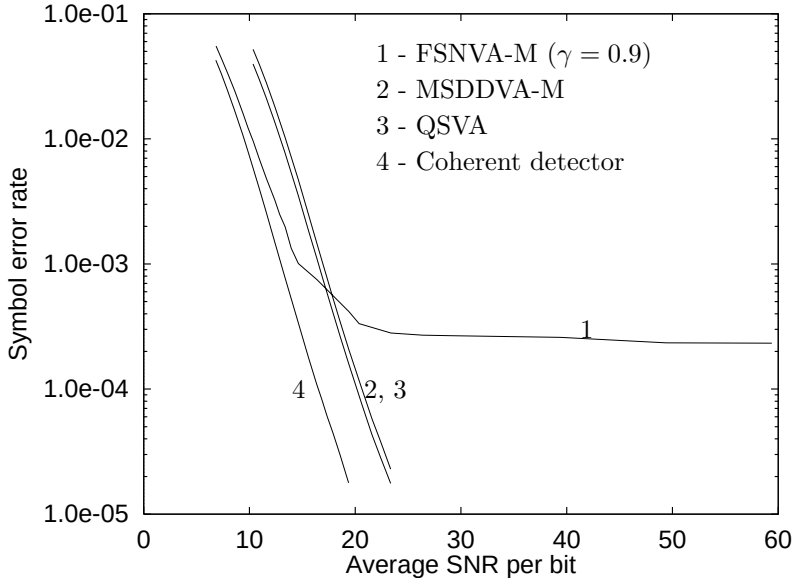

Figure 5.13: Simulation results for a Rician fading channel ($\rho = 0.995$, $K = 10$).

$\tilde{m}$ are known perfectly for all k. The coherent receiver decides in favour of that symbol $I^{(j)}$ in the M-ary constellation, $0 \leq j \leq M-1$, which minimizes

$$\eta^{(j)} = \left| \tilde{r}_k - \tilde{G}_k I^{(j)} \right|^2 . \tag{5.11}$$

For $\rho = 0.995$ and $K = 10$ (Figure 5.13), the FSNVA-M detector exhibits an error-floor at high SNR. This is because, the assumption that $\tilde{G}_k$ is nearly constant over many symbols is no longer valid. Note that the differential detectors perform much better than FSNVA-M at high SNR, since they assume $\tilde{G}_k$ is nearly constant only over two symbol durations. At low SNR, the FSNVA-M performs better than the differential detectors due to its inherent noise averaging capability.

It may be noted that the simulation model given by (5.8), is characterized by an exponential autocovariance function (also called the Kam's autocovariance function [Kam91b, MK97]). As mentioned earlier, in a realistic situation, the fade process is better characterized by a Bessel autocovariance function, which decays faster than the Kam's autocovariance function. Hence, we expect the FSNVA-M to show some performance degradation in a land-mobile fading model, compared to the model in (5.8).

5.5 Results for AWGN Channels

For the AWGN channel the simulation model is given by

$$\tilde{r}_k = I_k \mathrm{e}^{\mathrm{j}\phi} + \tilde{w}_k. \tag{5.12}$$

The average SNR per bit is defined by

$$\mathrm{SNR}_{\mathrm{AWGN}} = \frac{E\left[|I_k|^2\right]}{2\sigma_w^2 \log_2(M)} = \frac{E_{\mathrm{av}}}{2\sigma_w^2 \log_2(M)}. \tag{5.13}$$

In Figure 5.14 we give the simulation results for the SNVA-M and FSNVA-M de-

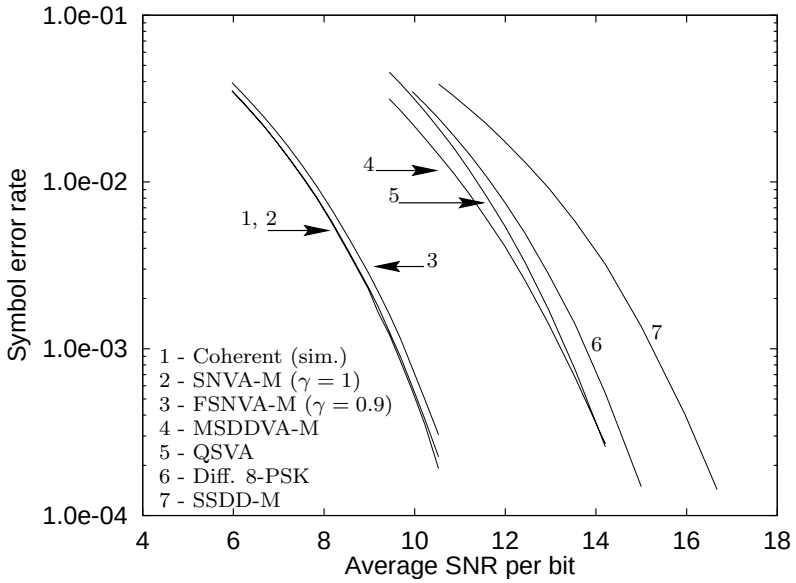

Figure 5.14: Simulation results for an AWGN channel.

tector for uncoded 8-QAM signalling, through an AWGN channel. *Unless explicitly mentioned, all results are for 8-QAM signalling.* The SNVA-M and FSNVA-M are initially trained (at the beginning of the simulation) with a known preamble of length ten symbols, as required by Property 3 in Section 3.4. Since the symbols are uncorrelated, the SNVA-M and the FSNVA-M operate on a single-state trellis with eight parallel transitions, since the constellation is 8-ary. Moreover, there is no detection delay, i.e., symbol decisions are immediate. The simulation was done over 10^6 symbols.

We find that the FSNVA-M receiver performs as well as the coherent receiver even for $\gamma = 0.9$. We also show the performance of the receivers based on differential detection of 8-QAM. The SNVA-M and the FSNVA-M receivers significantly

outperform those based on differential detection. For the differential schemes, the performance of differential 8-PSK is plotted as reference. The simulations also show that the performance of SSDD-M is poor, as expected. Note that the QSVA performs as well as MSDDVA-M at high SNR, but is slightly inferior at low SNRs.

5.6 Summary

In this chapter, we have presented computer simulation results for the proposed noncoherent detectors. The circular 8-QAM constellation was taken as an example. The simulation results were compared with the performance of the conventional differential detector for 8-PSK. For slow Rayleigh flat-fading channels, where the fade process varies from symbol-to-symbol, the Multiple Symbol Differential Detector for Multilevel signals (MSDDVA-M) performs better than the conventional two-symbol differential 8-PSK, and in fact, gives the best performance amongst the proposed differential detectors. The performance improvement of MSDDVA-M over differential 8-PSK, is higher for larger SNR. For a first-order fade process with $\rho = 0.9995$ and an SER of 10^{-2}, the performance improvement of MSDDVA-M over 8-PSK is only about 0.67 dB, with second-order diversity. However, for $\rho = 0.9995$, and an SER of 10^{-4}, the performance improvement of MSDDVA-M over differential 8-PSK is about 2 dB with second-order diversity. Thus, we can also conclude that the performance improvement increases as we approach the error-floor. The Quotient Space VA does not perform as well as the other differential detectors for diversities of order greater than one. In fact, with fourth-order diversity, the QSVA gives the worst performance.

The MSDDVA-M also performs better than the Suboptimal Linear Predictor-II (SLP-II), for a first-order fade process. However, this result is only of academic interest. For a third-order fade process, which is more realistic, the performance of the SLP detectors at high SNR is two orders of magnitude better than the proposed differential detectors, including the MSDDVA-M. This is because the SLP detectors take advantage of the memory in the prediction filter used to whiten the fade process. The SLP detectors, however, assume that the autocovariance of the

fade process is known perfectly. In practice there is some performance degradation in the SLP detectors, due to imperfect knowledge of the autocovariance of the fade process. The SLP detectors also have a computational complexity that increases exponentially with the order of the prediction filter used to whiten the fade process. The order of the prediction filter required, is in turn dependent on the autocovariance of the fade process. The complexity of the proposed differential detectors is independent of the autocovariance of the fade process. At low SNR, the performance of the SLP detectors deteriorates rapidly, whereas the differential detectors show a more graceful degradation. In fact, at low SNR, the differential detectors perform better than the SLP detectors.

For very slow Rayleigh flat-fading channels, where the fade process can be assumed to be constant over more than one symbol, the symbol-error-rate (SER) performance of the Suboptimal Noncoherent Viterbi Algorithm for Multilevel signals (SNVA-M) (with forgetting-factor, $\gamma = 1$) is better than MSDDVA-M, by a factor of two, for the same SNR and first-order diversity. However, with second-order diversity, the SER performance of SNVA-M is better than MSDDVA-M by a factor of four, for the same SNR. Simulation results were also obtained for the frame-dropping-rate (FDR) of the SNVA-M and MSDDVA-M detectors. To emulate the data communication application using TDMA, we considered frames containing 1000 symbols. The SNVA-M requires an extra 10 symbol known preamble for initialization. Frames with more than 10 symbol errors are dropped. For first-order diversity, the FDR performance of SNVA-M is better than MSDDVA-M by a factor of two. For second-order diversity, the FDR performance of SNVA-M is better than MSDDVA-M by a factor of four. Moreover, both the SER as well as the FDR performance of SNVA-M is as good as the coherent detector.

The Forgetting-factor-based Suboptimal Noncoherent Viterbi Algorithm for Multilevel signals (FSNVA-M) is also well suited for slow Rician flat-fading channels (having a large ratio of specular-to-diffuse power), and AWGN channels.

For slow Rician flat-fading channels, with a specular-to-diffuse power of $K = 10$, and for a first-order fade process with $\rho = 0.9995$, the FSNVA-M detector

performs as well as the coherent detector, for a forgetting factor $\gamma = 0.9$. However, for a first-order fade process with $\rho = 0.995$, the FSNVA-M detector with $\gamma = 0.9$, exhibits an error-floor at high SNR. At low SNR however (< 15 dB), the FSNVA-M with the same forgetting factor performs as well as the coherent detector.

Simulations were also carried out for different forgetting factors. For a first-order fade process with $\rho = 0.9995$, $K = 10$ and at high SNR, there is practically no difference in performance between $\gamma = 0.8$, $\gamma = 0.9$ and $\gamma = 0.95$. At low SNR (< 15 dB), $\gamma = 0.8$ suffers a 0.5 dB loss in performance for the same SER. For a first-order fade process with $\rho = 0.995$, the forgetting factors $\gamma = 0.8$, $\gamma = 0.9$ and $\gamma = 0.95$ exhibit an error-floor. The SER performance differs by a factor of two at the error-floor, with $\gamma = 0.8$ giving the best performance and $\gamma = 0.95$ giving the worst performance. At SNRs less than 15 dB, all the three forgetting factors give nearly the same performance.

CHAPTER 6

THE SPLIT-TRELLIS VITERBI ALGORITHM

6.1 Introduction

We have so far discussed efficient noncoherent detection strategies for flat-fading channels. We now present an efficient method of implementing the Viterbi Algorithm at Nyquist-rate or above, which is suitable for voiceband modem communications. The channels encountered in voiceband modem communications usually introduce intersymbol interference (ISI) and additive white Gaussian noise, but do not introduce fading.

The concept of Split-Trellis Viterbi Algorithm (STVA) has been discussed before in [Ung74] and more recently in [BC98]. In [Ung74], an adjustment algorithm for the joint estimation of the fractionally-spaced matched filter, the carrier phase and the symbol timing is also presented. Decoding of redundantly coded sequences is also discussed. In [BC98], a unified approach to the Forney receiver in [For72] and the Ungerboeck receiver in [Ung74], is given, where each receiver is derived from the other. Moreover in [BC98], the Ungerboeck receiver is extended to the case of a time-varying known channel. However, neither [Ung74] nor [BC98] discuss the computational advantage of the Ungerboeck receiver over the conventional Whitened Matched Filter approach of Forney [For72, Pro95].

It must also be mentioned that unlike the detection techniques introduced in the earlier chapters which are noncoherent, the Split Trellis approach requires coherent detection and a correct estimate of the channel. In this chapter, we assume perfect estimates of the carrier, timing and the channel coefficients. We also observe that since the bandwidth of the received signal is greater than $1/2T$ but less than $1/T$, where T denotes the symbol duration, sampling must be done at Nyquist-rate or above.

6.2 The Optimum Discrete-Time Receiver Operating at Nyquist-Rate or Above

The discrete-time, lowpass equivalent of a linearly modulated signal corrupted by ISI and AWGN [Pro95] is given by

$$\tilde{r}(nT_s) = \sum_{k=\lceil (n-P+1)T_s/T \rceil}^{\lfloor nT_s/T \rfloor} I_k \, \tilde{p}(nT_s - kT) + \tilde{w}(nT_s) \tag{6.1}$$

where T_s is the sampling period satisfying the Nyquist criterion, T is the symbol period, I_k denotes the complex symbol (drawn from an M-ary QAM constellation) occurring at time kT, $\tilde{p}(nT_s)$ is the overall channel response (assumed known at the receiver) and $\tilde{w}(nT_s)$ denotes samples of zero-mean, white Gaussian noise. The symbols I_k are assumed to be uncorrelated. The impulse response $\tilde{p}(nT_s)$ is assumed to have P taps, denoted by $\tilde{p}(0), \ldots, \tilde{p}((P-1)T_s)$. The limits in the summation in (6.1) are obtained by noting that

$$0 \leq nT_s - kT \leq (P-1)T_s. \tag{6.2}$$

In (6.1), $\lceil x \rceil$ denotes the smallest integer greater than or equal to x and $\lfloor x \rfloor$ denotes the largest integer less than or equal to x. To ensure steady-state values of $\tilde{r}(nT_s)$, we must have

$$(P-1)T_s \leq nT_s \leq (L\mathcal{C}-1)T_s \tag{6.3}$$

where L is the total number of transmitted symbols and $\mathcal{C} \triangleq T/T_s$, an integer, is the number of samples per symbol.

It is easy to show [Pro95] that the Maximum Likelihood (ML) detector is given by

$$\max_j \mathcal{M}_j = \sum_{n=P-1}^{L\mathcal{C}-1} 2\Re\left\{\tilde{r}(nT_s)\, \tilde{s}_j^*(nT_s)\right\} - |\tilde{s}_j(nT_s)|^2 \tag{6.4}$$

where $\Re\{\cdot\}$ denotes the real part and

$$\tilde{s}_j(nT_s) = \sum_{k=\lceil (n-P+1)T_s/T \rceil}^{\lfloor nT_s/T \rfloor} I_{k,\,j} \, \tilde{p}(nT_s - kT). \tag{6.5}$$

The subscript j in (6.4) and (6.5) lies in the range $0 \leq j \leq M^L - 1$. Note that the transmitted sequence (the summation term in (6.1)) is one amongst the M^L

sequences and we denote it by $\tilde{s}(nT_s)$. Figure 6.1 shows the block diagram of the maximum likelihood detector, using the Viterbi algorithm, operating at Nyquist-rate or above, based on (6.4).

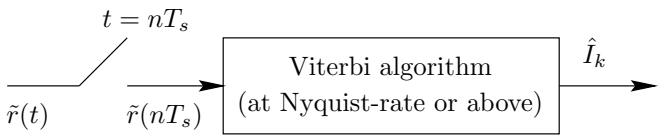

Figure 6.1: Viterbi algorithm at Nyquist-rate or above.

Substituting (6.5) in (6.4) and interchanging the order of summation, we get

$$\begin{aligned} \max_j \mathcal{M}_j &= \sum_{k=0}^{L-1} 2\Re\left\{ I^*_{k,\,j} \sum_{n=n1}^{n2} \tilde{r}(nT_s)\, \tilde{p}^*(nT_s - kT) \right\} \\ &\quad - \sum_{n=P-1}^{L\mathcal{C}-1} |\tilde{s}_j(nT_s)|^2 \end{aligned} \tag{6.6}$$

where

$$\begin{aligned} n1 &\triangleq \max\left(P-1, \left\lceil \frac{kT}{T_s} \right\rceil\right) \\ n2 &\triangleq \min\left(L\mathcal{C}-1, \left\lfloor \frac{(P-1)T_s + kT}{T_s} \right\rfloor\right). \end{aligned} \tag{6.7}$$

The limits n_1 and n_2 in the above equation are obtained from (6.2) and (6.3). Figure 6.2 shows the communication model based on (6.6), where we see that a fractionally-spaced matched filter is employed at the receiver. Note that the matched filter output must be sampled at the autocorrelation peaks [Pro95]. We refer to the approach in Figure 6.2, as the Split-Trellis Viterbi Algorithm (STVA). Observe that the STVA operates on symbol-rate samples, although it has been derived from the Nyquist-rate receiver in Figure 6.1.

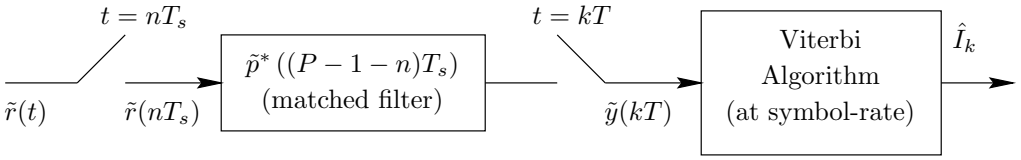

Figure 6.2: Block diagram of the proposed detector.

6.3 Equivalence Between the Whitened Matched Filter Approach and the Nyquist-Rate Approach

Since we have derived the Split-Trellis VA from the Nyquist-rate VA, we need to first establish an equivalence between the Nyquist-rate VA and the conventional Whitened Matched Filter (WMF) approach in [Pro95, For72]. In this section, we show that the Nyquist-rate VA based on (6.4) has the same number of states as the symbol-spaced VA in the WMF approach.

It is easy to see that $\tilde{s}(nT_s)$ (summation term in (6.1)) can be obtained by exciting a tapped-delay-line (TDL) by a train of discrete-time delta functions [PM92], weighted by the complex symbols, occurring every $\mathcal{C}$ samples. This is illustrated in Figure 6.3 for $P = 5$ and $\mathcal{C} = 2$. In general, $\mathcal{C}$ consecutive outputs

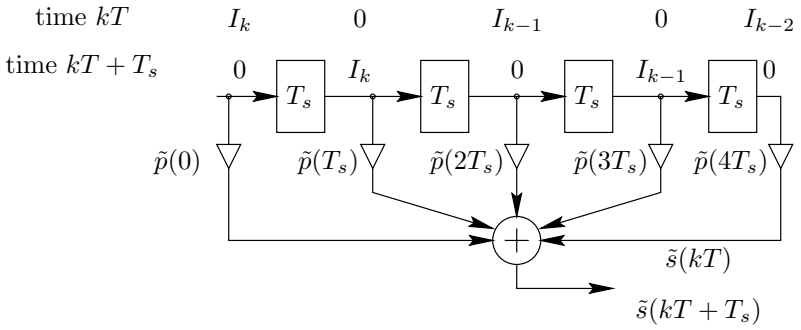

Figure 6.3: Transmitted samples at times kT and $kT + T_s$, for $P = 5$ and $\mathcal{C} = 2$.

of the TDL are obtained from the *same* set of input symbols, excepting perhaps for the last symbol (I_{k-2} in Figure 6.3). Therefore, the number of states in the trellis when M-ary signalling is used, is equal to M^{Q-1}, where Q is the *maximum* number of symbols in the TDL at any instant of time. In Figure 6.3, $Q = 3$ and in general

$$Q \triangleq \left\lceil \frac{P}{\mathcal{C}} \right\rceil . \tag{6.8}$$

We now show that the number of states in the trellis is the same as that in [Pro95], for a given impulse response $\tilde{p}(\cdot)$ and for integer values of $\mathcal{C}$. This can be proved as follows. We assume, for the purpose of comparision, that a discrete-time, fractionally-spaced matched filter is used in [Pro95]. Hence, the matched filter (MF) also has P taps. The length of the autocorrelation at the MF output is

thus $2P-1$ [PM92]. The length of the autocorrelation after symbol-rate sampling is equal to

$$\mathcal{L} \triangleq 1 + 2\left\lfloor \frac{P-1}{\mathcal{C}} \right\rfloor. \tag{6.9}$$

This is because, the autocorrelation must be sampled at the peak [Pro95]. This explains the term 1 in the above equation. Hence, we are left with $P-1$ samples on either side of the peak, out of which every $\mathcal{C}^{th}$ sample must be selected, starting from the peak. This explains the term $2\lfloor (P-1)/\mathcal{C} \rfloor$, since the number of samples selected on either side of the peak are identical. This is illustrated in Figure 6.4.

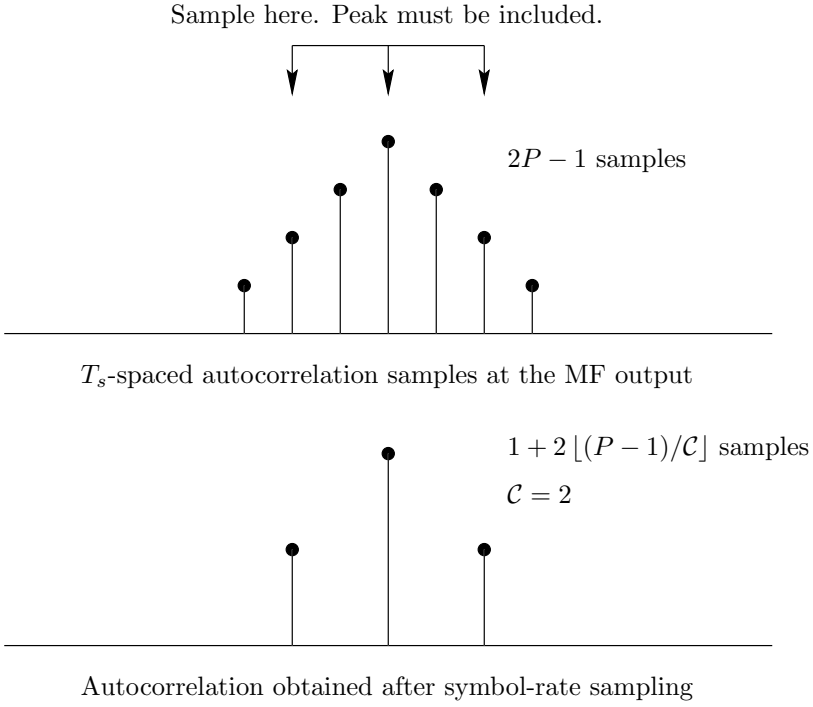

Figure 6.4: Relationship between fractionally-spaced and symbol-spaced autocorrelations.

Now, the order of the T-spaced autocorrelation in (6.9) is just $\mathcal{L}-1$, hence the order of the whitening filter is

$$\begin{aligned} \frac{\mathcal{L}-1}{2} &= \left\lfloor \frac{P-1}{\mathcal{C}} \right\rfloor \\ &= Q-1. \end{aligned} \tag{6.10}$$

The order of the pulse at the output of the whitening filter, which is referred to as the equivalent, symbol-spaced, discrete-time channel in [Pro95], is also equal to

$Q-1$ (the length of the channel is Q). Hence, the number of trellis states is equal to M^{Q-1}, which is identical to our approach.

6.4 Computational Complexity of Various Approaches

In this section, we compare the computational complexities of the Split-Trellis VA based on (6.6), the Nyquist-rate VA based on (6.4) and the WMF approach in [Pro95, For72].

6.4.1 The Split-Trellis Approach

The branch metric computation for the VA based on (6.6), between states $A \equiv \{I_k, I_{k-1}, \ldots, I_{k-Q+2}\}$ and $B \equiv \{I_{k+1}, I_k, \ldots, I_{k-Q+3}\}$, for an input symbol I_{k+1}, is given by

$$\Lambda_1(A,B) = \Re\left\{2\tilde{y}(mT)I^*_{k-Q+2}\right\} - E_{A,B} \tag{6.11}$$

where $\tilde{y}(mT)$ is the output of the matched filter sampled at symbol-rate (see Figure 6.2), and $E_{A,B}$ is given by

$$E_{A,B} = \sum_{i=0}^{\mathcal{C}-1}\left|\sum_{j=0}^{Q-1} I_{k+1-j}\,\tilde{p}(iT_s + jT)\right|^2. \tag{6.12}$$

Observe that the total number of distinct real multiplications (RMs) per symbol interval for computing $\Re\{\cdot\}$ in (6.11) is only $2M$, corresponding to M distinct complex symbols. Note that $2I^*_{k-Q+2}$ can be precomputed, and computing the real part of the product of two complex numbers involves two real multiplications and one real addition (RA).

Thus, the total number of RAs corresponding to the computation of $\Re\{\cdot\}$ is equal to M. The total number of RAs corresponding to computing the difference $\Re\{\cdot\} - E_{A,B}$ is equal to $M + M^Q$, since there are M^Q distinct values of $E_{A,B}$ in general. We assume that the "cost" of addition is the same as subtraction, and in fact in the Digital Signal Processors (DSPs), even the cost of multiplication is the same as addition. Observe that the term $E_{A,B}$ in (6.12) can be precomputed, if the channel is known.

In addition to the above computation, the complex matched filtering operation also involves extra RMs and RAs. Observe that computing a complex product involves 4 RMs and 2 RAs. Since the matched filter has P complex taps, $4P$ RMs and $2P$ RAs are required to compute P complex products. In addition to this, the P complex products have to be added to obtain one sample of $\tilde{y}(mT)$ every symbol interval, which implies an additional $2(P-1)$ RAs for both the real and imaginary parts. Thus, the computational complexity of the Split-Trellis approach per symbol interval can be summarized below:

Summary I:

(a) $2M + 4P$ RMs

(b) $M + M^Q + 2P + 2(P-1)$ RAs

It may be noted that multiplication by I^*_{k-Q+2} in (6.11) does not have any special significance. Any other symbol constituting the state A can also be used, and in fact, even the complex conjugate of the input symbol, I^*_{k+1}, can be used in (6.11).

We refer to the branch metric computation in (6.11) as the "Split-Trellis" approach because we can visualize the entire trellis to be "split" into M distinct sub-trellises. The product computation in each sub-trellis is identical. In other words, the trellis has M^{Q-1} states and M^Q branches. Since there are only M distinct products, there are M sub-trellises and each sub-trellis has M^{Q-1} branches with identical products. The energy term $E_{A,B}$ in (6.12) is however distinct in general, even within a sub-trellis. Observe that there are in general M^Q distinct values of $E_{A,B}$. Hence the overall branch metric given by (6.11) is distinct in general for the M^Q branches.

6.4.2 The Nyquist-Rate Approach

The branch metric computation for the VA based on (6.4) is given by

$$\Lambda_2(A,B) = \sum_{i=0}^{\mathcal{C}-1} \Re\left\{2\tilde{r}(mT+iT_s)\,\tilde{s}^*_{A,B}(iT_s)\right\} - E_{A,B} \tag{6.13}$$

where $\tilde{s}_{A,B}(\cdot)$ is the term inside the modulus in (6.12). The total number of distinct RMs for computing $\Re\{\cdot\}$ in (6.13) is equal to $2\mathcal{C}M^Q$, since there are $\mathcal{C}M^Q$ distinct values of $\tilde{s}_{A,B}(iT_s)$. Again, note that $2\tilde{s}^*_{A,B}(iT_s)$ can be precomputed.

The number of RAs for computing each $\Re\{\cdot\}$ in (6.13) is equal to 1, for each branch metric. The number of RAs required to compute $\sum \Re\{\cdot\}$ is equal to $\mathcal{C} + \mathcal{C} - 1$, for each branch metric. The number of RAs required for computing the difference $\sum \Re\{\cdot\} - E_{A,B}$ is equal to $\mathcal{C} + \mathcal{C} - 1 + 1 = 2\mathcal{C}$, for each branch metric. Thus, the total number of RAs per symbol interval is equal to $2\mathcal{C}M^Q$. Thus, the computational complexity of the approach given by (6.13), per symbol interval, can be summarized below:

Summary II:

(a) $2\mathcal{C}M^Q$ RMs

(b) $2\mathcal{C}M^Q$ RAs

It is important to note that the branch metrics in (6.11) and (6.13) are *not* identical. However, the metrics computed over the entire sequence are *exactly* identical, as seen from (6.4) and (6.6). Hence, both (6.4) and (6.6) implement the MLSE detector, and can be expected to have *identical* performance. In a VA-based implementation, identical performance can be achieved by having sufficient decision-delay. From computer simulations, it appears that at symbol-error-rates (SER) $> 10^{-2}$, VA-based implementation of (6.6) requires slightly larger decision-delay than (6.4), to get the same performance. This is due to the fact that the branch metrics (6.11) and (6.13) are not identical.

6.4.3 The Whitened Matched Filter Approach

The branch metric for the conventional VA in [Pro95] (whitened matched filter (WMF) approach) is identical to (6.13) excepting that $\mathcal{C} = 1$ and all samples are symbol-spaced. In addition, following the discussion prior to Summary I, the matched filtering operation requires $4P$ RMs and $2P + 2(P-1)$ RAs per symbol

interval. Similarly, the whitening filter requires $4Q$ RMs and $2Q + 2(Q-1)$ RAs. Thus, the computational complexity of the WMF approach [Pro95] is:

Summary III:

(a) $2M^Q + 4P + 4Q$ RMs

(b) $2M^Q + 2P + 2(P-1) + 2Q + 2(Q-1)$ RAs

There is yet another method of computing the branch metric as given below, where we again consider the WMF approach in [Pro95]:

$$\Lambda_3(A, B) = |\tilde{z}(mT) - \tilde{u}_{A,B}(mT)|^2 \tag{6.14}$$

where $\tilde{z}(mT)$ denotes the output of the whitening filter and $\tilde{u}_{A,B}(mT)$ denotes the corresponding noise-free sample. Observe that in the above equation, the minimum branch metric is propagated through the trellis, in contrast to (6.11) and (6.13), where the maximum branch metric is propagated. It is easy to see that the number of RMs for each branch metric is equal to 2. The number of RAs is equal to 3. Hence, the total number of RMs and RAs in the trellis, per symbol interval, are equal to $2M^Q$ and $3M^Q$ respectively. The complexity of matched filtering and noise whitening remain the same. Thus, the computational complexity of the WMF approach in [Pro95], using the branch metric computation in (6.14) is:

Summary IV:

(a) $2M^Q + 4P + 4Q$ RMs

(b) $3M^Q + 2P + 2(P-1) + 2Q + 2(Q-1)$ RAs

Thus, we find from the above four summaries that the Split-Trellis approach is much more efficient that the WMF approach in [Pro95], and the Nyquist-rate approach given by (6.4), both in terms of RMs as well as RAs.

6.5 Simulation Results

In Table 6.1 we show the simulation results for the circular 8-QAM constellation [Pro95]. As an example, the filter taps were taken to be $\tilde{p}(0) = \tilde{p}(3T_s) = 1 + \mathrm{j}$, $\tilde{p}(T_s) = \tilde{p}(4T_s) = -(1 + \mathrm{j})$ and $\tilde{p}(2T_s) = 0$, with $\mathcal{C} = 2$. Note that $M = 8$, $Q = 3$ and $P = 5$. For an SNR of 11 dB, the Split-Trellis VA (STVA) based on (6.6) gives a slightly larger SER. However, when the decision delay (DD) for the STVA based on (6.6) was increased to 24 symbols, the SER dropped to 47325×10^{-6}. The number of RMs per symbol interval, for the STVA based on (6.6) is only $2M + 4P = 36$, whereas for the Nyquist-rate VA based on (6.4) it is $2\mathcal{C}M^Q = 2048$. Even for the conventional VA in [Pro95, For72], the number of RMs in the VA alone (excluding the matched filtering and noise whitening operations) would be $2M^Q = 1024$ per symbol duration. Moreover, the Split-Trellis approach requires only about half the number of RAs per symbol interval, compared to the VA in [Pro95, For72].

Table 6.1: Results (20 symbol DD, 64-state trellis).

Average SNR per bit (dB)	Symbol-error-rate ($\times 10^{-6}$)	
	VA based on (6.4)	VA based on (6.6)
15.0	412	412
13.0	7016	7016
11.0	47326	47335

6.6 Summary

In this chapter, we have presented an efficient Viterbi Algorithm for multilevel signalling over ISI channels. The proposed technique significantly reduces the number of real multiplications in the trellis. For a channel of length Q symbols, the proposed Split Trellis Viterbi Algorithm requires approximately only $2M$ distinct real multiplications per symbol duration, for M-ary signalling. On the other hand, the Whitened Matched Filter (WMF) approach proposed in [Pro95, For72] requires approximately $2M^Q$ real multiplications per symbol duration, for the same channel

length. The Split Trellis approach also requires only about half the amount of real additions, compared to the Viterbi algorithm in [Pro95, For72].

CHAPTER 7

CONCLUSIONS AND SCOPE

This thesis has described several noncoherent detection strategies for multilevel signals transmitted through frequency-nonselective (flat) fading channels. First, we derived an approximate noncoherent Maximum Likelihood detector for frequency-nonselective, very slow fading channels, where the channel gain and phase remain constant, but unknown, over several symbol durations. In many high bit-rate, low-range indoor wireless applications like the wireless LAN or wireless PBX based on TDMA technology, this assumption of very slow and flat-fading may be simultaneously satisfied, even over an entire TDMA slot duration. The receiver is noncoherent in the sense that no knowledge is required about the channel gain or phase. In this respect, the problem discussed here is more general than in [DS94, LP92], which describe ML detectors for channels with unknown phase, but known gain. We refer to the proposed detector as the approximate Maximum Likelihood detector in Unknown Amplitude and Phase (ML-UAP), where a correlation metric suitable for multilevel signals was derived. We obtained the ML-UAP detector for Rician, Rayleigh and Uniform pdfs, and the correlation metric derived was found to be identical in all the three cases. We then discussed certain important properties of the correlation metric. Due to the property of isometry, the ML-UAP detector by itself is not very useful.

Next, we proposed a suboptimal VA-based approach whose complexity increases linearly with the sequence length to be detected, as opposed to the exponential complexity of the ML-UAP detector. We call this approach the Suboptimal Noncoherent VA for Multilevel signals (SNVA-M) [VGR98b, VGR98a]. The SNVA-M also solves the problem of distinguishing between isometric sequences, and can be viewed as a generalization of the earlier work on noncoherent detection of constant envelope signals [AAS86, AS89, DMV94, SK97, VGR97]. The next development was a Forgetting-factor-based SNVA-M (FSNVA-M), to deal with

slow variations in the channel gain and phase. The FSNVA-M detector eliminates the need to have explicit carrier phase estimation and received signal gain estimation, and the forgetting-factor enables fixed-point DSP implementations in a straightforward manner.

In order to deal with frequency-nonselective fading channels where the channel gain and phase vary from symbol to symbol, we modified the ML-UAP detector to accommodate differential encoding and decoding. Based on the ML-UAP detector, we proposed two differential detection techniques for 8-ary circular QAM namely, (i) Symbol-by-Symbol Differential Detector for Multilevel signals (SSDD-M) and, (ii) Multiple Symbol Differential Detector using the Viterbi Algorithm for Multilevel signals (MSDDVA-M). The MSDDVA-M takes advantage of the inherent memory in differential encoding, and hence performs better than SSDD-M. In particular, we have shown that the noncoherent minimum distance for MSDDVA-M is twice that of SSDD-M.

In [WHS91] and [Sve95], *quotient-space* symbol-by-symbol detectors have been proposed for differentially encoded star-QAM constellations over slow Rayleigh fading channels. That is, the quotient of two successive symbol-spaced samples is taken to determine whether an amplitude change has taken place. However, the inherent correlation in the quotient magnitudes is not exploited. In this thesis, we have proposed a Viterbi Algorithm-based detection in the quotient-space, for differentially encoded, circular-QAM signals. This Quotient Space VA (QSVA) technique exploits the fact that not all quotient sequences are valid, and hence is expected to perform better than the simple two-symbol quotient space approaches.

All the three differential detectors proposed, namely, SSDD-M, MSDDVA-M and the QSVA, are easily extended to include diversity reception, which greatly enhances their performance in slow Rayleigh fading channels, where the channel gain and phase vary from one symbol to next [VGR99a]. Computer simulation results indicate that Equal Gain Correlation Metric Combining (EGCMC) is best suited for SSDD-M and MSDDVA-M, whereas only Pre-detection Selection Diversity (Pre-SD) is possible for QSVA.

Computer simulation results, comparing the symbol-error-rate performance of the proposed noncoherent detectors for 8-QAM and 8-PSK signals transmitted through AWGN, Rayleigh and Rician fading channels were presented. The simulation results indicate that the FSNVA-M detector is best-suited for AWGN, very slow Rayleigh fading and slow Rician fading channels with large ratio of specular-to-diffuse power. The FSNVA-M performs as well as the coherent detector for very slow Rayleigh, slow Rician (with large ratio of specular-to-diffuse power), and AWGN channels. For very slow Rayleigh flat-fading channels and with second-order diversity, the symbol-error-rate performance of FSNVA-M is better than MSDDVA-M by a factor of four.

The FSNVA-M is however not suitable for slow Rayleigh flat-fading channels, where the fade process varies from symbol-to-symbol. For such channels, Multiple Symbol Differential Detector for Multilevel signals (MSDDVA-M) is best suited, and performs better than conventional differential 8-PSK. In fact, for second-order diversity, the MSDDVA-M gives a better performance by about 1.6 dB compared to 8-PSK, for SER of 10^{-2} and $\rho = 0.995$. For $\rho = 0.9995$ and the same SER, the performance improvement over 8-PSK is only about 0.67 dB. However, for $\rho = 0.9995$, with second-order diversity and SER of 10^{-4}, the performance improvement of MSDDVA-M over differential 8-PSK is about 2 dB. Thus, we can also conclude that the performance improvement of MSDDVA-M over differential 8-PSK, increases with decreasing SER. It is important to note that the simulation results without diversity (first-order diversity) are only of theoretical interest, since the error-floor is rather high (2×10^{-3} for $\rho = 0.9995$, which corresponds to slower fading compared to $\rho = 0.995$), and even this floor is attained at SNR greater than 40 dB. Since in practical situations, at least second-order diversity is used, the simulation results for second-order diversity are of practical importance.

The MSDDVA-M also performs better than the other two proposed differential detectors, namely, the Symbol-by-Symbol Differential detector for Multilevel signals (SSDD-M) and the Quotient Space Viterbi Algorithm (QSVA). In fact, QSVA does not perform well in the presence of diversity, for Rayleigh flat-fading

channels.

However, QSVA performs as well as MSDDVA-M in AWGN channels at high SNR. At low SNR however, the QSVA is slightly inferior to MSDDVA-M.

The MSDDVA-M also performs as well as the Suboptimal Linear Predictor-I (SLP-I) and SLP-II for a first-order fade process at high SNR. At low SNR, the MSDDVA-M performs better than the SLP detectors. For a third-order fade process and at high SNR, the performance of the SLP detectors is two orders of magnitude better than the proposed differential detectors, including the MSDDVA-M. This is because, the SLP detectors take advantage of the memory in the prediction filter used to whiten the fade process. Moreover, the SLP detectors make no assumption that the fade process is constant over two symbol durations, unlike the differential detectors. Recall that both SSDD-M and MSDDVA-M, which are derived from the ML-UAP detector, assume that the fade process is constant over two symbol durations. Even the quotient-space approach assumes that if the fade process is constant over two symbol durations, it can be eliminated by the quotient operation at high SNR. The SLP detectors however assume that the autocovariance of the fade process is known. In practice however, due to imperfect knowledge or inaccurate estimates of the autocovariance of the fade process, there is some performance degradation in the SLP detectors. The SLP detectors also have a computational complexity that increases exponentially with the order of the prediction filter, whereas the complexity of the differential detectors proposed in this thesis is independent of the autocovariance of the fade process. Moreover at low SNR, the performance of the SLP detectors deteriorates rapidly due to noise enhancement, while the differential detectors show a more graceful degradation. In fact, at low SNR, the differential detectors perform better than the SLP detectors.

Finally, we propose the *Split Trellis* VA for Intersymbol Interference (ISI), typically encountered in wireline communications. Unlike the other detectors proposed in this thesis which are noncoherent, the Split trellis VA is a coherent detector which requires estimation of channel, carrier phase and timing. Assuming

that the channel, carrier phase and timing are known perfectly at the receiver, it has been shown that the Split Trellis approach significantly reduces the number of real multiplications in the trellis. In particular, for a channel of length Q symbols, the number of real multiplications in the conventional Whitened Matched Filter (WMF) approach is $2M^Q$ per symbol duration, for M-ary signalling. However, the Split Trellis VA requires only $2M$ real multiplications per symbol duration. The number of real additions is also reduced by nearly a factor of two, in the Split Trellis approach, compared to the WMF approach.

Future work involves extending the FSNVA-M detector to frequency-selective fading, and data estimation in the presence of co-channel interference. The viability of a "blind initialization" approach (like the per-survivor processing proposed in [RPT95]) needs to be investigated. The constellation for the proposed differential detection strategies also needs to be optimized. It may be interesting to investigate diversity combining based on the Received Signal Strength (RSS) for the differential detection techniques, though we do not expect much improvement over Equal Gain Correlation Metric Combining (EGCMC). The isometry property in the Suboptimal Linear Predictors could be used to reduce the number of states. As an example, we have shown in Appendix D how the number of trellis states can be reduced for a first-order fade process and 8-PSK signalling. The LMS algorithm can be used to reduce the noise enhancement of the SLP detectors, and improve the performance at medium and low SNR.

In summary, it is hoped that the proposed family of computationally efficient noncoherent detectors will find use in many existing wireless communication systems based on standards like IS-136, GSM, DCS-1800 and DECT, and also in emerging standards like 3G. The Split Trellis VA will find use in high bit-rate wireline communications standards such as HDSL.

APPENDIX A

Suboptimal LP-Based Detector-I (SLP-I)

In SLP-I, we take the first (zeroth) coefficient of each of the $j = 1, \ldots, M^{k+1}$ filters as unity, namely, $\tilde{a}_{k,0}^{(j)} = 1$, which is the standard assumption in linear prediction theory. Substituting for $\tilde{R}_{p,q}$ from (2.11) in (2.17), we notice that the term $\left(I_{k-p}^{(j)}\right)^*$ is common in the p^{th} row (rows are numbered from 1 to k) and can be eliminated. Thus (2.17) becomes

$$\begin{bmatrix} \mu_0 & \cdots & \mu_{k-1} \\ \vdots & \vdots & \vdots \\ \mu_{k-1} & \cdots & \mu_0 \end{bmatrix} \begin{bmatrix} \tilde{a}_{k,1}^{(j)} I_{k-1}^{(j)} \\ \vdots \\ \tilde{a}_{k,k}^{(j)} I_0^{(j)} \end{bmatrix} = -I_k^{(j)} \begin{bmatrix} \mu_1 \\ \vdots \\ \mu_k \end{bmatrix}. \tag{A.1}$$

Let $b_{k,p}$ denote the p^{th} coefficient of the optimal k^{th}-order filter for the fade process $\tilde{G}_k$ alone. That is, if

$$\tilde{e}_k = \sum_{p=0}^{k} b_{k,p}\, \tilde{G}_{k-p} \tag{A.2}$$

then $b_{k,p}$ are given by (with $b_{k,0} = 1$)

$$\begin{bmatrix} \mu_0 & \cdots & \mu_{k-1} \\ \vdots & \vdots & \vdots \\ \mu_{k-1} & \cdots & \mu_0 \end{bmatrix} \begin{bmatrix} b_{k,1} \\ \vdots \\ b_{k,k} \end{bmatrix} = - \begin{bmatrix} \mu_1 \\ \vdots \\ \mu_k \end{bmatrix}. \tag{A.3}$$

Note that $b_{k,p}$ is *real*. The prediction error variance of the fade process alone is given by [PM92]

$$\frac{1}{2} E\left[|\tilde{e}_k|^2\right] \triangleq \sigma_{e,k}^2 = \frac{1}{2} \sum_{p=0}^{k} b_{k,p}\, \mu_p. \tag{A.4}$$

From (A.1) and (A.3) we see that (note that $\tilde{a}_{k,0}^{(j)} = 1$)

$$\tilde{a}_{k,p}^{(j)} = \left(\frac{I_k^{(j)}}{I_{k-p}^{(j)}}\right) b_{k,p} \qquad \text{for } 0 \le p \le k. \tag{A.5}$$

Hence, $\tilde{y}_k^{(j)}$ in (2.14) is given by

$$\tilde{y}_k^{(j)} = \sum_{p=0}^{k} \left(\frac{I_k^{(j)}}{I_{k-p}^{(j)}}\right) b_{k,p}\, \tilde{r}_{k-p} \tag{A.6}$$

where we have substituted for $\tilde{a}_{k,p}^{(j)}$ from (A.5). The average conditional prediction error variance is given by [PM92] (note that $\tilde{a}_{k,0}^{(j)} = 1$)

$$\frac{1}{2}E\left[\left|\tilde{y}_k^{(j)}\right|^2\right] \triangleq \left(\sigma_{y,k}^{(j)}\right)^2 = \frac{1}{2}\sum_{p=0}^{k} \tilde{a}_{k,p}^{(j)}\, \tilde{R}_{k-p,k} \tag{A.7}$$

where $\left(\sigma_{y,k}^{(j)}\right)^2$ denotes the prediction error variance of the optimal k^{th}-order predictor, given that the j^{th} sequence is transmitted. Substituting for $\tilde{R}_{p,q}$ from (2.11) and $\tilde{a}_{k,p}^{(j)}$ from (A.5) in the above equation and making use of the approximation in (2.16) we get

$$\left(\sigma_{y,k}^{(j)}\right)^2 = \frac{1}{2}\left|I_k^{(j)}\right|^2 \sum_{p=0}^{k} b_{k,p}\,\mu_p = \left|I_k^{(j)}\right|^2 \sigma_{e,k}^2 \tag{A.8}$$

where $\sigma_{e,k}^2$ is given in (A.4).

We now have the $L \times 1$ conditional prediction error vector given by

$$\begin{bmatrix} 1 & 0 & \dots & 0 \\ \tilde{a}_{1,1}^{(j)} & 1 & \dots & 0 \\ \vdots & \vdots & \vdots & \vdots \\ \tilde{a}_{L-1,L-1}^{(j)} & \tilde{a}_{L-1,L-2}^{(j)} & \dots & 1 \end{bmatrix} \begin{bmatrix} \tilde{r}_0 \\ \tilde{r}_1 \\ \vdots \\ \tilde{r}_{L-1} \end{bmatrix} = \begin{bmatrix} \tilde{y}_0^{(j)} \\ \tilde{y}_1^{(j)} \\ \vdots \\ \tilde{y}_{L-1}^{(j)} \end{bmatrix} \triangleq \tilde{\mathbf{y}}^{(j)}. \tag{A.9}$$

From linear prediction theory [PM92], the elements of $\tilde{\mathbf{y}}^{(j)}$ are mutually orthogonal in the statistical sense, that is

$$\frac{1}{2}E\left[\tilde{y}_k^{(j)}\left(\tilde{y}_l^{(j)}\right)^*\right] = \begin{cases} \left(\sigma_{y,k}^{(j)}\right)^2 & \text{for } k = l,\ 0 \le k,l \le L-1 \\ 0 & \text{for } k \ne l,\ 0 \le k,l \le L-1 \end{cases} \tag{A.10}$$

where $\sigma_{y,k}^{(j)}$ is given by (A.8). The conditional mean of the elements of $\tilde{\mathbf{y}}^{(j)}$, given that the j^{th} sequence has been transmitted, is given by

$$E\left[\tilde{y}_k^{(j)}\right] = \sum_{p=0}^{k} \tilde{a}_{k,p}^{(j)} E\left[\tilde{r}_{k-p}|\tilde{\mathbf{S}}^{(j)}\right] = 0. \tag{A.11}$$

Since the transformation in (A.9) is linear, the elements of $\tilde{\mathbf{y}}^{(j)}$ are Gaussian and are also jointly Gaussian. Thus, the maximization in (2.8) is equivalent to maximizing the joint conditional pdf

$$\max_j f\left(\tilde{\mathbf{y}}|\tilde{\mathbf{S}}^{(j)}\right) \triangleq \max_j f\left(\tilde{\mathbf{y}}^{(j)}\right). \tag{A.12}$$

Substituting for the conditional pdf in the above equation, we get

$$\max_j \frac{1}{(2\pi)^L \det\left(\tilde{\mathbf{R}}_2^{(j)}\right)} \exp\left[-\frac{1}{2}\left(\tilde{\mathbf{y}}^{(j)}\right)^H \left(\tilde{\mathbf{R}}_2^{(j)}\right)^{-1} \tilde{\mathbf{y}}^{(j)}\right] \tag{A.13}$$

where $\tilde{\mathbf{R}}_2^{(j)}$ is the $L \times L$ conditional autocovariance matrix containing only diagonal elements and is given by

$$\frac{1}{2}E\left[\tilde{\mathbf{y}}^{(j)}\left(\tilde{\mathbf{y}}^{(j)}\right)^H\right] \triangleq \tilde{\mathbf{R}}_2^{(j)} = \begin{bmatrix} \left(\sigma_{y,0}^{(j)}\right)^2 & \dots & 0 \\ \vdots & \vdots & 0 \\ 0 & \dots & \left(\sigma_{y,L-1}^{(j)}\right)^2 \end{bmatrix}. \tag{A.14}$$

Simplifying (A.13) we get

$$\max_j \frac{1}{(2\pi)^L \prod_{k=0}^{L-1}\left(\sigma_{y,k}^{(j)}\right)^2} \exp\left[-\frac{1}{2}\sum_{k=0}^{L-1}\frac{\left|\tilde{y}_k^{(j)}\right|^2}{\left(\sigma_{y,k}^{(j)}\right)^2}\right] \tag{A.15}$$

which can be further simplified to

$$\max_j \prod_{k=0}^{L-1}\frac{1}{\left(\sigma_{y,k}^{(j)}\right)^2} \exp\left[-\frac{\left|\tilde{y}_k^{(j)}\right|^2}{2\left(\sigma_{y,k}^{(j)}\right)^2}\right]. \tag{A.16}$$

Taking the natural logarithm of the above equation we finally get the SLP-I detector as

$$\min_j \sum_{k=0}^{L-1}\frac{\left|\tilde{y}_k^{(j)}\right|^2}{2\left(\sigma_{y,k}^{(j)}\right)^2} + \ln\left[\left(\sigma_{y,k}^{(j)}\right)^2\right] \tag{A.17}$$

which can now be implemented recursively.

Now, if $\tilde{G}_k$ in (2.1) is an Auto Regressive (AR) process of a finite order, say $\mathcal{P} \ll L$, then $\sigma_{e,k}^2$ attains the minimum value of $\sigma_{e,\mathcal{P}}^2$ for $k \geq P$. In such a situation, we can ignore the "transient" part of the above equation ($k < \mathcal{P}$) and consider only the "steady-state" part ($k \geq \mathcal{P}$). Thus, substituting for $\sigma_{y,k}^{(j)}$ from (A.8), the SLP-I detector can be approximated as

$$\min_j \sum_{k=\mathcal{P}}^{L-1}\frac{\left|\tilde{y}_k^{(j)}\right|^2}{2\left|I_k^{(j)}\right|^2\sigma_{e,\mathcal{P}}^2} + \ln\left[\left|I_k^{(j)}\right|^2\sigma_{e,\mathcal{P}}^2\right]. \tag{A.18}$$

It is clear from the above equation that the SLP-I detector requires knowledge of $\sigma_{e,\mathcal{P}}^2$. Theoretically, $\sigma_{e,\mathcal{P}}^2$ can be estimated from (A.4), for $k = \mathcal{P}$. From a practical point of view, we only know the autocovariance *model* and not the *exact*

autocovariance. For example, the autocovariance of the land-mobile fade model is popularly modelled as the zeroth-order Bessel function of the first kind [DS94], and is denoted by $J_0(\cdot)$. Hence, while the assumed autocovariance *model*, i.e. $J_0(\cdot)$, may be correct, the actual autocovariance is usually $cJ_0(\cdot)$, where c is a real constant which has to be estimated. Therefore, the estimation of $\sigma^2_{e,\mathcal{P}}$ is vital. It is important to note however that the predictor coefficients $b_{k,p}$ in (A.2) are *independent* of c. In the next subsection, we present the SLP-II detector, which does not require knowledge of $\sigma^2_{e,\mathcal{P}}$.

It is interesting to note that for M-ary PSK signalling, (A.18) reduces to

$$\min_j \sum_{k=\mathcal{P}}^{L-1} \left|\tilde{y}_k^{(j)}\right|^2. \tag{A.19}$$

In the presence of diversity, the SLP-I detector sums the squared prediction error from all the diversity arms. Hence (A.18) becomes

$$\min_j \sum_{k=\mathcal{P}}^{L-1} \sum_{l=1}^{\mathcal{D}} \left(\frac{\left|\tilde{y}_{k,l}^{(j)}\right|^2}{2\left|I_k^{(j)}\right|^2 \sigma^2_{e,\mathcal{P}}} + \ln\left[\left|I_k^{(j)}\right|^2 \sigma^2_{e,\mathcal{P}}\right] \right) \tag{A.20}$$

where

$$\tilde{y}_{k,l}^{(j)} = \sum_{p=0}^{k} \tilde{a}_{k,p}^{(j)}\, \tilde{r}_{k-p,l} \qquad \text{for } 0 \le k \le L-1,\ 1 \le l \le \mathcal{D} \tag{A.21}$$

is the prediction error from the l^{th} diversity arm and $\tilde{r}_{k-p,l}$ is the received sample at time $k-p$ in the l^{th} diversity arm. In the literature, many other ways of doing diversity combining have been proposed [Cox87]. We have not investigated the viability of any of these other approaches for the problem at hand.

APPENDIX B

Suboptimal LP-Based Detector-II (SLP-II)

In SLP-II, we assume that $\tilde{a}_{k,0}^{(j)} = 1/I_k^{(j)}$. As in the case of SLP-I, we substitute for $\tilde{R}_{p,q}$ from (2.11) in (2.17). We note that the term $\left(I_{k-p}^{(j)}\right)^*$ is common in the p^{th} row (rows are numbered from 1 to k) and can be eliminated. Thus (2.17) becomes

$$\begin{bmatrix} \mu_0 & \dots & \mu_{k-1} \\ \vdots & \vdots & \vdots \\ \mu_{k-1} & \dots & \mu_0 \end{bmatrix} \begin{bmatrix} \tilde{a}_{k,1}^{(j)} I_{k-1}^{(j)} \\ \vdots \\ \tilde{a}_{k,k}^{(j)} I_0^{(j)} \end{bmatrix} = - \begin{bmatrix} \mu_1 \\ \vdots \\ \mu_k \end{bmatrix}. \tag{B.1}$$

From the above equation and (A.3), it is easy to see that

$$\tilde{a}_{k,p}^{(j)} = \left(\frac{1}{I_{k-p}^{(j)}}\right) b_{k,p} \qquad \text{for } 0 \le p \le k \tag{B.2}$$

where $b_{k,0} = 1$. The average conditional prediction error variance given that the sequence $\tilde{\mathbf{S}}^{(j)}$ is transmitted, can be written as [PM92] (with $\tilde{a}_{k,0}^{(j)} = 1/I_k^{(j)}$)

$$\frac{1}{2} E\left[\left|\tilde{z}_k^{(j)}\right|^2\right] \triangleq \left(\sigma_{z,k}^{(j)}\right)^2 = \frac{1}{2}\left(\tilde{a}_{k,0}^{(j)}\right)^* \sum_{p=0}^{k} \tilde{a}_{k,p}^{(j)} \tilde{R}_{k-p,k} \tag{B.3}$$

where we have denoted the prediction error as $\tilde{z}_k^{(j)}$ to distinguish it from the prediction error $\tilde{y}_k^{(j)}$ of the SLP-I detector. Substituting for $\tilde{R}_{p,q}$ from (2.11) and $\tilde{a}_{k,p}^{(j)}$ from (B.2) in the above equation and making use of the approximation in (2.16), we get

$$\left(\sigma_{z,k}^{(j)}\right)^2 = \frac{1}{2} \sum_{p=0}^{k} b_{k,p}\, \mu_p = \sigma_{e,k}^2 \tag{B.4}$$

where $\sigma_{e,k}^2$ is given in (A.4). From the above equation, we see that the conditional prediction error is *independent* of $\tilde{\mathbf{S}}^{(j)}$.

We now have the conditional prediction error vector given by

$$\begin{bmatrix} 1/I_0^{(j)} & 0 & \dots & 0 \\ \tilde{a}_{1,1}^{(j)} & 1/I_1^{(j)} & \dots & 0 \\ \vdots & \vdots & \vdots & \vdots \\ \tilde{a}_{L-1,L-1}^{(j)} & \tilde{a}_{L-1,L-2}^{(j)} & \dots & 1/I_{L-1}^{(j)} \end{bmatrix} \begin{bmatrix} \tilde{r}_0 \\ \tilde{r}_1 \\ \vdots \\ \tilde{r}_{L-1} \end{bmatrix} = \begin{bmatrix} \tilde{z}_0^{(j)} \\ \tilde{z}_1^{(j)} \\ \vdots \\ \tilde{z}_{L-1}^{(j)} \end{bmatrix} \triangleq \tilde{\mathbf{z}}^{(j)}. \tag{B.5}$$

The conditional autocovariance of $\tilde{\mathbf{z}}^{(j)}$, given that $\tilde{\mathbf{S}}^{(j)}$ is transmitted, is given by the $L \times L$ diagonal matrix

$$\frac{1}{2} E\left[\tilde{\mathbf{z}}^{(j)} \left(\tilde{\mathbf{z}}^{(j)}\right)^H\right] = \begin{bmatrix} \sigma^2_{e,\,0} & \dots & 0 \\ \vdots & \vdots & 0 \\ 0 & \dots & \sigma^2_{e,\,L-1} \end{bmatrix}. \tag{B.6}$$

Proceeding as in the case of SLP-I, the SLP-II detector can be written as

$$\min_j \sum_{k=0}^{L-1} \frac{\left|\tilde{z}^{(j)}_k\right|^2}{2\sigma^2_{e,\,k}} + \ln\left(\sigma^2_{e,\,k}\right). \tag{B.7}$$

Now, if $\tilde{G}_k$ in (2.1) is an Auto Regressive (AR) process of a finite order, say $\mathcal{P} \ll L$, then $\sigma^2_{e,\,k}$ attains the minimum value of $\sigma^2_{e,\,\mathcal{P}}$ for $k \geq \mathcal{P}$. Once again in such a situation, we can ignore the transient part of the above equation ($k < \mathcal{P}$) and consider only the steady-state part ($k \geq \mathcal{P}$). Thus the SLP-II detector can be approximated as

$$\min_j \sum_{k=\mathcal{P}}^{L-1} \frac{\left|\tilde{z}^{(j)}_k\right|^2}{2\sigma^2_{e,\,\mathcal{P}}} + \ln\left(\sigma^2_{e,\,\mathcal{P}}\right) \tag{B.8}$$

which is equivalent to

$$\min_j \sum_{k=\mathcal{P}}^{L-1} \left|\tilde{z}^{(j)}_k\right|^2. \tag{B.9}$$

Thus, we find that unlike the SLP-I detector, the SLP-II detector does not require the estimation of $\sigma^2_{e,\,\mathcal{P}}$.

In the presence of diversity, the SLP-II detector sums the squared prediction error from all the diversity arms. Hence (B.9) becomes

$$\min_j \sum_{k=\mathcal{P}}^{L-1} \sum_{l=1}^{\mathcal{D}} \left|\tilde{z}^{(j)}_{k,\,l}\right|^2 \tag{B.10}$$

where

$$\tilde{z}^{(j)}_{k,\,l} = \sum_{p=0}^{k} \tilde{a}^{(j)}_{k,\,p}\, \tilde{r}_{k-p,\,l} \qquad \text{for } 0 \leq k \leq L-1,\ 1 \leq l \leq \mathcal{D} \tag{B.11}$$

is the prediction error from the l^{th} diversity arm. We have not investigated the other diversity techniques.

APPENDIX C

Isometry in SLP-I and SLP-II Detection

Here we show that differential encoding is necessary to overcome the problem of *isometry* in SLP-I and SLP-II. Though the concept of isometry is not new [VT95], it has not been exploited earlier to reduce the complexity of LP-based detection. In this appendix, we discuss the possibility of deriving such low-complexity, LP-based detectors.

Both SLP-I and SLP-II detection involves computing the squared prediction error. Let us now consider a $\mathcal{P}^{th}$-order predictor. Under steady-state conditions ($k \geq \mathcal{P}$) we have

$$\tilde{y}_k^{(j)} = \sum_{p=0}^{\mathcal{P}} \tilde{a}_{\mathcal{P},p}^{(j)} \tilde{r}_{k-p}. \tag{C.1}$$

For the SLP-I detector, $\tilde{a}_{\mathcal{P},p}^{(j)}$ is given by (A.5). Now, the regular M-ary QAM constellations and M-ary PSK constellations are invariant to certain discrete phase rotations. For example, M-ary QAM constellations are usually invariant to rotations that are an integer multiple of 90^o. Since the predictor coefficients in the above equation depend on the ratio of two symbols, they are also insensitive to phase rotation. In other words, two sets of symbols rotated by the same amount, yield the same predictor coefficients, and hence the same value of $\tilde{y}_k^{(j)}$, resulting in *isometry*. Thus, the SLP-I detector cannot differentiate between rotated versions of the symbol sequence. Hence, the symbols must be differentially encoded into *phase changes* (and *amplitude changes*, in the case of QAM), in order to recover the symbols at the receiver without any ambiguity.

In the case of the SLP-II detector, the predictor coefficients are given by (B.2). In this case, the predictor coefficients are sensitive to phase rotations of the symbols, which implies that the prediction error is also sensitive to phase rotations. However, the square of the prediction error (which is propagated in (B.9)) is insensitive to phase rotations, which results in isometry. Hence differential encoding is required to overcome this problem.

There is also another problem associated with the SLP-II detector. We illustrate this problem with an example. Let us consider 16-QAM signalling and let us assume that a continuous sequence of the complex symbol $1 + \mathrm{j}$ has been transmitted. At the receiver, the SLP-II detector decides in favour of the minimum accumulated squared prediction error, as given by (B.9). However, it is easy to see that the prediction error corresponding to a continuous sequence of $3 + \mathrm{j}3$, which is a valid symbol in the 16-QAM constellation, is *less* than that of a continuous sequence of $1 + \mathrm{j}$. In other words, substituting $I_{k-p}^{(j)} = 3 + \mathrm{j}3$ in (B.2) yields a lower prediction error than $I_{k-p}^{(j)} = 1 + \mathrm{j}$. Thus the SLP-II detector incorrectly decides in favour of the all $3 + \mathrm{j}3$ sequence. This problem can again be overcome by appropriate differential encoding. For example, if the differential encoding rules state that an input (uncoded) symbol number 0 (symbol numbers vary from 0 to 15, for 16-QAM signalling) does not result in either a phase change or an amplitude change, then the all $3 + \mathrm{j}3$ sequence will be differentially decoded as an all 0 input sequence. In fact, any continuous sequence of *identical* symbols corresponding to $I_{k-p}^{(j)}$ will be correctly decoded as the all 0 input sequence, *irrespective of the amplitude* of the symbols corresponding to $I_{k-p}^{(j)}$.

APPENDIX D

First-Order SLP Detectors for M-ary PSK

In this Appendix, we show that SLP-I and SLP-II become identical for M-ary PSK signalling. We also show that when $\tilde{G}_k$ in (1.8) is a first-order Auto Regressive (AR) process, SLP-I and SLP-II reduce to conventional symbol-by-symbol differential detection, for M-ary PSK signalling.

The complexity of the SLP-I and the SLP-II detectors increases exponentially with the order of the prediction filter. For a prediction filter of order $\mathcal{P}$ and M-ary signalling, the number of trellis states is equal to $M^{\mathcal{P}}$ [YP95]. We now show that for first-order prediction ($\mathcal{P} = 1$), the SLP detectors (both I and II) reduce to the conventional symbol-by-symbol differential detector for M-ary PSK, instead of requiring an M-state trellis. The proof involves three steps.

In the first step we prove that both SLP-I and SLP-II detectors are identical for M-PSK signalling, under steady-state conditions. Thus, we only need to prove that for a first-order prediction filter, the SLP-I detector reduces to the conventional symbol-by-symbol differential detector for M-ary PSK. A separate proof is not required for the SLP-II detector. The second step is to prove that computing the branch metric in the trellis is identical to symbol-by-symbol differential detection. In the third step, we show that by propagating the *survivor* branch metrics, all the trellis states have identical metrics, and hence can be merged into a single state, which reduces to symbol-by-symbol detection. Thus, due to steps 2 and 3, the overall detector reduces to a symbol-by-symbol differential detector. We now prove step 1, that is, SLP-I is identical to SLP-II for M-ary PSK signalling.

From (A.19) and (B.9) we find that the detection technique for both SLP-I and SLP-II are similar, only the prediction error is computed differently. We now show that the square of the prediction error for SLP-I and SLP-II are related by a constant. For SLP-I we have

$$\left|\tilde{y}_k^{(j)}\right|^2 = \left|\sum_{p=0}^{k} \frac{I_k^{(j)}}{I_{k-p}^{(j)}} b_p \tilde{r}_{k-p}\right|^2 \tag{D.1}$$

For SLP-II we have

$$\left|\tilde{z}_k^{(j)}\right|^2 = \left|\sum_{p=0}^{k} \frac{1}{I_{k-p}^{(j)}} b_p \tilde{r}_{k-p}\right|^2 \tag{D.2}$$

which is equivalent to

$$\left|\tilde{z}_k^{(j)}\right|^2 = \frac{1}{\left|I_k^{(j)}\right|^2} \left|\tilde{y}_k^{(j)}\right|^2. \tag{D.3}$$

Since $\left|I_k^{(j)}\right|^2$ is constant for M-ary PSK, it can be ignored. Thus, minimizing (A.19) is equivalent to minimizing (B.9) for M-ary PSK, and thus, SLP-I and SLP-II are equivalent.

We now prove that the branch metric computation in SLP-I (which is nothing but the computation of $\left|\tilde{y}_k^{(j)}\right|^2$ in the trellis) is identical to the symbol-by-symbol differential detector for M-ary PSK. We assume that $\tilde{G}_k$ in (2.1) is a 1^{st}-order AR process, which is obtained by exciting a 1^{st}-order IIR filter with a white Gaussian process. The transfer function of the IIR filter is of the form

$$H(z) = \frac{1}{1 - \rho z^{-1}} \tag{D.4}$$

where ρ is a real positive constant less than unity. This is similar to the fade model in (5.2). The corresponding branch prediction error of the SLP-I detector is given by

$$\tilde{y}_k^{(j)} = \tilde{r}_k - \rho \left(\frac{I_k^{(j)}}{I_{k-1}^{(j)}}\right) \tilde{r}_{k-1} \tag{D.5}$$

Minimizing the squared prediction error $\left|\tilde{y}_k^{(j)}\right|^2$ is equivalent to

$$\max_j \left|\tilde{Y}_k^{(j)}\right|^2 = \Re\left\{\tilde{r}_k r_{k-1}^* I_{k-1}^{(j)} \left(I_k^{(j)}\right)^*\right\} \tag{D.6}$$

which is *independent* of ρ and $\Re\{\cdot\}$ denotes the real-part. Note that $\left|\tilde{Y}_k^{(j)}\right|^2$ has to be *maximized*, as opposed to the *minimization* of $\left|\tilde{y}_k^{(j)}\right|^2$. In the above equation, we have used the fact that for M-ary PSK, $I_k^{(j)}/I_{k-1}^{(j)} = I_k^{(j)} \left(I_{k-1}^{(j)}\right)^*$. It is clear that the above equation is identical to that of symbol-by-symbol differential detection for M-ary PSK. This proves step 2.

In the third step, we prove that all the M states have identical survivor metrics and can be merged into a single state. The proof involves an exhaustive verification of the surviving metrics at each trellis state. This can be done only by computer

simulation. However, here we present the outline of the proof. We consider 8-PSK signalling for the purpose of illustration. The trellis has eight states, as shown in Figure D.1. All the transitions are not shown for the sake of clarity. Each state corresponds to a symbol in the PSK constellation. The states as well as the symbols are numbered from 0 to 7. Let us start from time $k = 0$ and assume that two consecutive transmitted symbols numbers are 3 and 7. If the detector does not make an error, then the surviving metric at state # 7 at time $k = 1$, is due to the transition from state # 3, at time 0. The surviving metric at state # 7 is dependent only on the *phase difference* between symbol # 7 and symbol # 3 (which is equal to $(2\pi \cdot 4/8)$). This is clear from (D.6). Due to isometry, the surviving metric at state # 0 at time $k = 1$ is due to the transition from state # 4 at time $k = 0$, and its value is exactly equal to the surviving metric at state # 7. Similarly, it is easy to show that the surviving metrics at the remaining states are all identical. By proceeding recursively in time, it is easy to see that all states have identical metrics and thus can be merged into a single state, which is equivalent to symbol-by-symbol detection.

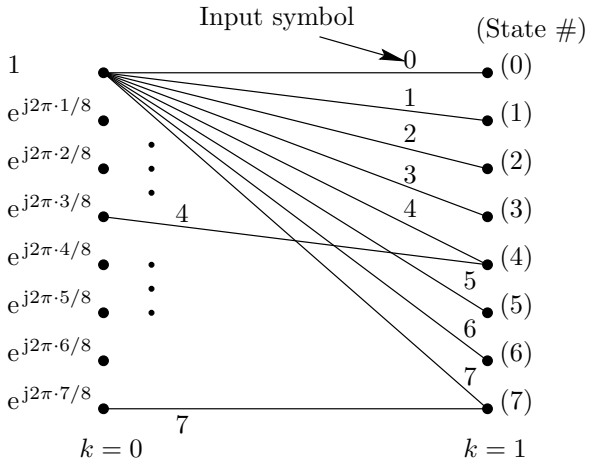

Figure D.1: Trellis for LP-based detection of 8-PSK.

Even if the detector makes an error (due to the presence of noise and fading) and the surviving (maximum) metric is due to a transition from an incorrect state, then due to isometry, all the other states will also have the same maximum metric. The phase difference between two states corresponding to the surviving transitions will also be identical. For example, let us assume that the receiver makes an error

and the surviving (maximum) metric at state # 7 at time $k = 1$, is due to a transition from state # 1 at time $k = 0$. The phase difference between state # 7 and state # 1 is equal to $(2\pi \cdot 6/8)$. The surviving metric at state # 0 at time $k = 1$, is due to a transition from state # 2 at time $k = 0$ (note that the phase difference between state # 0 and state # 2 is equal to $(2\pi \cdot 6/8)$). Moreover, due to isometry, the surviving metric at state # 0 has the same value as the surviving metric at state # 7. It is easy to show that due to isometry, the surviving metrics at the remaining states are identical. The proof for M-ary PSK is identical.

An interesting situation occurs when the transfer function of the IIR filter is of the form

$$H(z) = \frac{1}{1 + \rho z^{-1}} \tag{D.7}$$

where ρ is a real positive constant less than unity. In this case, the branch prediction error of the SLP-I detector is given by

$$\tilde{y}_k^{(j)} = \tilde{r}_k + \rho \left(\frac{I_k^{(j)}}{I_{k-1}^{(j)}} \right) \tilde{r}_{k-1}. \tag{D.8}$$

Minimizing the squared prediction error $\left| \tilde{y}_k^{(j)} \right|^2$ is equivalent to

$$\min_j \left| \tilde{Y}_k^{(j)} \right|^2 = \Re \left\{ \tilde{r}_k r_{k-1}^* I_{k-1}^{(j)} \left(I_k^{(j)} \right)^* \right\}. \tag{D.9}$$

Note that the conventional symbol-by-symbol differential detector for M-ary PSK is still given by (D.6) where $\left| \tilde{Y}_k^{(j)} \right|^2$ is *maximized*, as opposed to the *minimization* in the above equation. Hence the symbol-by-symbol differential detector is expected to give a significantly inferior performance, compared to SLP-I. This is confirmed from computer simulations.

In Table D.1, we show the simulated performance of the SLP detectors and the conventional differential detector for 8-PSK, when the fade model is given by (D.4). The SLP detectors have eight states and the detection delay was taken as ten symbols. We find that the performance is identical, as expected. However, for the fade model given by (D.7) the differential detector fails as expected. This is illustrated in Table D.2.

Table D.1: Simulation results for a Rayleigh fading channel. 1^{st}-order fade process given by (D.4), $\rho = 0.9995$.

Average SNR per bit (dB)	Symbol-error-rate	
	SLP-I (SLP-II)	Differential 8-PSK
Infinity	3.2×10^{-3}	3.2×10^{-3}
49	3.3×10^{-3}	3.3×10^{-3}
39	3.5×10^{-3}	3.5×10^{-3}
29	6.0×10^{-3}	6.0×10^{-3}
19	3.0×10^{-2}	3.0×10^{-2}

Table D.2: Simulation results for a Rayleigh fading channel. 1^{st}-order fade process given by (D.7), $\rho = 0.9995$.

Average SNR per bit (dB)	Symbol-error-rate	
	SLP-I (SLP-II)	Differential 8-PSK
Infinity	3.2×10^{-3}	9.0×10^{-1}
49	3.2×10^{-3}	9.0×10^{-1}
39	3.5×10^{-3}	9.0×10^{-1}
29	5.9×10^{-3}	9.0×10^{-1}
19	2.9×10^{-2}	9.0×10^{-1}

APPENDIX E

Probability of an Error Event for SNVA-M in AWGN

Here we derive the probability of an error event for the SNVA-M at high SNR in an AWGN channel. We assume that the received signal is given by (3.1). For notational convenience, we drop the subscript "1" in G_1 and ϕ_1. In the presence of noise, the correlation metric $\eta_{N+D}^{(i)}$ is given by

$$\eta_{N+D}^{(i)} = \frac{\left|GS^{(i)}\mathrm{e}^{\mathrm{j}\phi} + w_{0I} + \mathrm{j}\, w_{0Q} + GE^{(i)}\mathrm{e}^{\mathrm{j}\phi} + w_{1I} + \mathrm{j}\, w_{1Q}\right|^2}{S^{(i)} + E^{(i)}} \tag{E.1}$$

where $S^{(i)}$ and $E^{(i)}$ are as defined in (3.45),

$$\begin{aligned} w_{0I} + \mathrm{j}\, w_{0Q} &= \sum_{k=0}^{N-1} \tilde{w}_k \left(I_k^{(i)}\right)^* \\ w_{1I} + \mathrm{j}\, w_{1Q} &= \sum_{k=N}^{N+D-1} \tilde{w}_k \left(I_k^{(i)}\right)^* \end{aligned} \tag{E.2}$$

and $\tilde{w}_k$ is the noise term in (3.1). We now make the following assumptions:

$$S^{(i)} \gg E^{(i)}; \qquad S^{(i)} \gg |w_{0I} + \mathrm{j}\, w_{0Q}|^2 \qquad \text{and} \qquad S^{(i)} \gg |w_{1I} + \mathrm{j}\, w_{1Q}|^2. \tag{E.3}$$

The first assumption is valid for $N \gg D$. The last two assumptions are valid for high SNR. Using the above assumptions and after some simplifications we get

$$\begin{aligned} \eta_{N+D}^{(i)} \approx\ & G^2 S^{(i)} \Bigg[1 + \frac{E^{(i)}}{S^{(i)}} \\ & + \frac{2}{GS^{(i)}}(w_{0I}\cos(\phi) + w_{0Q}\sin(\phi)) \\ & + \frac{2}{GS^{(i)}}(w_{1I}\cos(\phi) + w_{1Q}\sin(\phi))\Bigg]. \end{aligned} \tag{E.4}$$

In the case of a coherent VA, where G and ϕ are known, the metric (say ξ) is given by

$$\xi_{N+D}^{(i)} = 2\Re\left\{\sum_{k=0}^{N+D-1} \tilde{r}_k \left(I_k^{(i)}\right)^* G\mathrm{e}^{-\mathrm{j}\phi}\right\} - G^2 \sum_{k=0}^{N+D-1} \left|I_k^{(i)}\right|^2. \tag{E.5}$$

Noting that $\tilde{r}_k = G\mathrm{e}^{\mathrm{j}\phi} I_k + \tilde{w}_k$, the above equation becomes

$$\begin{aligned}\xi_{N+D}^{(i)} &= G^2 S^{(i)} + G^2 E^{(i)} \\ &\quad + 2G\left[w_{0I}\cos(\phi) + w_{0Q}\sin(\phi)\right] \\ &\quad + 2G\left[w_{1I}\cos(\phi) + w_{1Q}\sin(\phi)\right] \end{aligned} \tag{E.6}$$

which is identical to the correlation metric in (E.4).

Similarly we have

$$\eta_{N+D}^{(j)} = \frac{\left|GS^{(i)}\mathrm{e}^{\mathrm{j}\phi} + w_{0I} + \mathrm{j}\, w_{0Q} + GE^{(ij)}\mathrm{e}^{\mathrm{j}(\phi+\phi_0)} + w_{2I} + \mathrm{j}\, w_{2Q}\right|^2}{S^{(i)} + E^{(j)}} \tag{E.7}$$

where $E^{(j)}$ is defined in (3.45) and

$$\begin{aligned} w_{2I} + \mathrm{j}\, w_{2Q} &= \sum_{k=N}^{N+D-1} \tilde{w}_k \left(I_k^{(j)}\right)^* \\ E_{ij} &= \sqrt{\left(X^{(ij)}\right)^2 + \left(Y^{(ij)}\right)^2} \\ \phi_0 &= \arctan\left(\frac{Y^{(ij)}}{X^{(ij)}}\right) \end{aligned} \tag{E.8}$$

and $X^{(ij)} + \mathrm{j}\, Y^{(ij)}$ is defined in (3.45). Again using the assumptions in (E.3) and simplifying we get

$$\begin{aligned}\eta_{N+D}^{(j)} &\approx G^2 S^{(i)}\left[1 + \frac{2}{S^{(i)}}E^{(ij)}\cos(\phi_0) - \frac{E^{(j)}}{S^{(i)}}\right. \\ &\quad + \frac{2}{GS^{(i)}}(w_{0I}\cos(\phi) + w_{0Q}\sin(\phi)) \\ &\quad \left. + \frac{2}{GS^{(i)}}(w_{2I}\cos(\phi) + w_{2Q}\sin(\phi))\right]. \end{aligned} \tag{E.9}$$

Again, in the case of a coherent VA, the corresponding metric is given by

$$\begin{aligned}\xi_{N+D}^{(j)} &= 2\Re\left\{\sum_{k=0}^{N-1}\tilde{r}_k\left(I_k^{(i)}\right)^* G\mathrm{e}^{-\mathrm{j}\phi} + \sum_{k=N}^{N+D-1}\tilde{r}_k\left(I_k^{(j)}\right)^* G\mathrm{e}^{-\mathrm{j}\phi}\right\} \\ &\quad - G^2\sum_{k=0}^{N-1}\left|I_k^{(i)}\right|^2 - G^2\sum_{k=N}^{N+D-1}\left|I_k^{(j)}\right|^2. \end{aligned} \tag{E.10}$$

Substituting for $\tilde{r}_k$ we find that $\xi_{N+D}^{(j)}$ becomes

$$\begin{aligned}\xi_{N+D}^{(j)} &= G^2 S^{(i)} + 2G^2 E^{(ij)}\cos(\phi_0) - G^2 E^{(j)} \\ &\quad + 2G\left[w_{0I}\cos(\phi) + w_{0Q}\sin(\phi)\right] \\ &\quad + 2G\left[w_{2I}\cos(\phi) + w_{2Q}\sin(\phi)\right] \end{aligned} \tag{E.11}$$

which is again identical to the correlation metric in (E.9). Thus we observe that the correlation metric is approximately equal to the corresponding coherent metric at high SNR, when the accumulated correlation metric corresponding to the correct path is high.

Note that $\eta_{N+D}^{(i)}$ and $\eta_{N+D}^{(j)}$ in (E.4) and (E.9) respectively are Gaussian random variables. We now define

$$Z \triangleq \eta_{N+D}^{(i)} - \eta_{N+D}^{(j)}. \tag{E.12}$$

It is easy to see that

$$E[Z] = m_Z = d_c^2(i,j) \tag{E.13}$$

where $d_c^2(i,j)$ is given in (3.48). The variance of Z is given by

$$\begin{aligned} E[(Z-m_Z)^2] = \sigma_Z^2 &= 4G^2 E\left[(w_{1I}\cos(\phi) + w_{1Q}\sin(\phi)\right. \\ &\quad \left. - w_{2I}\cos(\phi) - w_{2Q}\sin(\phi))^2\right]. \end{aligned} \tag{E.14}$$

Substituting for the noise terms from (E.2) and (E.8) and noting that the in-phase and quadrature components of $\tilde{w}_k$, defined in (3.1) are self and mutually-uncorrelated, σ_Z^2 reduces to

$$\sigma_Z^2 = 4d_c^2(i,j)\sigma_w^2 \tag{E.15}$$

where $d_c^2(i,j)$ is defined in (3.48) and σ_w^2 is the variance of the in-phase and quadrature components of $\tilde{w}_k$. The probability of the error event given that the sequence i was transmitted, is now equal to $P[Z<0|i]$ and it is easy to see that

$$P[Z<0|i] = \frac{1}{2}\text{erfc}\left(\sqrt{\frac{d_c^2(i,j)}{8\sigma_w^2}}\right). \tag{E.16}$$

Note that (E.16) is also the probability of the error event when coherent detection is employed (G and ϕ are known at the receiver). Thus we find that for an AWGN channel, the probability of an error event for the SNVA-M detector is identical to that of a coherent receiver at high SNR. Moreover, since the coherent detector and the SNVA-M detector use the same trellis for detecting the data, we also expect the symbol-error-probability to be identical.

Table E.1: Results showing the near-optimality of SNVA-M at high SNR and suboptimality of SNVA-M at low SNR.

Average SNR per bit (dB)	$\phi = 0$		
	1	2	3
10.5	2.2×10^{-4}	2.2×10^{-4}	5
3	1.5×10^{-1}	1.5×10^{-1}	101971

1 - Symbol-error-rate of SNVA-M ($\gamma = 1$)
2 - Symbol-error-rate of coherent detector
3 - Number of symbols in which the survivor sequences of SNVA-M and coherent detectors differ (out of 10^7 symbols)

In Table E.1, we compare the performance of SNVA-M (with $\gamma = 1$) with a coherent detector for a phase offset of $\phi = 0$ in (5.12). We find that the symbol-error-rates of SNVA-M and the coherent detector are comparable even at an SNR of 2.95 dB. In fact, the difference in symbol-error-rates is 0.24% at an SNR of 2.95 dB, and only 0.04% at an SNR of 10.53 dB. However, the SNVA-M is suboptimal at low SNR because, there is a significant increase in the number symbols in which the survivor sequences of the SNVA-M and the coherent detectors differ. In other words, the survivor sequence of the SNVA-M deviates significantly from the Maximum Likelihood sequence of the coherent detector (although their error-rates are equal). This is clear from the column numbered 3 in Table E.1. Similar results were obtained for other phase offsets.

REFERENCES

[AAS86] J. B. Anderson, T. Aulin, and C. E. Sundberg. *Digital Phase Modulation.* New York: Plenum, 1986.

[Ada93] F. Adachi. Postdetection Optimal Diversity Combiner for DPSK Differential Detection. *IEEE Trans. on Veh. Technol.*, 42(3):326–337, Aug. 1993.

[Ada94] Fumiyuki Adachi. MLSE Differential Phase Detection for M-ary DPSK. *IEE Proc. Commun.*, 141(6):407–412, Dec. 1994.

[Ada95a] Fumiyuki Adachi. Bit Error Rate Analysis of Reduced-State Viterbi Differential Detection of M-ary DPSK Signals. *Electronics Letters*, 31(24):2069–2070, Nov. 1995.

[Ada95b] Fumiyuki Adachi. Reduced-State Viterbi Differential Detection using a Recursively Estimated Phase Reference for M-ary PSK. *IEE Proc. Commun.*, 142(4):263–270, Aug. 1995.

[Ada96a] Fumiyuki Adachi. Adaptive Differential Detection of M-ary DPSK. *IEE Proc. Commun.*, 143(1):21–28, Feb. 1996.

[Ada96b] Fumiyuki Adachi. Adaptive Reception of MPSK signals in Fast Fading and AWGN Channels. *Electronics Letters*, 32(21):1944–1945, Oct. 1996.

[Ada96c] Fumiyuki Adachi. Error Rate Analysis of Differentially Encoded and Detected 16APSK Under Rician Fading. *IEEE Trans. on Veh. Technol.*, 45(1):1–11, Feb. 1996.

[Ada98] Fumiyuki Adachi. Adaptive Differential Detection Using Linear Prediction for M-ary DPSK. *IEEE Trans. on Veh. Technol.*, 47(3):909–918, Aug. 1998.

[AI94] Fumiyuki Adachi and Masaharu Ikura. Postdetection Diversity using Differential Phase Detection for M-ary DPSK. *Electronics Letters*, 30(21):1745–1746, Oct. 1994.

[AS65] Milton Abramowitz and Irene A. Stegun, editors. *Handbook of Mathematical Functions: with Formulas, Graphs and Mathematical Tables.* Dover Publications, first edition, 1965.

[AS89] S. Torgny Andersson and N. Arne B. Svensson. Noncoherent Detection of Convolutionally Encoded Continuous Phase Modulation. *IEEE J. on Select. Areas in Commun.*, 7(9):1402–1414, Dec. 1989.

[AS92a] F. Adachi and M. Sawahashi. Performance Analysis of Various 16 Level Modulation Schemes Under Rayleigh Fading. *Electronics Letters*, 28(17):1579–1581, Aug. 1992.

[AS92b] F. Adachi and M. Sawahashi. Viterbi-Decoding Differential Detection of DPSK. *Electronics Letters*, 28(23):2196–2197, Nov. 1992.

[AS93] F. Adachi and M. Sawahashi. Decision Feedback Differential Detection of 16-DAPSK Signals. *Electronics Letters*, 29(16):1455–1456, Aug. 1993.

[AS94] Fumiyuki Adachi and Mamoru Sawahashi. Error Rate Analysis of MDPSK and CPSK with Diversity Reception Under very Slow Rayleigh Fading and Cochannel Interference. *IEEE Trans. Veh. Technol.*, 43(2):252–263, May 1994.

[AS95] Fumiyuki Adachi and Mamoru Sawahashi. Decision Feedback Differential Phase Detection of M-ary DPSK Signals. *IEEE Trans. on Veh. Technol.*, 44(2):203–210, May 1995.

[AS96] Fumiyuki Adachi and Mamoru Sawahashi. Decision Feedback Differential Detection of Differentially Encoded 16APSK Signals. *IEEE Trans. on Commun.*, 44(4):416–418, April 1996.

[BC98] Gregory E. Bottomley and Sandeep Chennakesu. Unification of MLSE Receivers and Extension to Time-Varying Channels. *IEEE Trans. on Commun.*, 46(4):464–472, April 1998.

[BMM93] Dimitrios P. Bouras, P. Takis Mathiopoulos, and Dimitrios Makrakis. Optimal Detection of Coded Differentially Encoded QAM and PSK Signals with Diversity Reception in Correlated Fast Rician Fading Channels. *IEEE Trans. on Veh. Technol.*, 42(3):245–258, Aug. 1993.

[Chu97] Char-Dir Chung. Differentially Amplitude and Phase-Encoded QAM for the Correlated Rayleigh Fading Channel with Diversity Reception. *IEEE Trans. on Commun.*, 45(3):309–321, March 1997.

[CNM92] Y. C. Chow, A. R. Nix, and J. P. McGeehan. Analysis of 16-APSK Modulation in AWGN and Rayleigh Fading Channel. *Electronics Letters*, 28(17):1608–1610, Aug. 1992.

[CNM93] Y. C. Chow, A. R. Nix, and J. P. McGeehan. Diversity Improvement for 16-DAPSK in Rayleigh Fading Channel. *Electronics Letters*, 29(4):387–389, Feb. 1993.

[Cox87] Donald C. Cox. Universal Digital Portable Radio Communications. *Proc. IEEE*, 75(4):436–477, April 1987.

[DMV94] Aldo N. D'Andrea, Umberto Mengali, and Giorgio M. Vitetta. Approximate ML Decoding of Coded PSK with No Explicit Carrier Phase Reference. *IEEE Trans. on Commun.*, 42(2/3/4):1033–1039, Feb/March/April 1994.

[DS90] Dariush Divsalar and Marvin K. Simon. Multiple-Symbol Differential Detection of MPSK. *IEEE Trans. on Commun.*, 38(3):300–308, March 1990.

[DS94] Dariush Divsalar and Marvin K. Simon. Maximum-Likelihood Differential Detection of Uncoded and Trellis Coded Amplitude Phase Mod-

ulation over AWGN and Fading Channels-Metrics and Performance. *IEEE Trans. on Commun.*, 42(1):76–89, Jan. 1994.

[EQ88] M. Vedat Eyuboğlu and Shahid U. H. Qureshi. Reduced-State Sequence Estimation with Set Partitioning and Decision Feedback. *IEEE Trans. on Commun.*, 36(1):13–20, Jan. 1988.

[For72] G. D. Forney. Maximum-Likelihood Sequence Estimation of Digital Sequences in the Presence of Intersymbol Interference. *IEEE Trans. Info. Theory*, 18(3):363–378, May 1972.

[GL97] Michael J. Gertsman and John H. Lodge. Symbol-by-Symbol MAP Demodulation of CPM and PSK Signals on Rayleigh Flat-Fading Channels. *IEEE Trans. on Commun.*, 45(7):788–799, July 1997.

[GR94] I. S. Gradshteyn and I. M. Ryzhik. *Table of Integrals, Series and Products*. Academic Press, fifth edition, 1994.

[Hay83] Simon Haykin. *Communication Systems*. Wiley Eastern, second edition, 1983.

[HF92] P. Ho and D. Fung. Error Performance of Multiple-Symbol Differential Detection of PSK Signals Transmitted Over Correlated Rayleigh Fading Channels. *IEEE Trans. on Commun.*, 40(10):1566–1569, Oct. 1992.

[IA94] Masaharu Ikura and Fumiyuki Adachi. Postdetection Phase Combining Diversity. *IEEE Trans. Veh. Technol.*, 43(2):298–303, May 1994.

[Jr.74] W. C. Jakes Jr. *Microwave Mobile Communications*. Wiley, New York, 1974.

[Kai60] Thomas Kailath. Correlation Detection of Signals Perturbed by a Random Channel. *IRE Trans. Info. Theory*, 6(3):361–366, June 1960.

[Kam91a] Pooi Yuen Kam. Bit Error Probabilities of MDPSK Over the Nonselective Rayleigh Fading Channel with Diversity Reception. *IEEE Trans. on Commun.*, 39(2):220–224, Feb. 1991.

[Kam91b] Pooi Yuen Kam. Optimal Detection of Digital Data Over the Nonselective Rayleigh Fading Channel with Diversity Reception. *IEEE Trans. on Commun.*, 39(2):214–219, Feb. 1991.

[KT84] Pooi Yuen Kam and Cho Huak Teh. An Adaptive Receiver with Memory for Slowly Fading Channels. *IEEE Trans. on Commun.*, 32(6):654–659, June 1984.

[LM90] John H. Lodge and Michael L. Moher. Maximum Likelihood Sequence Estimation of CPM Signals Transmitted Over Rayleigh Flat-Fading Channels. *IEEE Trans. on Commun.*, 38(6):787–794, June 1990.

[LP92] Harry Leib and Subbarayan Pasupathy. Noncoherent Block Demodulation of MSK with Inherent and Enhanced Encoding. *IEEE Trans. on Commun.*, 40(9):1430–1441, Sept. 1992.

[MK97] Aarne Mämmelä and Veli-Pekka Kaasila. Smoothing and Interpolation in a Pilot-Symbol Assisted Diversity System. *Intl. J. of Wireless Info. Networks*, 4(3):205–214, June 1997.

[MMB94] Dimitrios Makrakis, P. Takis Mathiopoulos, and Dimitrios P. Bouras. Optimal Decoding of Coded PSK and QAM Signals in Correlated Fast Fading Channels and AWGN: A Combined Envelope, Multiple Differential and Coherent Detection Approach. *IEEE Trans. on Commun.*, 42(1):63–75, Jan. 1994.

[Mon80] Peter Monsen. Fading Channel Communications. *IEEE Commun. Mag.*, 18(1):16–25, Jan. 1980.

[MS79] Robert E. Morley, Jr. and Donald L. Snyder. Maximum Likelihood Sequence Estimation for Randomly Dispersive Channels. *IEEE Trans. on Commun.*, 27(6):833–839, June 1979.

[PM92] John G. Proakis and Dimitris G. Manolakis. *Digital Signal Processing: Principles, Algorithms and Applications*. Maxwell MacMillan, second edition, 1992.

[Pro95] John G. Proakis. *Digital Communications*. McGraw Hill, third edition, 1995.

[RPT95] R. Raheli, A. Polydoros, and C. K. Tzou. Per-Survivor Processing: A General Approach to MLSE in Uncertain Environments. *IEEE Trans. on Commun.*, 43(2/3/4):354–364, Feb/March/April 1995.

[SF95] James P. Seymour and Michael P. Fitz. Near Optimal Symbol-by-Symbol Detection Schemes for Flat Rayleigh Fading. *IEEE Trans. on Commun.*, 43(2/3/4):1525–1533, Feb/March/April 1995.

[SK97] Yew Kong Some and Pooi Yuen Kam. Efficient Estimation of Continuous Phase Modulation With Unknown Carrier Phase. *IEEE Trans. on Commun.*, 45(7):765–767, July 1997.

[Skl97] Bernard Sklar. Rayleigh Fading Channels in Mobile Digital Communication Systems: Parts I and II. *IEEE Commun. Mag.*, 35(7):90–109, July 1997.

[Sve95] N. Arne B. Svensson. On Differentially Encoded Star 16QAM with Differential Detection and Diversity. *IEEE Trans. on Veh. Technol.*, 44(3):586–593, Aug. 1995.

[Ung74] G. Ungerboeck. Adaptive Maximum Likelihood Receiver for Carrier Modulated Data Transmission Systems. *IEEE Trans. on Commun.*, 22(5):624–635, May 1974.

[VGR97] K. Vasudevan, K. Giridhar, and Bhaskar Ramamurthi. Nyquist-Rate Detection of CPM Signals Using the Viterbi Algorithm. In *Proc. of the Third National Conf. on Commun.*, pages 85–90, Indian Institute of Technology Madras, India, Feb. 1997.

[VGR98a] K. Vasudevan, K. Giridhar, and Bhaskar Ramamurthi. DSP-Based Noncoherent Detectors for Multilevel Signals in Flat Fading Channels. In *Proc. of the* 7^{th} *IEEE International Conference on Universal Personal Communications*, pages 1313–1317, Florence, Italy, Oct. 1998.

[VGR98b] K. Vasudevan, K. Giridhar, and Bhaskar Ramamurthi. Noncoherent Sequence Estimation of Multilevel Signals in Slowly Fading Channels. In *Proc. of the Fourth National Conf. on Commun.*, pages 18–23, Indian Institute of Science Bangalore, India, Jan. 1998.

[VGR99a] K. Vasudevan, K. Giridhar, and Bhaskar Ramamurthi. Differential Detection of Multilevel Signals in Frequency Nonselective Rayleigh Fading Channels with Diversity. In *Proc. of the IEEE International Conference on Personal Wireless Communications*, pages 188–192, Jaipur, India, Feb. 1999.

[VGR99b] K. Vasudevan, K. Giridhar, and Bhaskar Ramamurthi. Noncoherent Detection of Multilevel Signals in Frequency Nonselective Fading Channels. *Signal Processing Journal, Elsevier Science Publishers*, 78(2):159–176, Oct. 1999.

[VT95] Giorgio M. Vitetta and Desmond P. Taylor. Viterbi Decoding of Differentially Encoded PSK Signals Transmitted over Rayleigh Frequency-Flat Fading Channels. *IEEE Trans. on Commun.*, 43(2/3/4):1256–1259, Feb/March/April 1995.

[WHS91] W. T. Webb, L. Hanzo, and R. Steele. Bandwidth Efficient QAM schemes for Rayleigh Fading Channels. *IEE Proceedings-I*, 138(3):169–175, June 1991.

[YP95] Xiaoyong Yu and Subbarayan Pasupathy. Innovations-Based MLSE for Rayleigh Fading Channels. *IEEE Trans. on Commun.*, 43(2/3/4):1534–1544, Feb/March/April 1995.

LIST OF PAPERS BASED ON THESIS

1. K. Vasudevan, K. Giridhar and Bhaskar Ramamurthi, "Split-Trellis Viterbi Decoder: A New Computationally Efficient MLSE," *Proc. of the Second National Conf. on Commun.*, Indian Institute of Technology, Bombay, pp. 59–62, Feb. 1996.

2. K. Vasudevan, K. Giridhar and Bhaskar Ramamurthi, "Nyquist-Rate Detection of CPM Signals Using the Viterbi Algorithm," *Proc. of the Third National Conf. on Commun.*, Indian Institute of Technology, Madras, pp. 85–90, Feb. 1997.

3. K. Vasudevan, K. Giridhar and Bhaskar Ramamurthi, "Noncoherent Sequence Estimation of Multilevel Signals in Slowly Fading Channels," *Proc. of the Fourth National Conf. on Commun.*, Indian Institute of Science, Bangalore, pp. 18–23, Jan. 1998.

4. K. Vasudevan, K. Giridhar and Bhaskar Ramamurthi, "Efficient VA for Signals with ISI," *Electronics Letters*, vol. 34, no. 7, pp. 629–631, April 1998.

5. K. Vasudevan, K. Giridhar and Bhaskar Ramamurthi, "DSP-Based Noncoherent Detectors for Multilevel Signals in Flat Fading Channels", *Proc. of the IEEE International Conference on Universal Personal Communications*, Florence, Italy, pp. 1313–1317, Oct. 1998.

6. K. Vasudevan, K. Giridhar and Bhaskar Ramamurthi, "Differential Detection of Multilevel Signals in Frequency Nonselective Rayleigh Fading Channels with Diversity", *Proc. of the IEEE International Conference on Personal Wireless Communications*, Jaipur, pp. 188–192, Feb. 1999.

7. K. Vasudevan, K. Giridhar and Bhaskar Ramamurthi, " Noncoherent Detectors for Multilevel Signals in Frequency Nonselective Fading Channels", *Signal Processing Journal*, (Elsevier Science), vol. 78, issue 2, pp. 159–176, Oct. 1999.

CURRICULUM VITAE

1. NAME : K. Vasudevan

2. DATE OF BIRTH : 6th April 1969

3. EDUCATIONAL QUALIFICATIONS

1991 Bachelor of Technology, Honours (B.Tech.(Hons))

Institution : Indian Institute of Technology, Kharagpur

Specialization : Electronics and Electrical Communication Engineering

1996 Master of Science (by Research)

Institution : Indian Institute of Technology, Madras

Specialization : Electrical Engineering

Doctor of Philosophy (Ph.D.)

Institution : Indian Institute of Technology, Madras

Registration Date : 17-11-1995

DOCTORAL COMMITTEE

CHAIRPERSON: Dr. Ashok Jhunjhunwalla
Professor and Head
Department of Electrical Engineering

GUIDES: Dr. Bhaskar Ramamurthi
Associate Professor
Department of Electrical Engineering

Dr. K. Giridhar
Assistant Professor
Department of Electrical Engineering

MEMBERS: Dr. V. V. Rao
Professor
Department of Electrical Engineering

Dr. B. Yegnanarayana
Professor
Department of Computer Science and Engineering

Dr. R. Kalyanakrishnan
Professor
Department of Computer Science and Engineering